



Cite this: *EES Catal.*, 2025, **3**, 1196

## Advances in catalysing the hydrogen storage in main group metals and their tetrahydroborates and tetrahydroaluminates

Melinda Krebsz,  <sup>†\*ab</sup> Tibor Pasinszki,  <sup>c</sup> Sooraj Sreenath<sup>a</sup> and Valeska P. Ting<sup>bd</sup>

Hydrogen is a promising clean and renewable energy source; however, its efficient storage is one of the key challenges in establishing the sustainable hydrogen economy. The light main group metals and their tetrahydroborates and tetrahydroaluminates show great potential for high hydrogen storage capacity close to ambient conditions; however, their high hydrogenation and dehydrogenation temperatures, sluggish kinetics, and limited reversibility have always been an obstacle for practical applications. Large efforts have been devoted to modifying the thermodynamic and kinetic properties of these systems, and reviewing these efforts and highlighting future directions are the aims of the present review. Based on recent research, the application of multicomponent systems utilizing multiple modification methods, such as catalysis, nanoconfinement, alloying, and structure engineering, is essential for enhancing the storage conditions. The synergistic effect of multiple catalysts is now a key requirement to address various steps of the overall process, including forming/breaking the H–H and metal–H bonds, transporting hydrogen and heat, and suppressing the formation of side products. Compared to pristine systems, tremendous improvement has been achieved. Catalysed  $\text{AlH}_3$  decomposition can now operate as a one-way hydrogen source below 100 °C and the Mg/MgH<sub>2</sub> hydrogen storage system exhibits good cyclic performance at elevated temperatures. Metal hydrides, tetrahydroborates, tetrahydroaluminates, and their composite systems face challenges in achieving close to ambient operating conditions and cyclic stability. As the demand for improved hydrogen energy storage is expected to grow, further research for the enhancement of these systems will continue to advance the state of hydrogen storage technology.

Received 30th April 2025,  
Accepted 18th July 2025

DOI: 10.1039/d5ey00134j

rsc.li/eescatalysis

### Broader context

Development of effective storage technologies for the hydrogen industry will support decarbonisation and shifting away from fossil fuels. Mobile applications require safe and robust technologies operating close to ambient conditions. To address this, storage materials capable of delivering and absorbing hydrogen under mild conditions need to be explored. Promising material groups for mobile hydrogen storage are the light main group metals and their tetrahydroborates and tetrahydroaluminates. We demonstrate in our present study the possibility of improving the storage performances of these compounds by tuning their thermodynamic and kinetic properties utilizing multiple modification methods, such as multi-component catalysis, nanoconfinement and alloying. Given the potential of these techniques, findings presented in this review may enable the much-needed improvements in solid-phase hydrogen storage to develop high-capacity storage systems operating close to ambient conditions.

## 1. Introduction

Three of the most difficult challenges facing mankind today are global warming caused by air pollution, increasing energy demand, and depleting sources of fossil fuels. The three are interconnected as current energy production is heavily based on fossil fuels,<sup>1</sup> the combustion of fossil fuels leads to about three quarters of global greenhouse gas emissions,<sup>1</sup> and depleting fossil fuel sources endanger energy supply.<sup>2</sup> 76.5% of the global primary energy consumed in 2023 was based on fossil fuels,<sup>1</sup> and the mass of carbon in the atmosphere has increased

<sup>a</sup> School of Engineering, STEM College, RMIT University, Bundoora, Victoria 3083, Australia. E-mail: melinda.krebsz@anu.edu.au

<sup>b</sup> Research School of Chemistry, College of Science and Medicine, The Australian National University, Canberra, ACT 2601, Australia

<sup>c</sup> School of Sciences, College of Engineering and TVET, Fiji National University, Suva, P.O. Box 3722, Fiji

<sup>d</sup> Department of Mechanical Engineering, University of Bristol, Bristol, BS8 1TR, UK  
<sup>†</sup> Current address: Research School of Chemistry, College of Science and Medicine, The Australian National University, Canberra, ACT 2601, Australia.



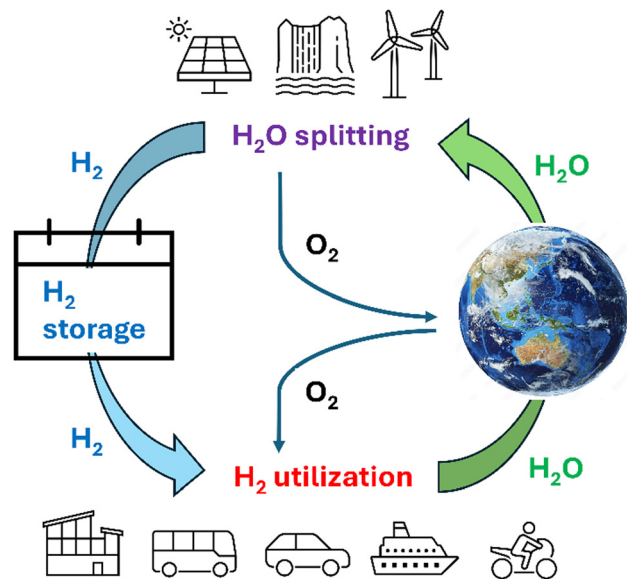


Fig. 1 The carbon-free hydrogen energy cycle.

by 48% from eighteenth century pre-industrial levels.<sup>3</sup> The world therefore needs an alternative energy source and technology to shift away from fossil fuels. Water is abundant on Earth and splitting water into hydrogen and oxygen and using hydrogen to generate energy if needed would provide a sustainable and carbon-free energy cycle if hydrogen is generated by utilizing renewable energy (Fig. 1). Several governments around the globe have realised the need for technology change and abandoning dependence on fossil fuels and started to build a ‘hydrogen-powered economy’.<sup>4–8</sup> Key enabling technologies to realize these plans are needed for the production, storage, distribution, and application of hydrogen. The storage of hydrogen, however, is challenging due to its inherent nature; hydrogen is a low-density gas under ambient conditions ( $0.0813 \text{ kg m}^{-3}$  at 1 bar and  $25 \text{ }^\circ\text{C}$ )<sup>9</sup> and storage, transport and utilization, especially in mobile applications, require high storage densities. The U.S. Department of Energy (DOE) technical system targets for onboard hydrogen storage for light-duty fuel cell vehicles highlight these challenges and formulate targets for industry and academic research (Table 1).<sup>10</sup> Considering these, a 615-fold increase of the density of hydrogen in the storage system must be achieved compared to that of ambient gas, which is even more demanding for the storage material as the storage vessel also has volume and mass.

The hydrogen storage system needs to fulfill several requirements, including safety, high gravimetric and volumetric storage

capacity, sufficient rate of hydrogen delivery and recharging, close to ambient operating conditions, easy handling, abundant resources, and competitive price. None of the current systems can fulfill all these requirements. There are several research directions reflecting application needs, and hydrogen may be stored in molecular form or in compounds. The current most advanced molecular hydrogen storage methods are storage of hydrogen as a pressurized gas at ambient temperatures (technology readiness level<sup>11</sup> (TRL) = 9) and as liquified hydrogen at cryogenic temperatures (TRL = 9). Drawbacks of these methods include the safety issues and cost of compressing hydrogen to pressures up to 700 bar, the low volumetric density of the pressurized gas and the high production cost of high pressure storage containers for high pressure gaseous storage, and the cost of liquefaction, bulky insulation to maintain low temperatures ( $< 33 \text{ K}$ ) and the control of the boil off for liquid hydrogen storage.<sup>12–15</sup> Large efforts have been devoted to developing hydrogen storage based on molecular hydrogen adsorption on solid materials such as doped carbons, metal organic frameworks (MOFs), covalent organic frameworks (COFs) and porous aromatic frameworks (PAFs).<sup>16–19</sup> However, high storage capacity can only be achieved at cryogenic temperatures (TRL = 5); ambient temperature storage satisfying DOE targets is not yet feasible for storage of hydrogen *via* adsorption.<sup>16–19</sup> Storing hydrogen in compounds is an alternative to molecular hydrogen storage and has several advantages such as the stability of many hydrogen compounds under ambient conditions, the high gravimetric and volumetric hydrogen capacity (up to about 20 wt% or  $150 \text{ kg m}^{-3}$ ), and the relatively easy storage and transport.<sup>20–23</sup> Hydrogen compounds for storage may be classified into three groups, namely (1) molecular hydrides (*e.g.*, ammonia, perhydro-dibenzyltoluene, methylcyclohexane), (2) interstitial hydrides of transition metals and their alloys (*e.g.*, TiFe,  $\text{Nd}_2\text{Ni}_7$ , high entropy alloys such as  $\text{V}_{35}\text{Ti}_{30}\text{Cr}_{25}\text{Fe}_5\text{Mn}_5$ ), or (3) ionic and polymeric hydrides (*e.g.*, LiH,  $\text{MgH}_2$ ). An advantage of currently considered liquid organic molecular hydrides is that they closely resemble conventional fuels and existing infrastructures could be used to store and transport them safely.<sup>24–27</sup> However, industrial environments are required for the hydrogenation and purification of the hydrogen-lean and hydrogen-rich forms of storage compounds and mobile applications can consider these hydrogen carriers only as “off-board” regenerable materials. None of the currently considered molecular liquid hydrogen carriers fulfill all storage requirements, namely low melting ( $< -30 \text{ }^\circ\text{C}$ ) and high boiling ( $> 300 \text{ }^\circ\text{C}$ ) point, high volumetric and gravimetric hydrogen storage capacities, stability for long lifespan, low dehydrogenation temperatures, low

Table 1 DOE technical system targets for onboard hydrogen storage for light-duty fuel cell vehicles<sup>10</sup>

|                 | System properties          |  |   |                        |                        |                              |
|-----------------|----------------------------|--|---|------------------------|------------------------|------------------------------|
|                 | Gravimetric capacity (wt%) | Volumetric capacity ( $\text{kg m}^{-3}$ ) | Min/max delivery temperature ( $^\circ\text{C}$ ) | System fill time (min) | Operational cycle life | Dormancy <sup>a</sup> (days) |
| 2025 target     | 5.5                        | 40   | –40/85  | 3–5                    | 1500                   | 10                           |
| Ultimate target | 6.5                        | 50   | –40/85  | 3–5                    | 1500                   | 14                           |

<sup>a</sup> Considering that the vehicle is parked at an ambient temperature of  $35 \text{ }^\circ\text{C}$ ; minimum until first release from initial 95% usable capacity.



production cost, and low toxicity. The toluene/methylcyclohexane system is technologically the most advanced (TRL = 9); a demonstration project has been carried out by hydrogenating toluene in a chemical plant in Brunei, shipping methylcyclohexane to Japan, dehydrogenating methylcyclohexane in Japan, and shipping toluene back to Brunei.<sup>26,28</sup> Storing hydrogen in interstitial, ionic or polymeric metal hydrides solves the problem of volatility of molecular hydrides; however, it introduces new challenges. The hydrogen storage in interstitial hydrides has several advantages such as reversibility, fast kinetics, and the ability of several transition metals and alloys to absorb and desorb hydrogen under ambient and near ambient conditions, as well as the tunability of operating pressure and temperature, including the region in which electrolyzers and fuel cells operate (between 1 and 10 bar pressure and below 100 °C) (TRL = 9).<sup>22,29,30</sup> Disadvantages, however, are the high cost and low gravimetric storage capacity, well below the DOE targets, which prevent their wide scale use. Nonetheless, interstitial hydrides are successfully applied as hydrogen storage materials in vehicles where the heavy storage material is not a weight penalty, for example in forklifts, submarines, and canal boats.<sup>31–33</sup>

Promising groups of hydride compounds for hydrogen storage, that may fulfill storage requirements in the future and bypass the limitations of storage methods mentioned above, are the ionic and polymeric binary hydrides of light main group metals (alkali and alkali earth elements and aluminium) and their tetrahydroborates and tetrahydroaluminates (which can be considered to be complexes of metal hydrides and BH<sub>3</sub> and AlH<sub>3</sub>, respectively), as well as their mixtures (reactive hydride composites, RHCs) due to their high gravimetric and volumetric hydrogen storage capacities (Table 2). These

compounds are stable under ambient conditions in an inert atmosphere and several of the relevant metals, *e.g.* Mg and Al, are cheap, light, and abundant on Earth, which makes them very attractive for both mobile and stationary storage systems. Inherent properties of these compounds, namely the high temperatures and pressures needed for hydrogen uptake and release, the sluggish kinetics, and the partial- or non-reversibility of hydrogen release and uptake, as well as the formation of side products, however, have impeded their wide scale application to date (TRL = 3–5 depending on the compound). Due to their potential in filling the gap in reversible and high-capacity hydrogen storage under close to ambient conditions, large efforts have been devoted during the last few decades to bring operation conditions closer to ambient conditions by improving the kinetics and thermodynamics of the hydrogenation and dehydrogenation reactions using additives and catalysts. Considering this and the increasing demand for effective storage materials, as well as the rapidly changing hydrogen storage industry, the aim of the present work is to review advances in improving hydrogen storage properties of binary hydrides of light main group metals and their tetrahydroborates and tetrahydroaluminates, and to highlight their advantages, limitations, and challenges, as well as to point out future trends in developing storage materials for the hydrogen industry. We consider DOE initiatives and the operation conditions of fuel cells as research targets, namely storage capacities of 6.5 wt% and 50 kg m<sup>-3</sup> and lower than 10 bar pressure and 100 °C temperature (note that the DOE target is the storage system target and the storage material must perform better, but to keep discussion simple we use these target numbers for the storage material in this article). Additives to hydrides which

Table 2 Gravimetric storage capacity of main group metal hydrides and alkali and alkali earth tetrahydroborates and tetrahydroaluminates<sup>ab</sup>

| Metal hydride    | Grav. capacity (wt.%) | Vol. capacity (kg·m <sup>-3</sup> H <sub>2</sub> ) | Tetrahydroborate                  | Grav. capacity (wt.%) | Vol. capacity (kg·m <sup>-3</sup> H <sub>2</sub> ) | Tetrahydroaluminate                | Grav. capacity (wt.%) | Vol. capacity (kg·m <sup>-3</sup> H <sub>2</sub> ) |
|------------------|-----------------------|--|-----------------------------------|-----------------------|--|------------------------------------|-----------------------|--|
| LiH              | 12.68                 | 98.3   | LiBH <sub>4</sub>                 | 18.51                 | 122.2  | LiAlH <sub>4</sub>                 | 10.62                 | 96.6   |
| NaH              | 4.20                  | 57.2   | NaBH <sub>4</sub>                 | 10.66                 | 114.1  | NaAlH <sub>4</sub>                 | 7.47                  | 94.9   |
| KH               | 2.51                  | 35.9   | KBH <sub>4</sub>                  | 7.47                  | 87.4   | KAlH <sub>4</sub>                  | 5.75                  | 71.6   |
| BeH <sub>2</sub> | 18.28                 | 118.8  | Be(BH <sub>4</sub> ) <sub>2</sub> | 20.84                 | 146.3  | Be(AlH <sub>4</sub> ) <sub>2</sub> | 11.35                 | ---  |
| MgH <sub>2</sub> | 7.66                  | 111.1  | Mg(BH <sub>4</sub> ) <sub>2</sub> | 14.94                 | 147.8  | Mg(AlH <sub>4</sub> ) <sub>2</sub> | 9.34                  | 97.7   |
| CaH <sub>2</sub> | 4.79                  | 91.1   | Ca(BH <sub>4</sub> ) <sub>2</sub> | 11.56                 | 126.5  | Ca(AlH <sub>4</sub> ) <sub>2</sub> | 7.90                  | ---  |
| AlH <sub>3</sub> | 10.08                 | 148.9  | Al(BH <sub>4</sub> ) <sub>3</sub> | 16.92                 | 92.9   | AlH <sub>3</sub> <sup>c</sup>      | 10.08                 | 148.9  |

<sup>a</sup> Calculated in this work using atomic masses and the density of hydrides.<sup>35,39–44</sup> <sup>b</sup> BeH<sub>2</sub>, MgH<sub>2</sub>, and AlH<sub>3</sub> have a polymeric structure with three-centre M–H–M bonds (M = Be, Mg, or Al). Colour codes: above the DOE target (green and yellow, green is higher than yellow and primary target), below the DOE target (pink), and not considered for hydrogen storage (no colour). <sup>c</sup> Al(BH<sub>4</sub>)<sub>3</sub> = AlH<sub>3</sub>.



do not contain hydrogen decreases the storage capacity; therefore large amounts of additives used to alter reaction conditions are not considered in this review. Considering gravimetric capacities in Table 2, pristine NaH, KH, CaH<sub>2</sub>, and KAlH<sub>4</sub> do not satisfy DOE targets (Table 1), but can be considered as one of the components of RHCs. Heavier I–III group metals are not relevant for hydrogen storage due to their weight, toxicity, and/or low abundance. Although beryllium compounds have exceptionally high hydrogen storage capacity (Table 2), they are not considered for hydrogen storage because beryllium ores are not abundant, beryllium is expensive, and beryllium salts, including the hydride, are extremely toxic.<sup>34,35</sup> Al(BH<sub>4</sub>)<sub>3</sub> is a volatile pyrophoric liquid at room temperature, explosive in air, has poor storage stability, and releases also diborane upon heating; therefore, its practical use in hydrogen storage is restricted.<sup>36–38</sup> To discuss the highlighted topic, this review is organised in subchapters according to the chemical groups of hydrogen compounds.

## 2. Results and discussion

### 2.1. General considerations and experimental determination of thermodynamic and kinetic parameters of hydrogen absorption and release

The hydrogen absorption by metals is a multiple-step process, and involves several consecutive steps, namely (a) physisorption

of hydrogen, (b) dissociation of hydrogen into atoms on the surface, (c) penetration of hydrogen atoms in the subsurface, (d) hydrogen diffusion in the bulk material, and (e) nucleation and growth of the hydride phase. The reverse process, hydrogen release, follows the opposite multistep process, starting with the dissociation of the metal–hydrogen bond. Each step of both absorption and desorption processes must overcome a range of activation energy barriers, and decreasing these energy barriers, especially that of the rate determining step, is of crucial importance for improving the rate and/or decreasing the reaction temperature of hydrogen absorption and desorption. Covalent and ionic bonds are strong; therefore, dissociation of molecular hydrogen and the metal–hydrogen bond is, in general, rate determining and thermodynamically limiting. The overall thermodynamics and kinetics govern the hydrogen uptake and release and altering these is an effective strategy for improving hydrogen storage properties in metals.

Thermodynamically, the hydrogenation reaction occurs if the Gibbs free energy ( $\Delta G$ ) of the reaction, related to the enthalpy of formation ( $\Delta H$ ), entropy of formation ( $\Delta S$ ), and temperature ( $T$ ), is negative ( $\Delta G = \Delta H - T\Delta S$ ). Since heat is released and entropy is reduced during the hydrogenation reaction (as hydrogen is moving from the gas phase into its bonded solid phase), the enthalpy and entropy both have negative signs; consequently, thermodynamically, and depending on the concrete value of  $\Delta H$ ,

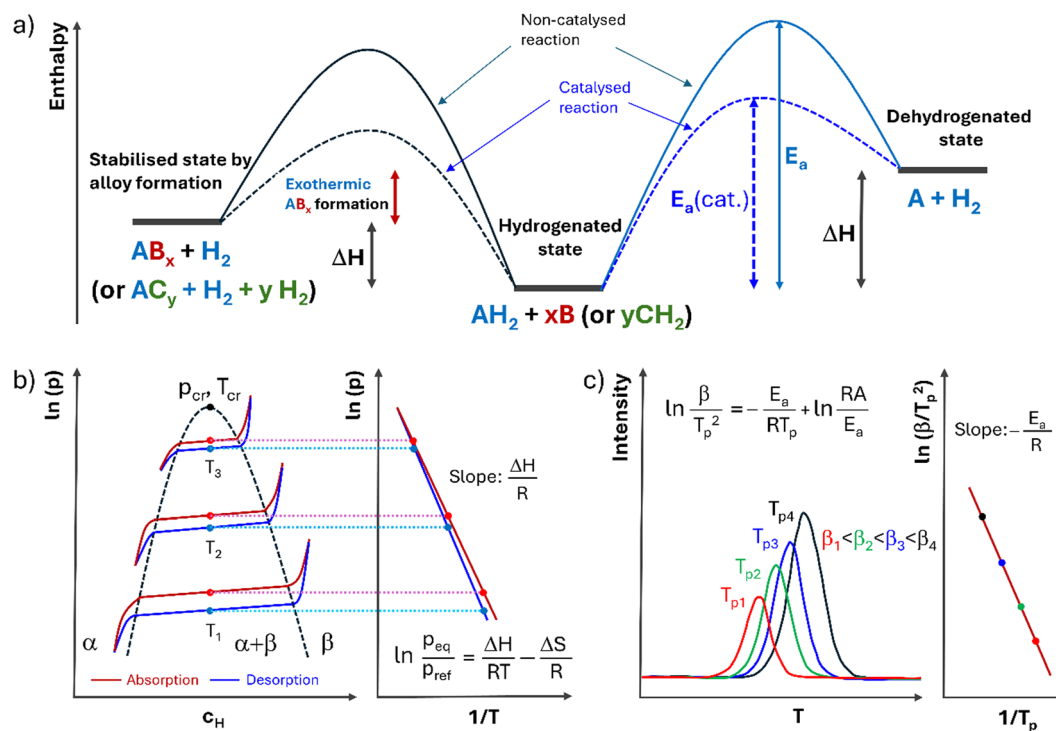


**Fig. 2** (a) Generalized enthalpy diagram showing the effect of a catalyst on the kinetics and the effect of alloy formation on the thermodynamics for a hypothetical metal/metal hydride system ( $A = \text{Li, Na, K, Mg, Ca}$  or  $\text{Al}$ ;  $B = \text{non-hydrating alloying element}$ ;  $C = \text{hydrating alloying element}$ ), (b) schematic PCT phase diagram on the left hand side and the van't Hoff equation and the corresponding van't Hoff lines on the right hand side for hydrogen absorption and desorption on a typical metal ( $c_H = \text{hydrogen concentration in the solid phase}$ ,  $p = \text{hydrogen pressure}$ ,  $p_{eq} = \text{mid-plateau equilibrium pressure}$ ,  $p_{ref} = \text{reference pressure of 1 bar}$ ,  $p_{cr} = \text{critical pressure}$ ,  $R = \text{universal gas constant}$ ,  $T = \text{absolute temperature}$ ,  $T_{cr} = \text{critical temperature}$ ), and (c) schematic representation of a thermal event at various heating rates on the left hand side and the Kissinger line on the right hand side ( $\beta = \text{heating rate}$ ,  $T_p = \text{peak temperature}$ ,  $E_a = \text{apparent activation energy}$ ,  $A = \text{pre-exponential factor}$ ).



the hydrogenation is favoured at lower temperatures, but the reverse reaction, dehydrogenation, is favoured at higher temperatures when  $\Delta G$  becomes positive. Considering an ideal hydrogen storage system using temperature swing, a right balance between  $\Delta H$  and  $T \cdot \Delta S$  must exist where  $|\Delta H| > |T \cdot \Delta S|$  at charging (hydrogenation at lower temperature, ideally under ambient conditions) and  $|\Delta H| < |T \cdot \Delta S|$  at discharging (hydrogen release at elevated temperature). With very large  $\Delta H$ , which is related to the strength of the metal–hydrogen bond, hydrogen release requires high temperatures. Considering that the entropy change during hydrogen absorption corresponds mostly to the change from molecular hydrogen gas to bonded hydrogen in solid hydrides,  $\Delta S$  is approximately equal to the standard entropy of hydrogen for all metal–hydrogen systems, namely  $-130 \text{ J K}^{-1} \text{ mol}^{-1} \text{ H}_2$ .<sup>45,46</sup> The thermodynamic properties of metal–hydrogen systems are therefore usually characterized by the reaction enthalpy. (The same principle can be applied to tetrahydroborates and tetrahydroaluminates, too.) One way to alter thermodynamics is the application of additives which form alloys during dehydriding (see Fig. 2a). Non-hydriding additives decrease hydrogen storage capacity, as they dilute the metal; however, hydriding additives can preserve or even increase hydrogen storage capacity (Fig. 2a), which highlights the advantage of RHCs. In this sense, the formation of metal borides and alloys during the dehydrogenation reactions of tetrahydroborates, tetrahydroaluminates, and RHCs (formally the mixtures of two or more binary hydrides) is crucial for the desired thermodynamics of the system; the separation of metallic and boron phases is unfavourable (as will be discussed below). Thermodynamic parameters of hydrogen absorption and desorption are usually determined using the pressure–composition–temperature (PCT) phase diagram and the van't Hoff equation (Fig. 2b).<sup>45–48</sup> Considering a metal–hydrogen system and the Gibbs phase rule, the system has two degrees of freedom (due to the presence of two phases and two components) when hydrogen starts to absorb. Hydrogen first dissolves in the metal lattice and forms a solid solution phase ( $\alpha$ -phase), which has the same crystal structure as the bare metal and has low hydrogen concentration. In the  $\alpha$ -phase region the concentration of hydrogen in the solid phase increases as the hydrogen pressure increases. At a certain point, nucleation of a higher concentration phase ( $\beta$ -phase) occurs. Due to the occurrence of an additional phase and thus the presence of three phases ( $\alpha$ ,  $\beta$  and gas), the system's degree of freedom is decreased to one, and the pressure stays constant (equilibrium pressure,  $p_{\text{eq}}$ ) until the  $\alpha$ - and  $\beta$ -phases coexist. After the disappearance of the  $\alpha$ -phase, hydrogen enters the  $\beta$ -phase (solid solution) and the system's degree of freedom is two again and the concentration of hydrogen increases as the pressure is increased. As Fig. 2b shows, there are three phase regions in the PCT diagram, the  $\alpha$ ,  $\alpha + \beta$ , and  $\beta$  regions separated by the transition dome curve (dotted line). The two-phase region ( $\alpha + \beta$ ) ends in a critical point, characterized by the critical temperature ( $T_{\text{cr}}$ ) and pressure ( $p_{\text{cr}}$ ), above which the transition from the  $\alpha$ - to  $\beta$ -phase is continuous. When  $\alpha$  and  $\beta$  phases coexist, there is a plateau in the isotherms, the pressure hardly changes during the  $\alpha \rightarrow \beta$  phase transition, therefore a significant amount of hydrogen is absorbed with

small pressure increases. The plateau region ( $\alpha + \beta$  isotherm), however, is not entirely flat due to the expansion of the lattice and small changes of  $\Delta H$  as a function of hydrogen concentration. In addition, the absorption pressure is slightly higher than the desorption pressure due to unequal accommodation of elastic and plastic energies, which causes a 'hysteresis'.<sup>48</sup> The hysteresis, in general, decreases with increasing temperature.<sup>49</sup> Typical hysteresis magnitudes ( $\Delta p/p_{\text{des}}$ , where  $\Delta p = p_{\text{abs}} - p_{\text{des}}$ ) for selected systems as examples are 0.015 (at 401 °C) and 0.007 (at 497 °C) for Mg,<sup>50</sup> 0.51 (at 0 °C) and 0.24 (at 80 °C) for LaNi<sub>5</sub>,<sup>49</sup> and 1.43 (at 25 °C) and 0.97 (at 85 °C) for TiFe.<sup>51</sup> The pressure–temperature–concentration relationship can be expressed for both absorption and desorption by the extended van't Hoff equation; by setting the hydrogen concentration to the value at the middle of the  $\alpha + \beta$  phase region, the equation is simplified and the pressure–temperature relationship can be used to determine  $\Delta H$  values experimentally (see Fig. 2b).

The rates of the hydrogenation and dehydrogenation reactions are of crucial importance for practical storage applications. They depend on the activation energy barrier of the absorption and desorption processes and on the temperature and hydrogen pressure, as well as on the surface area of the solid. Nanosizing metals and alloys to increase the rate of the heterogeneous hydrogenation reaction is an obvious step to increase the rate. Current research on improving the kinetics of hydrogen absorption/desorption aims to reduce the activation energy barrier using catalysts to allow milder reaction conditions (temperature and pressure) for practical applications. The Kissinger method is currently overwhelmingly popular to estimate the apparent activation energy ( $E_a$ ) for both hydrogen absorption and desorption due to its simplicity (even if complex processes may not be well represented by a single activation energy).<sup>52,53</sup> The Kissinger equation is shown in Fig. 2c. The method is based on measuring a chemical (or physical) thermal event at several non-isothermal tests conducted at constant heating rates ( $\beta$ ), using *e.g.* DSC, DTG, DTA, or MS, and measuring the peak (or onset) temperature of the event ( $T_p$ ). A plot of  $\ln(\beta/T_p^2)$  versus  $1/T_p$  leads to a straight line with the slope equal to  $-E_a/R$  (Fig. 2c). Although this method is simple, it oversimplifies the process by assuming single-step kinetics with first-order reaction. If the reaction model is not first order, its dependence on the heating rate introduces an inaccuracy which increases with decreasing  $E_a/RT$ . This error has been shown to be below 5% as long as  $E_a/RT$  is larger than 10;<sup>53,54</sup> therefore the  $E_a/RT > 10$  relationship may be considered as a prerequisite for using the Kissinger method.<sup>53</sup> In addition, the linear heating rate is an integral part of the Kissinger equation; therefore nonlinear heating programs can be applied only if the extent of conversion of the reactant to products doesn't vary significantly with the heating rate at the event peak.<sup>53</sup> Further drawbacks of the method are its inability to detect complexity of processes (namely multiple steps covered by one event peak) and inapplicability to any data obtained on cooling.<sup>53</sup> The appearance of multiple peaks in experimental data requires treating them separately (note that a single peak doesn't necessarily mean a single-step process). If peaks are overlapping, they



need to be deconvoluted and the Kissinger method should be applied separately to each individual peak to estimate activation energies of specific processes. Considering its limitations, the Kissinger method should be used for quick estimation of apparent activation energies in comparative studies of simple transformations, rather than providing details of process kinetics. An alternative, although less frequently used and more time consuming, way to obtain activation energies is based on calculating rate constants at several temperatures using the Johnson–Mehl–Avrami–Kolmogorov (JMAK)<sup>55,56</sup> equation [“linearized” form:  $\ln[-\ln(1 - \alpha)] = \eta \ln(k) + \eta \ln(t)$ , where  $k$  = rate constant,  $\alpha$  = converted reaction fraction,  $\eta$  = growth dimensionality,  $t$  = time] by fitting (de)hydrogenation curves and calculating the activation energy using the Arrhenius equation (the slope of  $\ln(k)$  versus  $1/T$  is equal to  $-E_a/R$ ). The JMAK model includes simultaneous nucleation, growth and impingement and offers a more detailed model of phase transformation kinetics than the Kissinger method. Limitations may arise from model specifics, namely assuming phase transformation by random nucleation and growth, a zero critical nucleus size, requirement of a large number of nuclei for accurate prediction, and nucleation and growth following a predetermined law.<sup>56–59</sup> It is important to note that although the limitations of the Kissinger model have been stretched, its popularity continues;<sup>53,60</sup> however, this may change in the future by wider application of more sophisticated, currently underutilised kinetic models for hydrogen storage materials.<sup>56</sup>

Macroscopic PCT and thermal analyses are the most widely used methods for obtaining information about the kinetics and thermodynamics of the system due to easy accessibility and cost of the instrumentation, but modern *operando* tools (e.g., synchrotron radiation X-ray power diffraction (SR-XRPD), neutron scattering (NS), and *in situ* transmission electron microscopy (TEM)) can allow direct observation of phase evolution and kinetics. The SR-XRPD light source is more intense than those of laboratory XRPD instruments, highly collimated, tuneable in a wide energy spectrum, and has a short pulse time structure; therefore SR-XRPD allows high-resolution and time-resolved studies to investigate microstructures of materials, including crystal structure, crystallite size, phase composition, defect and strain.<sup>61,62</sup> Recording *in situ* SR-XRPD data throughout the whole hydrogenation/dehydrogenation reaction can provide information on the reaction mechanism, transient phases, and kinetics of phase transitions. Hydrogen has a high scattering cross section with neutrons; therefore, neutron scattering techniques, including neutron diffraction (ND), total neutron scattering (TNS), inelastic neutron scattering (INS), quasi-elastic neutron scattering (QENS) and small-angle neutron scattering (SANS), are valuable tools for studying hydrogen storage materials.<sup>63–68</sup> ND and TNS can locate hydrogen atoms in the crystal structure which is practically impossible with XRD. TNS is also powerful for studying amorphous materials. Using neutrons also has the benefit of being able to put the sample under a greater range of pressures, temperatures and gas environments, compared to X-ray instruments, as the neutrons can pass through thick stainless-steel cells and

instruments. This makes them particularly useful for *operando* measurements. INS and QENS are conceptually similar to infrared and Raman spectroscopy and provide information on molecular and crystal vibrations as well as diffusion and liberation of hydrogen, but in contrast to IR and Raman all vibrations are visible (no selection rules) and the spectrum is dominated by hydrogen displacements due to the approximately order of magnitude higher scattering cross section of neutrons for hydrogen as compared to other elements. The SANS pattern contains information on atomic positions and shapes of particles and can therefore be used to obtain information on the size, shape, and interaction of nanoparticles. Both SR-XRPD and NS facilities are uncommon and accessing them can be expensive and highly competitive. *In situ* TEM is a much cheaper and more widely available technique suited to follow phase transformations and kinetics.<sup>69–71</sup> Real-time observations during dehydrogenation can be readily performed in the high vacuum environment of the instrument; however, studying hydrogenation (which requires a high-pressure hydrogen atmosphere) is challenging. The reactant and hydrogen must be sealed within a tiny space of a gas cell equipped with electron-transparent windows, allowing a gas layer only a few micrometres thick and separated from the other parts of the microscope. An advantage of the sealed-gas-cell approach is that normal TEM instruments can be modified to run *in situ* hydrogen absorption experiments by modifying the sample holder.<sup>71</sup>

The hydrogen release from binary hydrides is a one-step chemical reaction, but it is multi-step for tetrahydroborates, tetrahydroaluminates, and RHCs involving the formation and decomposition of alkali and earth alkali hydrides in the last step. Fig. 3 shows a simplified decomposition scheme for hydrogen release from these compounds and a more complex scheme for  $\text{Mg}(\text{BH}_4)_2$ <sup>72</sup> to illustrate the complexity of the problem. Phase separation of metals or metals and boron is an issue for reversibility, and the formation of alloys or borides is favourable for the overall thermodynamics of the system (see Fig. 2a). In addition, passivation of metal surfaces during hydrogenation influences kinetics negatively. The diffusion of hydrogen in LiH and  $\text{MgH}_2$  was found to be much slower than in respective metals (there is a three–five order of magnitude difference in diffusion coefficients);<sup>73–75</sup> therefore the hydride layer passivates the surface. As a result, for example, only partial hydriding was observed on magnesium particles larger than 50  $\mu\text{m}$  due to fast hydride formation.<sup>75</sup> Downsizing metals and alloys has a positive effect in solving this issue and improves kinetics as mentioned above. Since the hydrogen absorption/desorption leads to nanocrystalline solids, due to volume expansion and contraction,<sup>45</sup> downsizing is a natural phenomenon after one hydrogen absorption/desorption cycle. Nanosizing and activation by removing the passivating oxide layer is therefore essential before the first hydrogen absorption step. General strategies to activate metal surfaces, in addition to nanosizing, are thermal annealing and surface functionalization and doping. Thermal annealing creates cracks on the passivating oxide film and surface metal vacancies, thereby exposing the metal to hydrogen and reducing the energy barrier of hydrogen dissociation, respectively.<sup>76</sup> The most widely



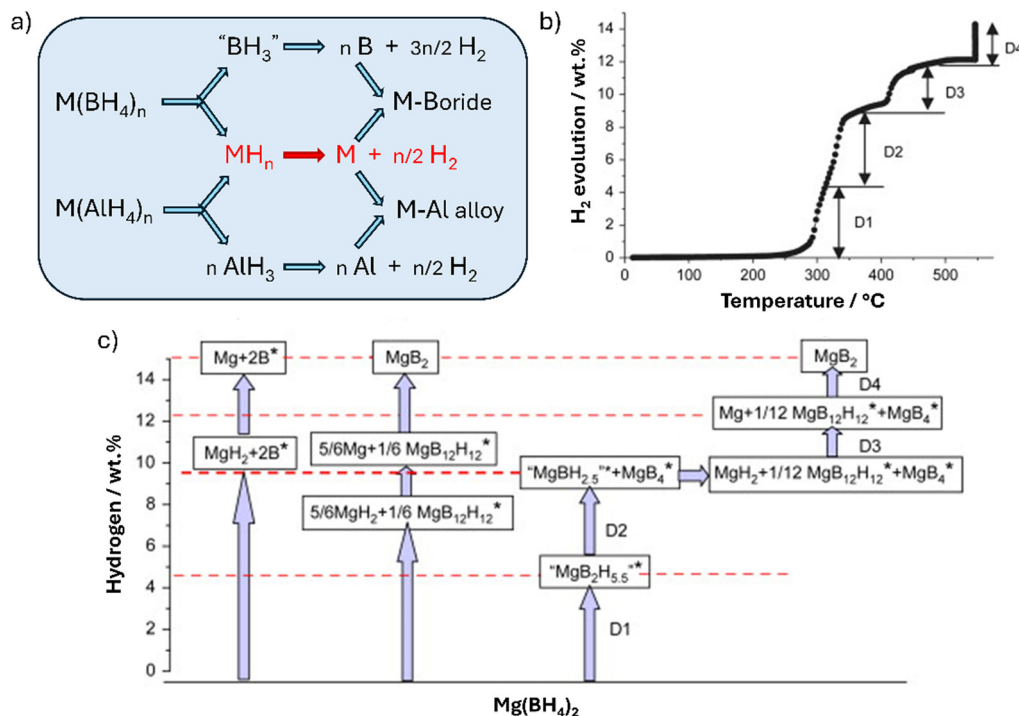


Fig. 3 (a) Simplified decomposition scheme for metal hydrides, tetrahydroborates, and tetrahydroaluminates, (b) volumetric temperature programmed desorption curve of  $Mg(BH_4)_2$  and (c) decomposition pathways of  $Mg(BH_4)_2$  (observed hydrogen evolution steps, see panel (b), marked by dashed lines; amorphous phases denoted by asterisks). Reproduced from ref. 72 with permission from Elsevier Ltd, copyright 2008.

used method for surface modification and functionalization to create more active sites for molecular hydrogen dissociation and hydrogen atom diffusion on the material surface is currently ball milling with additives and/or catalysts. In general, ball milling introduces mechanical stress and modifies the structure, additives open diffusion channels and catalysts facilitate hydrogen dissociation.<sup>77–79</sup>

## 2.2. Tuning the hydrogen storage in lithium, magnesium, and aluminium

Li, Mg, and Al have high hydrogen storage capacities (Table 1, Be is not considered and the capacities of Na, K, and Ca are below the DOE target); however, their practical application faces different challenges. LiH is extremely stable, and the formation enthalpy is  $-181.2 \text{ kJ mol}^{-1} H_2$  ( $-90.6 \text{ kJ mol}^{-1} LiH$ , Table 3); therefore the dehydrogenation of LiH requires very high temperatures (the main desorption peak is observed at 671  $^{\circ}C$ ).<sup>73</sup> In addition, there is an activation energy of  $52.8 \text{ kJ mol}^{-1}$  for the

reaction of  $H_2$  with molten lithium.<sup>80</sup> Consequently, lithium reacts with hydrogen at high temperatures or pressures (at temperatures above 700  $^{\circ}C$  under ambient pressure or at 500 bar pressure at room temperature).<sup>73,81,82</sup> LiH therefore cannot be considered as a practical hydrogen storage material as it is economically unviable for cyclic energy storage. Destabilizing the LiH phase and catalysing the hydrogenation and dehydrogenation reactions would be essential to reach milder reaction conditions. To underpin the idea, it is important to note that Wang *et al.* synthesized LiH nanoparticles with a Ni shell at the surface (composition 85.5 wt% Li, 14.0 wt% Ni and 0.5 wt% Ti, corresponding to an overall hydrogen capacity of 10.8 wt%  $H_2$ ) and achieved full hydrogen release/uptake in less than 50 min at 350  $^{\circ}C$ .<sup>73</sup> Extensive cycling, however, could not be achieved at this temperature due to the formation of large particles behaving like bulk LiH and thus not cycling hydrogen at 350  $^{\circ}C$ ; the reversible storage capacity of LiH/nano-Ni remained limited to 2 wt% instead of the potential 10.8 wt%  $H_2$ . The experiment, however, demonstrated the possibility of tuning the Li/LiH

Table 3 Comparison of thermodynamic and kinetic properties of  $AlH_3$ , LiH and  $MgH_2$

| Hydride | $\Delta_f H^a$ (s) ( $\text{kJ mol}^{-1}$ ) | $\Delta_f S^b$ (s) ( $\text{J mol}^{-1} \text{K}^{-1}$ ) | $\Delta_f G^c$ ( $\text{kJ mol}^{-1}$ ) | $E_a$ (des.) <sup>d</sup> ( $\text{kJ mol}^{-1} H_2$ ) | Cycling properties <sup>e</sup> |
|---------|---|--|---|--|---------------------------------|
| $AlH_3$ | -9.9  | -194.3   | 48.0                                    | 102.2  | n.a.                            |
| LiH     | -90.6                                       | -74.1  | -68.5                                   | n.a.   | n.a.                            |
| $MgH_2$ | -76.2                                       | -132.3   | -36.7                                   | 160  | 515 (ca. 60%)                   |

<sup>a</sup> Enthalpy of formation from elements at 25  $^{\circ}C$  from ref. 9 and 86. <sup>b</sup> Entropy change of the hydride formation reaction at 25  $^{\circ}C$ , calculated using  $S^{\circ}$  (298 K) values from ref. 9. <sup>c</sup> At 25  $^{\circ}C$ . <sup>d</sup> Overall activation energy of hydrogen release from ref. 87 and 88. <sup>e</sup> Number of stable cycles and capacity retention (in parenthesis) from ref. 89; n.a. = not available.



system for hydrogen storage. Thermodynamic tuning of the Li/LiH system was reported earlier,<sup>83–85</sup> but reversible hydrogen cycling at the level of DOE targets could not be achieved. Alloying Li with porous silicon nanowires (molar ratio: 4.4:1), for example, resulted in a reduced hydrogen absorption enthalpy of  $-118 \text{ kJ mol}^{-1} \text{ H}_2$  ( $-59 \text{ kJ mol}^{-1} \text{ LiH}$ ) and the alloy could reach a maximum observed  $\text{H}_2$  absorption capacity of 3.95 wt% at 400 °C and 40 bar.<sup>83</sup> Hydrogen storage properties of LiH were demonstrated to be size dependent; LiH nanoconfined in high surface area graphite could release 1.9 wt% hydrogen with a peak at 340 °C and could reversibly absorb 1 wt% hydrogen at 300 °C and 60 bar hydrogen pressure.<sup>81</sup>

$\text{AlH}_3$ , in contrast to LiH, is metastable at room temperature; although the formation enthalpy is slightly negative ( $-9.9 \text{ kJ mol}^{-1}$  for  $\alpha\text{-AlH}_3$ ), the Gibbs free energy ( $\Delta G$ ) is positive ( $+48 \text{ kJ mol}^{-1}$  at 25 °C) (Table 3).  $\text{AlH}_3$  fully decomposes in the 100–200 °C temperature region, and the activation energy of decomposition can be decreased by using alkali hydrides and transition metal compounds.<sup>90–92</sup> The hydrogenation of aluminium, however, requires extremely high pressures (above 25 000 bar);<sup>90,91,93</sup> therefore  $\text{AlH}_3$  can be considered only as a one-way hydrogen storage material and cannot be regenerated on-board a vehicle.<sup>90,93</sup> The findings from recent research to bring the  $\text{AlH}_3$  decomposition temperature below 100 °C by doping catalytic amounts of various metal compounds into the  $\text{AlH}_3$  matrix through ball milling are summarized in Table 4. Substantial improvement in reaction kinetics was observed compared to pristine  $\text{AlH}_3$ , promoted by metal hydrides, metals, and solid solutions, formed *in situ* or by the accordion structure of MXene additives (Table 4). The catalytic effect of these materials is based on lattice distortion,<sup>92</sup> destruction of the aluminium oxide layer by  $\text{Ti}_3\text{C}_2$ ,<sup>96</sup> enhanced electron transfer and hydrogen diffusion by *in situ* formed transition metals or metal compound species,<sup>94,95,97,98</sup> and/or destabilization of  $\text{AlH}_3$  through increased Al–H bond length.<sup>98–100</sup> As an example, the multivalent conversion of  $\text{TiO}_2$  and  $\text{Pr}_6\text{O}_{11}$  promoted the electron transfer of  $\text{H}^-$  in  $\text{AlH}_3$ , and the newly generated  $\text{PrH}_{2.37}$  hydrogen diffusion pathway promoted the release of hydrogen (Fig. 4a). It seems that the DOE system targets considering storage capacity and hydrogen release temperature can be met with catalysed  $\text{AlH}_3$  decomposition, which makes  $\text{AlH}_3$  a

promising one-way hydrogen source medium for mobile applications. Cheap production or regeneration of the hydride, however, is not solved yet.

Considering the extreme stability of LiH and the thermodynamic instability of  $\text{AlH}_3$ , the Mg/ $\text{MgH}_2$  system seems to be the golden middle road for reversible hydrogen storage. Hydrogen absorption in Mg and especially desorption from  $\text{MgH}_2$ , however, require high temperatures. Considering the van't Hoff equation (Fig. 2b), the enthalpy of  $\text{MgH}_2$  formation of  $-74 \text{ kJ mol}^{-1} \text{ H}_2$ <sup>101</sup> and an entropy change of  $130 \text{ J K}^{-1} \text{ mol}^{-1} \text{ H}_2$ , the temperature required to reach 1 bar hydrogen equilibrium pressure at  $\text{MgH}_2$  desorption is about 300 °C. If  $\text{MgH}_2$  could be destabilized to have a desorption enthalpy below  $48.5 \text{ kJ mol}^{-1}$  ( $T\Delta S$  at 100 °C), hydrogen release would be thermodynamically favoured at 100 °C. Improving both thermodynamics and kinetics of the Mg/ $\text{MgH}_2$  system is therefore essential for reversible hydrogen storage; however, there is a limit of 15 wt% for the additive concerning the ultimate DOE target of 6.5 wt% and the theoretical  $\text{MgH}_2$  storage capacity of 7.66 wt%. Alloying Mg with Al was found to improve both kinetics and thermodynamics of the system;<sup>102,103</sup> however, Al served only as a diluent due to the instability of  $\text{AlH}_3$  (see above). Despite improvements, the kinetics of hydrogen absorption in the  $\text{Mg}_{90}\text{Al}_{10}$  alloy (11 wt% Al) was still slow, namely 2.7 wt% and 4.6 wt% hydrogen capacity could be achieved at 260 °C and 380 °C, respectively, at 30 bar hydrogen pressure within 2 hours.<sup>102</sup> The Mg–Zn alloy containing 17 wt% Zn performed better and could absorb 5.0 wt% hydrogen in 20 min at 300 °C and had a hydrogen storage capacity of 6.1 wt% at this temperature (but below the DOE target); the enhanced hydrogen storage properties for this system were attributed to improved kinetics (low hydrogen absorption activation energy of  $56.3 \text{ kJ mol}^{-1}$ ) rather than the change in enthalpy.<sup>104</sup> Mg has also been alloyed with Li; however, the hydrogenation of Mg–Li alloys always leads to a mixture of  $\text{MgH}_2$  and LiH, from which  $\text{MgH}_2$  could be thermally decomposed up to 450 °C, but LiH remained stable.<sup>105</sup> Considering this, Mg–Li alloys are not good candidates for reversible hydrogen storage because their reversibility and stability are very similar to those of pure Mg, but with lower storage capacity.

Early long term hydrogen cycling experiments on Mg in 1984,<sup>89</sup> involving 515 cycles and using high purity hydrogen

Table 4 Effect of catalysts on the hydrogen release properties of  $\text{AlH}_3$

| Catalyst precursor                               | Active form <sup>a</sup> | Capacity <sup>b</sup> (wt%) | Decomp. temp. <sup>c</sup> onset/peak (°C) | Isothermal $\text{H}_2$ release wt%/°C/min | $E_a$ (des.) (kJ mol <sup>-1</sup> $\text{H}_2$ ) | Ref. |
|--|--------------------------|-----------------------------|--|--|---|------|
| $\text{TiB}_2$ (2.5 wt%)                         | Al–Ti–B ss               | 8.7                         | 78/n.a.                                    | 5.3/80/200<br>7.3/110/60                   | 86  | 92   |
| $\text{NbF}_5$ (1 mol%)                          | Nb, $\text{AlF}_3$       | 6                           | 60/122                                     |  | 96  | 94   |
| $\text{LaNi}_5$ (10 wt%)                         | Ni                       | 8.6                         | 86/n.a.                                    | 6.3/100/60<br>7.7/120/30                   | 98  | 95   |
| $\text{Ti}_3\text{C}_2$ (4 wt%)                  | $\text{Ti}_3\text{C}_2$  | 8.1                         | 61/n.a.                                    | 6.9/100/20                                 | 40  | 96   |
| $\text{CeO}_2$ (1 mol%)                          | $\text{CeH}_{2+x}$       | 7.8                         | 114/n.a.                                   | 6.5/100/100                                | 69  | 97   |
| $\text{TiO}_2\text{-Pr}_6\text{O}_{11}$ (1 mol%) | $\text{PrH}_{2.37}$      | 8.3                         | 43/119                                     | 5.9/100/60                                 | 56  | 98   |
| Bi@C (5 wt%)                                     | Bi                       | 8.0                         | 80/n.a.                                    | 5.4/120/40                                 | 87  | 99   |
| Fe@C (3 wt%)                                     | Fe@C                     | 8.5                         | 94/n.a.                                    | 6.2/120/40                                 | 78  | 100  |

<sup>a</sup> Catalytically active component formed during ball milling of precursors; ss = solid solution. <sup>b</sup> Experimentally determined maximum storage capacity. <sup>c</sup> n.a. = not available.



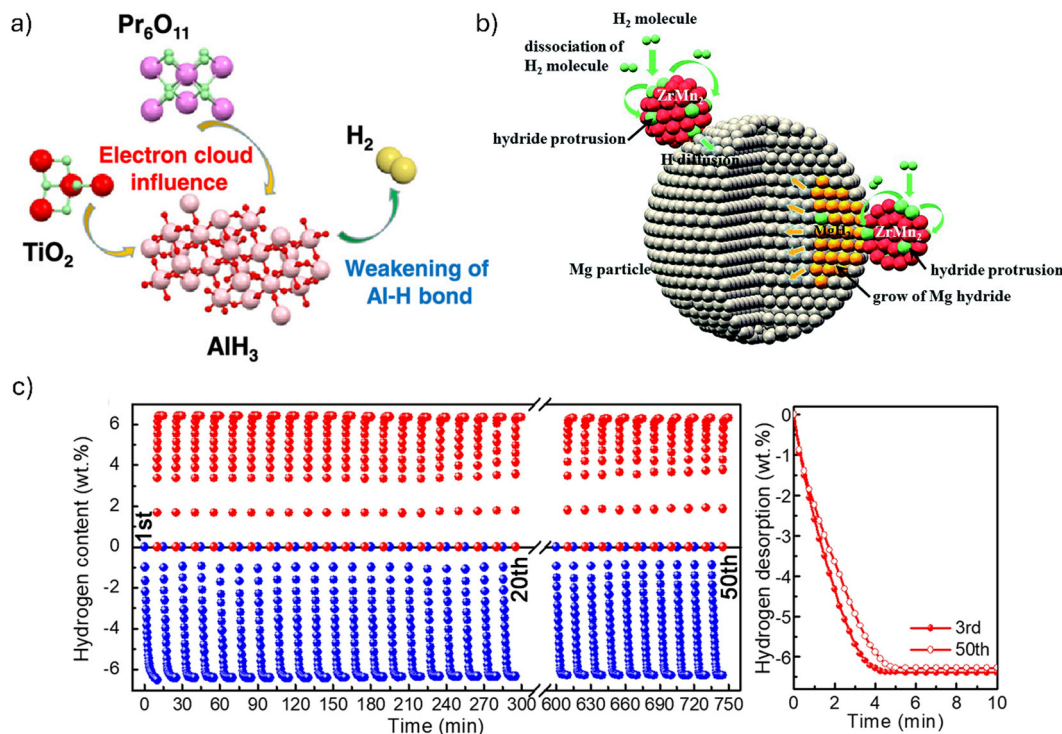


Fig. 4 (a) Mechanism for the catalytic effect of  $\text{TiO}_2$  and  $\text{Pr}_6\text{O}_{11}$  on  $\text{AlH}_3$ . Reproduced from ref. 98 with permission from the American Chemical Society, copyright 2021, (b) mechanism for the hydrogenation of Mg catalysed by  $\text{ZrMn}_2$  nanoparticles. Reproduced from ref. 118 with permission from the Royal Society of Chemistry, copyright 2019, and (c) dehydrogenation/hydrogenation cyclic curves of  $\text{MgH}_2$  with 10 wt%  $\text{TiO}_2$ - $\text{ZrO}_2$ - $\text{V}_2\text{O}_5$  catalyst at 300 °C. Reproduced from ref. 127 with permission from Elsevier Ltd, copyright 2024.

(99.9997%), an operating temperature of 390 °C, and 30 min charging and discharging time at 32 bar  $\text{H}_2$  pressure and vacuum, respectively, highlighted the potential of reversible hydrogen storage in Mg and challenges as well, namely the high operating temperature and pressure, decreasing storage capacity by cycle numbers and the sensitivity of magnesium to oxygen and nitrogen impurities in repeated experiments.<sup>106</sup> The high activity of freshly prepared pure magnesium to oxygen, water and nitrogen was pointed out recently.<sup>107,108</sup> To bring operating conditions closer to ambient conditions and improve hydrogen cycling properties, a very wide range of metal compounds have been screened during the last few decades to find effective catalysts to improve kinetic and cycling properties for magnesium by reducing activation energies;<sup>74,101,109–115</sup> these included transition and rare earth metals, alloys, oxides, halides, carbides, carbonitrides, nitrides, sulphides, hydrides, carbon materials, MXenes, and their mixtures. The catalytic activity of these compounds was based on various mechanisms,<sup>114–144</sup> namely absorbing and delivering hydrogen to Mg thereby acting as a “hydrogen pump”,<sup>114,116–118,123,129,130,133,135,137,139,142,144</sup> providing channels for fast hydrogen diffusion,<sup>114,115,121,125,128,130,131,137,139,142</sup> providing nucleation sites,<sup>115,119,121,125,135</sup> providing abundant oxygen vacancies in oxides,<sup>116,127,132</sup> and weakening the Mg–H and/or H–H bond strength.<sup>114,120,123,124,136,138,141,143</sup> The addition of carbon nanotubes (CNTs) or carbon was found to be advantageous for preventing the aggregation of  $\text{Mg}/\text{MgH}_2$  particles, thereby preserving stable cycle properties,<sup>122,130,142,143</sup> as well

as aiding hydrogen diffusion and heat transfer.<sup>141</sup> The catalytic mechanism can be structured into three groups: (1) kinetic facilitation of dehydrogenation/hydrogenation processes (e.g.,  $\text{LiCoO}_2$ ,<sup>114</sup>  $\text{TiO}_{2-x}$ ,<sup>115</sup>  $\text{V}_2\text{O}_5$ ,<sup>116</sup>  $\text{NiV}_2\text{O}_6$ ,<sup>117</sup>  $\text{ZrMn}_2$ ,<sup>118</sup>  $\text{TiFe}$ ,<sup>122</sup>  $\text{Ni}_3\text{ZnC}_{0.7}$ ,<sup>123</sup>  $\text{Nb}_2\text{CTx}$  MXene,<sup>124</sup>  $\text{TiO}_2@\text{MnCo}_2\text{O}_{4.5}$ ,<sup>125</sup>  $\text{TiMn}_2$ ,<sup>126</sup>  $\text{TiO}_2$ - $\text{ZrO}_2$ - $\text{V}_2\text{O}_5$ ,<sup>127</sup>  $\text{Ti}_2\text{VC}_2$  MXene,<sup>128</sup> shell-like  $\text{Ni}/\text{Mo}_2\text{N}$ ,<sup>129</sup>  $\text{Ni}_3\text{Fe}/\text{Ni}/\text{NiFe}_2\text{O}_4@\text{C}$ ,<sup>130</sup>  $\text{Nb}_2\text{O}_5$ - $\text{C}/\text{Ti}_3\text{C}_2\text{Tx}$  MXene,<sup>131</sup>  $\text{MoO}_{3-x}$ ,<sup>132</sup> MXene  $\text{Ti}_3\text{C}_2@\text{NiO}$ ,<sup>133</sup>  $\text{NiSe}_2$ ,<sup>135</sup>  $\text{Ni}/\text{TiO}_2$ ,<sup>136</sup>  $\text{Ce}_{0.6}\text{Zr}_{0.4}\text{O}_2$ ,<sup>137</sup>  $\text{Co}_3\text{V}_2\text{O}_8$ ,<sup>138</sup>  $\text{NaNbO}_3$ ,<sup>139</sup>  $\text{Al}_3\text{V}$ ,<sup>140</sup>  $\text{Ti}_{0.9}\text{Zr}_{0.1}\text{Mn}_{1.5}\text{V}_{0.3}$ ,<sup>141</sup>  $\text{NiS}@\text{C}$ ,<sup>142</sup>  $\text{Ni}/\text{Mo}_2\text{C}@\text{C}$ ,<sup>143</sup>  $\text{Ni}_3\text{Mn}$ <sup>144</sup>), (2) structural stabilization of nanoparticles (e.g.,  $\text{V}_2\text{O}_5$ ,<sup>116</sup>  $\text{CoFeB}/\text{CNT}$ ,<sup>121</sup>  $\text{CNT}$ ,<sup>122</sup> carbon<sup>123,142,143</sup>), and (3) thermodynamic tuning (e.g.,  $\text{TiH}_2$ <sup>119</sup>). Most of the materials in catalyst groups 1 and 2 did little to reduce the thermodynamic stability of  $\text{MgH}_2$ . In general, transition metal oxides acted as precursors for *in situ* formation of catalytically active species (see Table 5).

Each step of the multistep hydrogenation and dehydrogenation processes must be addressed for effective catalysis, including bond dissociation, hydrogen transfer, bond formation, phase transformation, and heat transfer. In addition, uniform distribution and prevention of phase separation of catalysts and controlling the surface area of  $\text{MgH}_2/\text{Mg}$  particles by blocking large particle growth and aggregation are also of key importance. *In situ* formed hydride/metal or hydride/alloy couples that more easily release and accept hydrogen than  $\text{MgH}_2/\text{Mg}$  in the material matrix can serve as “hydrogen pumps” by removing/delivering hydrogen to  $\text{MgH}_2/\text{Mg}$ ; examples are  $\text{Mg}_2\text{Co}/\text{Mg}_2\text{CoH}_5$ ,<sup>114</sup>





Table 5 Effect of catalysts on the hydrogen absorption and desorption kinetics of Mg/MgH<sub>2</sub><sup>a</sup>

| Catalyst (active form)  | Isothermal absorption |     |     | Non-isoth. des. onset/peak |          |     | Isothermal desorption |       |     | Cycles/capacity retention |      |      | E <sub>a</sub> (abs/des)<br>kJ mol <sup>-1</sup> H <sub>2</sub> | Ref.      |     |
|---|-----------------------|-----|-----|----------------------------|----------|-----|-----------------------|-------|-----|---------------------------|------|------|---|-----------|-----|
|   | wt%                   | °C  | bar | min                        | °C/°C    | wt% | °C                    | bar   | min | wt%                       | °C   | No.  |   |           | %   |
| (no catalyst) <sup>b</sup>  | 1.3                   | 210 | 32  | 10                         | 310/n.a. | 1.1 | 325                   | 0.003 | 10  | n.a.                      | n.a. | n.a. | n.a.  | 81/156    | 114 |
| LiCoO <sub>2</sub> (7 wt%)  | 6.1                   | 270 | 32  | 10                         | 180/n.a. | 7.1 | 375                   | 0.003 | 10  | n.a.                      | n.a. | n.a. | n.a.  | 45/49     | 114 |
| (Mg <sub>2</sub> Co-Mg <sub>2</sub> CoH <sub>5</sub> )  | 2.2                   | 125 | 32  | 10                         | 180/n.a. | 5.5 | 250                   | 0.003 | 60  | 6.2                       | 300  | 20   | 94  |           |     |
|   | 3.8                   | 150 | 32  | 10                         |          | 6.6 | 325                   | 0.003 | 10  |                           |      |      |   |           |     |
|   | 6                     | 200 | 32  | 10                         |          |     |                       |       |     |                           |      |      |   |           |     |
| 5% K-TiO <sub>2-x</sub>   | 4                     | RT  | 80  | 6                          | 194/247  | 6.7 | 300                   | 0.001 | 10  | 6.5                       | 300  | 30   | 100   | n.a./69   | 115 |
| (K <sub>2</sub> Ti <sub>2</sub> O <sub>3</sub> )  | 6                     | RT  | 80  | 180                        |          |     |                       |       |     |                           |      |      |   |           |     |
|   | 6.7                   | 200 | 30  | 60                         |          |     |                       |       |     |                           |      |      |   |           |     |
| 10% H-V <sub>2</sub> O <sub>5</sub>   | 2.4                   | 30  | 30  | 60                         | 185/n.a. | 4.4 | 225                   | 0.1   | 10  | 5.7                       | 275  | 100  | 99  | 43/85     | 116 |
| (VH <sub>2</sub> , V)   | 4.1                   | 100 | 30  | 30                         |          | 6   | 275                   | 0.1   | 5   |                           |      |      |   |           |     |
| 10% NiV <sub>2</sub> O <sub>6</sub>   | 2.2                   | 75  | 30  | 50                         | n.a.     | 4.5 | 250                   | 0.01  | 75  | 6.1                       | 325  | 50   | 90  | 25/93     | 117 |
| (Mg <sub>2</sub> Ni, V <sub>2</sub> O <sub>5</sub> )  | 5.6                   | 150 | 30  | 50                         |          | 5.2 | 300                   | 0.01  | 10  |                           |      |      |   |           |     |
| 10% ZrMn <sub>2</sub>   | 4.3                   | 50  | 30  | 40                         | 182/251  | 6.7 | 300                   | —     | 5   | 6.5                       | 275  | 10   | 85  | 22/82     | 118 |
|   | 5.3                   | 100 | 30  | 10                         |          |     |                       |       |     |                           |      |      |   |           |     |
| 10% TiH <sub>2</sub>  | 4                     | RT  | 20  | 240                        | 180/n.a. | 4   | 240                   | 0.001 | 20  | 6                         | 300  | 80   | 100   | n.a./58   | 119 |
|   | 5                     | 240 | 20  | 1                          |          |     |                       |       |     |                           |      |      |   |           |     |
| 5% Fe NS  | 6                     | 200 | 32  | 10                         | 182/223  | 5.4 | 300                   | 0.03  | 10  | 6                         | 300  | 50   | 83  | n.a./41   | 120 |
| 10% CoFeB/CNT (Co <sub>3</sub> MgC, Fe, CoFe)   | 6.2                   | 150 | 50  | 10                         | 177/n.a. | 6.5 | 300                   | vac.  | 30  | 6.4                       | 300  | 20   | 99  | n.a./83.2 | 121 |
| TiFe + CNT (10 + 5 wt%)   | 4.5                   | 125 | 30  | 60                         | 210/n.a. | 6.1 | 275                   | 0.03  | 30  | 6.2                       | 300  | 10   | 100   | 61/n.a.   | 122 |
|   |                       |     |     |                            |          | 6.2 | 300                   | 0.03  | 14  |                           |      |      |   |           |     |
| Ni <sub>3</sub> ZnCo <sub>7</sub> @C (2.5 wt%) (Mg <sub>2</sub> Ni, MgZn <sub>2</sub> )               | 5.2                   | 150 | 50  | 3                          | 312/360  | 5.7 | 400                   | 0.001 | 5   | 4.5                       | 400  | 20   | 95  | 42/101    | 123 |
| Nb <sub>2</sub> CT <sub>x</sub> -5Na (5 wt%)  | 4                     | 100 | 30  | 1                          | n.a.     | 5.6 | 250                   | 0.01  | 12  | 6.2                       | 300  | 40   | 90  | n.a./70   | 124 |
|   | 5.5                   | 125 | 30  | 1                          |          | 6.4 | 300                   | 0.01  | 3   |                           |      |      |   |           |     |
| TiO <sub>2</sub> @MnCo <sub>2</sub> O <sub>4.5</sub> (6 wt%)  | 2                     | 30  | 30  | 30                         | n.a./290 | 5   | 225                   | 0.01  | 120 | 6.2                       | 325  | 30   | 79  | n.a./76   | 125 |
|   | 5.1                   | 150 | 30  | 3                          |          | 6.4 | 300                   | 0.01  | 30  |                           |      |      |   |           |     |
| TiMn <sub>2</sub> (10 wt%)  | 5.1                   | 225 | 10  | 2                          | n.a.     | 5.1 | 225                   | 0.2   | 8   | 5.8                       | 225  | 414  | 100   | 19/83     | 126 |
| TiO <sub>2</sub> -ZrO <sub>2</sub> -V <sub>2</sub> O <sub>5</sub> (10 wt%)                            | 5.1                   | 50  | 40  | 30                         | 220/n.a. | 6.5 | 300                   | 0.001 | 5   | 6.4                       | 300  | 50   | 98  | n.a./66   | 127 |
| Ti <sub>3</sub> VC <sub>2</sub> (10 wt%)  | 3.2                   | 25  | 60  | 60                         | 170/n.a. | 4.5 | 225                   | 0.1   | 60  | 6.2                       | 325  | 100  | 98  | n.a./71   | 128 |
|   | 5.5                   | 150 | 60  | 10                         |          | 6.2 | 300                   | 0.1   | 5   |                           |      |      |   |           |     |
| Ni/Mo <sub>2</sub> N (6 wt%)  | 5.1                   | 125 | 20  | 10                         | 186/n.a. | 5.9 | 265                   | —     | 30  | 6.7                       | 330  | 10   | 98  | n.a./76   | 129 |
| (Mg <sub>2</sub> Ni)  | 5.5                   | 150 | 20  | 15                         |          | 6.8 | 325                   | —     | 5   |                           |      |      |   |           |     |
| Ni <sub>3</sub> Fe/Ni/NiFe <sub>2</sub> O <sub>4</sub> @C (10 wt%)                                    | 4.2                   | 100 | 30  | 10                         | n.a./290 | 3.6 | 250                   | 0.2   | 60  | 6.4                       | 300  | 10   | 100   | n.a./91   | 130 |
|   | 5.8                   | 150 | 30  | 1                          |          | 5.8 | 325                   | 0.2   | 5   |                           |      |      |   |           |     |
| Nb <sub>2</sub> O <sub>5</sub> -C/Ti <sub>3</sub> C <sub>2</sub> (10 wt%)                             | 5.5                   | 100 | 40  | 15                         | n.a.     | 5.8 | 300                   | 0.001 | 3   | 6.3                       | 300  | 50   | 99  | n.a./63   | 131 |
| MoO <sub>3-x</sub> (10 wt%)   | 4.6                   | 175 | 30  | 8                          | 200/n.a. | 5.9 | 300                   | 0.05  | 8   | 6.1                       | 300  | 50   | 99  | n.a./71   | 132 |
| Ti <sub>3</sub> C <sub>2</sub> @NiO (9 wt%) (Mg <sub>2</sub> Ni, Ti)                                  | 4                     | 100 | 30  | 10                         | 184/n.a. | 6.7 | 300                   | 0.01  | 10  | 6.7                       | 300  | 20   | 96  | n.a./53   | 133 |
|   | 5.2                   | 150 | 30  | 10                         |          |     |                       |       |     |                           |      |      |   |           |     |
| Cr <sub>1</sub> Mn <sub>1</sub> Fe <sub>1</sub> Co <sub>1</sub> Ni-oxide (10 wt%)                     | 5.2                   | 75  | 30  | 50                         | 184/n.a. | 6.7 | 250                   | n.a.  | 12  | 6.5                       | 250  | 50   | 98  | 17/55     | 134 |
| NiSe <sub>2</sub> (5 wt%) (MgSe, Mg <sub>2</sub> NiH <sub>4</sub> )                                   | 5.2                   | 100 | 30  | 80                         | n.a./319 | 6   | 300                   | 0.2   | 20  | 6.2                       | 360  | 20   | 100   | n.a./71   | 135 |
|   | 5.7                   | 200 | 30  | 4                          |          |     |                       |       |     |                           |      |      |   |           |     |
| Ni/TiO <sub>2</sub> (7 wt%) (Mg <sub>2</sub> Ni)  | 5.4                   | 150 | 25  | 1                          | 181/n.a. | 6   | 250                   | 0.001 | 30  | 5.5                       | 200  | 20   | 95  | n.a./78   | 136 |
|   |                       |     |     |                            |          | 6.3 | 300                   | 0.001 | 5   |                           |      |      |   |           |     |
| Ce <sub>0.6</sub> Zr <sub>0.4</sub> O <sub>2</sub> (7 wt%) (CeH <sub>2.73</sub> /CeO <sub>2-x</sub> ) | 4.4                   | 100 | 50  | 5                          | 201/n.a. | 3.9 | 230                   | 0.001 | 40  | 5.8                       | 270  | 20   | 99  | n.a./69   | 137 |
|   | 6                     | 150 | 50  | 3                          |          | 6.2 | 270                   | 0.001 | 8   |                           |      |      |   |           |     |
| Co <sub>3</sub> V <sub>2</sub> O <sub>8</sub> (6 wt%) (Co, V <sub>2</sub> O <sub>3</sub> )            | 1.3                   | RT  | 30  | 30                         | n.a.     | 3.4 | 225                   | 0.09  | 120 | 6                         | 300  | 30   | 73  | n.a./69   | 138 |
|   | 3.9                   | 100 | 30  | 30                         |          | 5.9 | 300                   | 0.09  | 5   |                           |      |      |   |           |     |
|   | 5.9                   | 300 | 30  | 1                          |          | 6.4 | 325                   | 0.09  | 3   |                           |      |      |   |           |     |
| NaNbO <sub>3</sub> (5 wt%) (NbH <sub>x</sub> , Nb, NaMgH <sub>3</sub> )                               | 3.5                   | 30  | 30  | 90                         | n.a.     | 6.2 | 260                   | 0.01  | 12  | 6.3                       | 300  | 40   | 100   | n.a./85   | 139 |
|   | 4.7                   | 125 | 30  | 5                          |          |     |                       |       |     |                           |      |      |   |           |     |
| Al <sub>3</sub> V (5 wt%)   | 6.3                   | 300 | 50  | 10                         | 291/n.a. | 6.5 | 400                   | 0.001 | 6   | 6                         | 400  | 20   | 97  | n.a./86   | 140 |

Table 5 (continued)

| Catalyst (active form)   | Isothermal absorption |      |     | Non-isoth. des. onset/peak |          |     | Isothermal desorption |       |     | Cycles/capacity retention |     |     | $F_a$ (abs/des)<br>kJ mol <sup>-1</sup> H <sub>2</sub> | Ref.    |     |
|--|-----------------------|------|-----|----------------------------|----------|-----|-----------------------|-------|-----|---------------------------|-----|-----|--|---------|-----|
|  | wt%                   | °C   | bar | min                        | °C/°C    | wt% | °C                    | bar   | min | wt%                       | °C  | No. |  |         | %   |
| Ti <sub>0.9</sub> Zr <sub>0.1</sub> Mn <sub>1.3</sub> V <sub>0.3</sub> /CNT (10 + 1 wt%) | 2.4                   | 25   | 30  | 60                         | 195/n.a. | 6.1 | 300                   | 0.001 | 5   | 6.2                       | 325 | 100 | 97   | n.a./86 | 141 |
| NiS/C (5 wt%) (Mg <sub>2</sub> Ni, MgS)  | 4.8                   | 150  | 30  | 10                         | 235/n.a. | 3.5 | 300                   | 0     | 60  | 6.5                       | 400 | 20  | 97   | 24/67   | 142 |
| Ni/Mo <sub>2</sub> C@C (7.5 wt%) (Mg <sub>2</sub> Ni)                                    | n.a.                  | n.a. | 35  | n.a.                       | 240/318  | 6.4 | 300                   | 0.001 | 20  | 6.5                       | 300 | 20  | 98   | n.a./97 | 143 |
| Ni <sub>3</sub> Mn (9 wt%) (Mg <sub>2</sub> Ni)  | 3.5                   | 75   | 30  | 60                         | 190/n.a. | 4.4 | 235                   | 0.03  | 60  | 6.6                       | 295 | 20  | 94   | 39/87   | 144 |
| CuNi (10 wt%) <sup>c</sup> (Mg <sub>2</sub> Ni/Cu)                                       | 6.1                   | 150  | 30  | 10                         | n.a./245 | 6.6 | 295                   | 0.03  | 5   | 6.1                       | 277 | 15  | 95   | n.a./81 | 146 |

<sup>a</sup> RT = room temperature, NS = nanosheet, CNT = carbon nanotube, n.a. = not available. <sup>b</sup> As-prepared MgH<sub>2</sub>. <sup>c</sup> Solar heating under a light density of 3.5 W cm<sup>-2</sup>.

VH<sub>2</sub>/V,<sup>116</sup> Mg<sub>2</sub>Ni/Mg<sub>2</sub>NiH<sub>4</sub>,<sup>117,123,129,130,133,135,136,142–144</sup> and ZrMn<sub>2</sub>/Zr<sub>4</sub>Mn<sub>8</sub>H<sub>10.99</sub> (Fig. 4b).<sup>118</sup> Another “hydrogen pump” mechanism is found to be the facilitation of electron transfer between Mg<sup>2+</sup> and H<sup>-</sup> by transition metal compounds, which promotes the dissociation and recombination of H<sub>2</sub>, observed *e.g.* for TiFe,<sup>122</sup> and multi-valent transition-metal related species formed during hydrogen cycling from Nb<sub>2</sub>Ctx MXene,<sup>124</sup> TiO<sub>2</sub>@MnCo<sub>2</sub>O<sub>4.5</sub>,<sup>125</sup> Nb<sub>2</sub>O<sub>5</sub>-C/Ti<sub>3</sub>C<sub>2</sub>Tx MXene,<sup>131</sup> Ni/TiO<sub>2</sub>,<sup>136</sup> Ce<sub>0.6</sub>Zr<sub>0.4</sub>O<sub>2</sub>,<sup>137</sup> or NaNbO<sub>3</sub>.<sup>139</sup> In addition, transition metals promote the dissociation of H<sub>2</sub> molecules<sup>121</sup> and rupture of the Mg–H bond by weakening the interaction and elongating the bond length (see *e.g.*, the ZrMn<sub>2</sub>-MgH<sub>2</sub>,<sup>118</sup> Fe–MgH<sub>2</sub>,<sup>120</sup> Co–H<sub>2</sub>,<sup>138</sup> V<sub>2</sub>O<sub>3</sub>-MgH<sub>2</sub>,<sup>138</sup> Ti<sub>0.9</sub>Zr<sub>0.1</sub>Mn<sub>1.5</sub>V<sub>0.3</sub>-MgH<sub>2</sub> interactions<sup>141</sup>). Oxygen vacancies of transition metal oxide catalysts have been found to have a promoting effect on dehydrogenation/rehydrogenation by accelerating electron transfer and creating a “hydrogen pump” (*e.g.* V<sub>2</sub>O<sub>5</sub>)<sup>116</sup> or by enhancing the hydrogen adsorption ability of the oxide (*e.g.* MoO<sub>3-x</sub>).<sup>132</sup> There are multiple effects and processes during hydrogenation and dehydrogenation of magnesium, and to utilise all of these, synergistic use of multiple catalytic phases is required. The *in situ* generated phases can collectively constitute an efficient catalytic system. For example the coexistence of Mg<sub>6</sub>MnO<sub>8</sub>, Mn, Ti<sub>2</sub>O<sub>3</sub>, and CoO phases generated *in situ* from TiO<sub>2</sub>@MnCo<sub>2</sub>O<sub>4.5</sub><sup>125</sup> exhibits abundant diffusion pathways and nucleation sites for hydrogen absorption and desorption reactions.<sup>125</sup> Another example is the Ni<sub>3</sub>Fe/Ni/NiFe<sub>2</sub>O<sub>4</sub>@C catalyst system where the *in situ* formed Mg<sub>2</sub>Ni/Mg<sub>2</sub>NiH<sub>4</sub> acts as a “hydrogen pump”, Fe<sup>0</sup> facilitates electron transfer and creates hydrogen diffusion channels, and carbon effectively prevents particle agglomeration.<sup>130</sup> The catalyst Mg/MgH<sub>2</sub> interfaces play a key role in hydrogen transfer. Catalysts can cause morphological defects and could boost the nucleation by reducing the nucleation energy of Mg/MgH<sub>2</sub> and thereby improve the hydrogen diffusion rate.<sup>115</sup> 2D nanomaterial sheets and layered materials, *e.g.* MXenes, are effective in creating abundant active sites and enabling faster hydrogen boundaries diffusion along the interfaces.<sup>120,128</sup> They are also effective in hindering powder agglomeration.<sup>134</sup>

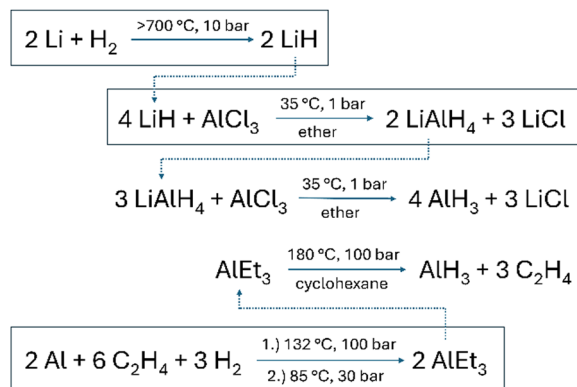
It is becoming clearer that effective hydrogen storage in magnesium requires both addressing each step of the multi-step hydrogenation/dehydrogenation processes by benefiting from the synergistic catalytic effect of multiple phases of multiple compounds and limiting the growth of Mg and MgH<sub>2</sub> particles. Developing composite materials seems to be the best strategy to achieve long term cyclic goals. Significant, 50–70%, reduction of the overall activation energies could be achieved in dehydrogenation/rehydrogenation considering recent efforts; good performers, also tested for cycling, are provided in Table 5. It is now possible to recharge Mg below 100 °C; however, hydrogen release requires much higher temperatures (Table 5). Although the reduction of operation temperatures is a fundamental aim of research efforts, the excellent cycling stability is also crucial for practical applications; therefore, recent research is increasingly focusing on cycling stability (Table 5, Fig. 4c). To date, cycling tests have been conducted at relatively high temperatures between 275 and 400 °C due to slow hydrogen release at lower temperatures. Capacity retention close to 100% could be achieved



for cycles ranging from 10 up to 414 (Table 5), but long-term cyclic stability evaluation as per DOE requirements is yet to be conducted. The high temperature of the hydrogen release of  $\text{MgH}_2$ , however, remains problematic for practical applications; therefore the  $\text{Mg}/\text{MgH}_2$  hydrogen storage system still cannot work in the operational range of PEM fuel cells. Its application is currently limited to high-temperature fuel cells or stationary applications, or the released hydrogen must be cooled for PEM fuel cells. An example for high-temperature  $\text{MgH}_2$ -based storage is the application of the  $0.9\text{MgH}_2\text{-}0.1\text{TiH}_2\text{-}5\text{ wt\% C}$  nanocomposite in a storage tank which could deliver 185 normal litre hydrogen in temperature swing operation involving charging at  $150\text{ }^\circ\text{C}$  and discharging at  $370\text{ }^\circ\text{C}$ .<sup>145</sup>

It is important to note the recent novel concept of solar-driven reversible hydrogen storage for magnesium, which integrates the photothermal localized heat and catalytic action by a single-component phase that simultaneously exhibits photothermal and catalytic effects.<sup>146</sup> Incorporating 10 wt% NiCu into Mg resulted in the formation of  $\text{Mg}_2\text{Ni}(\text{Cu})$  which acted as a  $\text{Mg}_2\text{Ni}(\text{Cu})/\text{Mg}_2\text{Ni}(\text{Cu})\text{H}_4$  hydrogen pump in cycling and also weakened the Mg–H bond. Reversible hydrogen storage was achieved with 6.1 wt% capacity and 95% retention.<sup>146</sup> The photodecomposition and rehydrogenation of the LiH surface under illumination at ambient temperature was also observed recently (dehydrogenated LiH could uptake 0.08 wt% hydrogen at 1 bar hydrogen pressure),<sup>147</sup> highlighting a new path for the development of hydrogen storage methods.

Among Li, Mg, and Al, which exhibit hydrogen storage properties, currently, only magnesium has the potential to become a reversible hydrogen storage material. Although it is still not satisfying all DOE targets, it seems to be on track to meet long-term cycling goals under close to ambient conditions. Strategies that might enable this are expected to use multielement and multiphase systems which can address kinetics of all steps of the multistep hydrogenation and dehydrogenation process and can control phase transfer and growth. A key advantage of magnesium is that it is abundant, non-poisonous, recyclable and a relatively cheap material. Mg is produced on a large scale in the smelting industry (1 million tonnes in 2024)<sup>148</sup> and can be hydrogenated directly in a rotary autoclave at  $300\text{--}400\text{ }^\circ\text{C}$  and 100–150 bar hydrogen pressure, or in THF solvent at  $60\text{--}70\text{ }^\circ\text{C}$  and 80 bar in the presence of catalysts.<sup>149</sup> A major disadvantage is its sensitivity to oxygen and water, with Mg nanopowders reacting violently with air and presenting the hazard of dust explosions.<sup>150</sup> Pure and finely divided  $\text{MgH}_2$  is also pyrophoric.<sup>149</sup> The application of Li as a hydrogen storage material is not practical due to the high temperatures required for hydrogen absorption and release and competing demand for Li for batteries. LiH is produced in the industry by reacting molten lithium with hydrogen at temperatures above  $700\text{ }^\circ\text{C}$ .<sup>149</sup> Although Al is highly abundant and  $\text{AlH}_3$  releases hydrogen upon moderate heating (temperatures below  $100\text{ }^\circ\text{C}$  if catalysed), regeneration of  $\text{AlH}_3$  is not feasible by the direct  $\text{Al} + \text{H}_2$  reaction due to thermodynamic instability.  $\text{AlH}_3$  is currently not produced in industry; the main small scale laboratory production methods are based on the reaction of  $\text{LiAlH}_4$  with  $\text{AlCl}_3$  in a diethylether solvent (Scheme 1).<sup>149,151</sup> The energy intensive



Scheme 1 Synthesis of  $\text{AlH}_3$  and LiH (industrial processes are indicated by the boxes).<sup>149–153</sup>

nature of the desolvation process and conversion of the LiCl by-product to lithium limits the potential of this method for large scale production. An alternative to this synthetic route could be the thermal decomposition of  $\text{Al}(\text{Et})_3$  (triethylaluminium), produced on an industrial scale from Al,  $\text{H}_2$  and ethylene in a two-step process;<sup>152</sup> however, the current synthesis at the laboratory scale is still suffering from low yields (19%).<sup>153</sup> Due to the lack of convenient synthesis/regeneration of  $\text{AlH}_3$ , currently,  $\text{AlH}_3$  cannot compete with other potential one-way storage systems such as ammonia and LOHCs. In addition, the handling of Al and  $\text{AlH}_3$  nanopowders is more problematic compared to that of LOHCs, as these nanopowders present the same dust explosion hazards as finely divided/powdered magnesium.

### 2.3. Alkali and alkali earth metal tetrahydroborates

Tetrahydroborates exhibit higher hydrogen storage capacity than metal hydrides due to the light boron atom constituent but have high decomposition temperatures (above  $400\text{ }^\circ\text{C}$ ), the kinetics of hydrogen desorption are sluggish, and the multi-step decomposition reaction is not or only partially reversible and only at high hydrogen pressures.<sup>72,154–167</sup> In addition, the tetrahydroborate decomposition may generate stable intermediates, such as borate cluster anions, or volatile by-products, like diborane,<sup>72,167</sup> and the evaporation of volatile alkali metals, namely Na and K, is an issue for practical applications. The latter issue might explain the paucity of experimental work on the thermal decomposition of sodium and potassium tetrahydroborates. Alkali and alkali earth tetrahydroborates, therefore, are not suited for reversible hydrogen storage without modifying the thermodynamics and kinetics of hydrogen absorption/desorption and establishing lower operating temperatures and reversibility for these reactions. It is, however, an advantage of tetrahydroborates compared to metal hydrides that they can tolerate larger amounts of additives/catalysts to satisfy DOE targets due to larger hydrogen storage capacities; the amount of additive in an additive +  $\text{LiBH}_4$  mixture can be as high as 75 wt% to satisfy the DOE target of 6.5 wt% hydrogen storage capacity, but it is only 13 wt% for  $\text{KBH}_4$  (see Tables 1 and 2). The possible higher additive load and storage capacity therefore opens the door for storage techniques that are not feasible for the  $\text{Mg}/\text{MgH}_2$  system considering the DOE target,



such as combining (nano)confinement and catalysis or applying only partial dehydrogenation by limiting the temperature and stopping before full decomposition, typically neglecting the final high temperature hydrogen release. An example is  $\text{LiBH}_4$  decomposition due to the formation of thermally stable  $\text{LiH}$  whose hydrogen release proceeds only at very high temperatures ( $\text{LiBH}_4 \rightarrow \text{LiH} + \text{B} + 3/2\text{H}_2$ ).

The role of additives/catalysts is multiple in the tetrahydroborate systems as they should decrease the overall activation energy barrier of decomposition and hydrogen absorption, alter thermodynamics, and prevent the formation of stable intermediates and the separation of elemental boron by establishing an alternative lower energy pathway to metal borides (which are thermodynamically more stable reaction products than elemental boron). Considerable work has been dedicated to date to tailor the hydrogen absorption and desorption properties of tetrahydroborates using transition metal oxides, halides, and carbides, transition, rare earth and main group metals, and carbon-based materials.<sup>46,167–210</sup> Achieving reversible cycling is seemingly the most challenging (Table 6). The formation and accumulation of stable intermediates, for example  $\text{Li}_2\text{B}_{12}\text{H}_{12}$ , loss of nanoconfinement effects due to increasing particle size, and segregation of B and metal hydride phases are possibly the main reasons for the decrease in cyclic hydrogen capacity.<sup>185,186,189</sup> The mechanism of catalytic action of various additives may involve weakening B–H bonds,<sup>181,186,188,191,193</sup> facilitating hydrogen diffusion,<sup>181,187,194,200,201,204–206</sup> inhibiting  $\text{B}_{12}\text{H}_{12}^{2-}$  formation,<sup>185,188,191,192,194,198</sup> suppressing the formation of  $\text{B}_2\text{H}_6$ ,<sup>192,203</sup> enhancing the effect of nanoconfinement,<sup>185,186</sup> providing nucleation sites,<sup>189,204</sup> establishing B reservoirs by boride formation,<sup>197</sup> and limiting particle size growth.<sup>191</sup> Carbonaceous materials, *e.g.* CNTs, can facilitate heat management as they effectively increase the thermal conductivity of the confined system.<sup>187</sup> As a new approach, the light-driven dehydrogenation of  $\text{LiBH}_4$ , without thermal heating, was achieved recently by incorporating  $\text{TiO}_2$  for the photocatalytic effect and  $\text{TiF}_3$  for enhanced dehydrogenation; the  $\text{LiBH}_4$ - $8\text{TiF}_3$ - $2\text{TiO}_2$  composite could release about 3.12 wt% hydrogen in 30 min under a light intensity of  $0.76 \text{ W cm}^{-2}$ .<sup>209</sup>  $\text{LiBH}_4$  nanoconfined in ultralow-content Ni-doped structured mesoporous carbon could release 11.02 wt% hydrogen of  $\text{LiBH}_4$  (not considering the template matrix) in 150 min under  $3.5 \text{ W cm}^{-2}$  light irradiation and maintain a capacity retention of 85% after 5 cycles due to the nanoconfinement effect, trace amounts of Ni, and photogenerated vacancies in the  $\text{LiH}$  product which thermodynamically destabilize B–H bonds.<sup>210</sup> Transition metals and alloys, such as Ti,<sup>201,204,209</sup> Ni,<sup>192,205</sup> and CoNi,<sup>193</sup> and transition metal compounds, such as  $\text{NbB}_2$ ,<sup>186,202</sup>  $\text{LiTiO}_2$  and  $\text{TiB}_2$ ,<sup>187</sup>  $\text{FeB}$  and  $\text{Fe}_2\text{B}$ ,<sup>188,190</sup>  $\text{Ni}_2\text{B}$ ,<sup>191</sup>  $\text{Li}_3\text{BO}_3$  and  $\text{NbH}$ ,<sup>194</sup>  $\text{Co}_2\text{B}/\text{Ni}_2\text{B}$ ,<sup>197</sup>  $\text{V}_x\text{B}_y$  and  $\text{Ni}_x\text{B}_y$ ,<sup>198</sup>  $\text{VH}_{2,01}$ ,<sup>201</sup>  $\text{TiH}_2$ ,<sup>203</sup>  $\text{TiH}_{1,924}$ ,  $\text{TiB}$ , and  $\text{TiB}_2$ ,<sup>204</sup> and  $\text{NbVH}$ ,<sup>206</sup> generated *in situ* from oxide, carbide and halide precursors, as well as additives, such as MXenes ( $\text{Ti}_3\text{C}_2$ ,  $\text{Ti}_2\text{C}$ ,  $\text{Nb}_2\text{C}$ ),<sup>181</sup> were found to destabilize the  $\text{BH}_4^-$  anion by weakening the B–H bond and decreasing thereby hydrogen dissociation energy for hydrogen desorption due to electronic interactions/electron transfer.  $\text{NbVH}$  nanoparticles, for example, operated as

“bidirectional hydrogen pumps” combining both hydrogen spillover and hydrogen diffusion.<sup>206</sup> The bidirectional charge-transfer catalytic mechanisms of  $\text{FeB}$  and  $\text{Fe}_2\text{B}$  were revealed wherein they act as electron acceptors accepting electrons from  $\text{BH}_4^-$  and electron donors donating electrons to boron, which enhances their reactivity for dehydrogenation and hydrogenation, respectively.<sup>188,190</sup> In addition to kinetic facilitation of dehydrogenation/hydrogenation processes, *in situ* formed borides contribute to thermodynamic tuning of the system. An example is the reversible transformation between  $\text{NiB}/\text{CoB}$  and  $\text{Ni}_2\text{B}/\text{Co}_2\text{B}$ , acting as boron reservoirs, in the dehydrogenation and hydrogenation reactions of  $\text{NaBH}_4$ .<sup>197</sup> A problematic side product of tetrahydroborate decomposition is  $\text{B}_2\text{H}_6$ , a poisonous and flammable gas, which results in boron loss and/or in the formation of a stable  $\text{B}_{12}\text{H}_{12}^{2-}$  dodecaborate anion *via* the  $\text{B}_2\text{H}_6 + \text{BH}_4^-$  reaction at elevated temperatures.<sup>192</sup> The accumulation of  $\text{B}_{12}\text{H}_{12}^{2-}$  or boron loss during cycling gradually decreases storage capacity. Strategies to prevent these reactions include lowering the temperature below the temperature required to generate  $\text{B}_2\text{H}_6$  (below  $300 \text{ }^\circ\text{C}$ )<sup>192</sup> or catalytically decomposing  $\text{B}_{12}\text{H}_{12}^{2-}$ . The nanoconfinement effect has also been found to suppress the release of  $\text{B}_2\text{H}_6$  and inhibit  $\text{B}_{12}\text{H}_{12}^{2-}$  formation during the dehydrogenation process.<sup>185,210</sup> Concerning the stable dodecaborate anion, reactive lithium ferrites and catalysis from iron borides were shown to effectively promote the decomposition of  $\text{Li}_2\text{B}_{12}\text{H}_{12}$ .<sup>188</sup> *In situ* formed  $\text{Ni}_x\text{B}$  or the synergistic action of  $\text{Li}_3\text{BO}_3$  and  $\text{NbH}$  were also found to inhibit the formation of  $\text{Li}_2\text{B}_{12}\text{H}_{12}$  during hydrogenation.<sup>194,210</sup> Carbonaceous materials (*e.g.*, graphene, CNTs) and MXenes have multiple roles, as they provide structural support, interfaces for electron conduction and hydrogen diffusion, and also have a catalytic effect on hydrogenation and dehydrogenation processes.<sup>181,201</sup> The decomposition of  $\text{LiBH}_4$ , for example, is believed to preferably occur at the graphene- $\text{LiBH}_4$  interface, than within bulk  $\text{LiBH}_4$ , as an interface reaction.<sup>185</sup> Graphene was also shown to weaken both the Mg–H and B–B bonds of  $\text{MgH}_2$  and  $\text{B}_2\text{H}_6$ , respectively.<sup>200</sup> Nanoconfinement shortens the hydrogen diffusion pathway, and this effect is believed to be responsible for the decrease of activation energy.<sup>185</sup> Table 6 lists recent examples, focusing on those where hydrogen cycling has also been investigated, and highlights challenges for the application of alkali and alkali earth tetrahydroborates in hydrogen storage, namely the high temperature for hydrogen absorption/desorption and poor cycling stability. Obviously, the utilization of the synergistic effects of catalysts, nanoconfinement, improved surface interaction between various phases in the systems, and enhanced thermal transfer has already resulted in marked improvement of hydrogen storage properties. Fig. 5 shows, as an example, the fabrication of a multi-metal catalyst system for enhancing hydrogen release from  $\text{NaBH}_4$  and the energy diagram illustrating altered thermodynamics and kinetics compared to pristine  $\text{NaBH}_4$ . There is a large variability for combining catalyst, confinement, and support; the most promising results, in terms of cycle number and capacity retention, are obtained by the nano-synergy of carbon materials and transition metal compounds, such as nitrogen-doped carbon nanocages/ $\text{NbF}_5$ ,<sup>186</sup> few-layer



Table 6 Effect of catalysts on the hydrogen absorption and desorption kinetics of tetrahydroborates<sup>a</sup>

| Catalyst (active form)   | Isothermal absorption |      |      | Non-isoth. des. |              |            | Isothermal desorption |      |      | Cycles/capacity retention |      |              | $E_a$ (des)<br>kJ mol <sup>-1</sup> H <sub>2</sub> | Ref. |          |     |
|--|-----------------------|------|------|-----------------|--------------|------------|-----------------------|------|------|---------------------------|------|--------------|--|------|----------|-----|
|  | wt%                   | °C   | bar  | min             | °C/°C        | onset/peak | wt%                   | °C   | bar  | min                       | wt%  | °C           |  |      | No.      | %   |
|  |                       |      |      |                 |              |            |                       |      |      |                           |      |              |  |      |          |     |
| LiBH <sub>4</sub>  |                       |      |      |                 |              |            |                       |      |      |                           |      |              |  |      |          |     |
| GMF (30 wt%)   | 5.8                   | 400  | 100  | 55              | n.a./327     |            | 8.0                   | 320  | vac  | 100                       | 8.0  | <sup>b</sup> | 10   | 54   | 107      | 185 |
| NC-NbF <sub>5</sub> (50 wt%) (NbB <sub>2</sub> )   | 6.3                   | 300  | 120  | 96              | 141/311      |            | 5.9                   | 280  | vac  | 159                       | 6.3  | 300          | 20   | 93   | 83       | 186 |
|  |                       |      |      |                 |              |            | 7.6                   | 320  | vac  | 39                        |      |              |  |      |          |     |
| (CNT@C@TiO <sub>2</sub> ) (40%) (LiTiO <sub>2</sub> , TiB <sub>2</sub> )                                   | 6.8                   | 400  | 100  | 300             | 224/318      |            | 7.3                   | 320  | vac  | 60                        | 8.4  | <sup>b</sup> | 20   | 61   | 96       | 187 |
| Fe <sub>3</sub> O <sub>4</sub> (30 wt%) (FeB, Fe <sub>2</sub> B)   | 6.4                   | 450  | 100  | 40              | 183/n.a.     |            | 7.9                   | 375  | vac  | 100                       | 6.4  | <sup>c</sup> | 10   | 70   | 83       | 188 |
|  |                       |      |      |                 |              |            | 8.3                   | 400  | vac  | 50                        |      |              |  |      |          |     |
| FL-GR (30 wt%)   | 7                     | 350  | 100  | 400             | 230/359      |            | 5.5                   | 300  | vac  | 400                       | 7.1  | 350          | 10   | 100  | 116      | 189 |
|  |                       |      |      |                 |              |            | 7.2                   | 350  | vac  | 60                        |      |              |  |      |          |     |
| FeF <sub>2</sub> /FeO <sub>x</sub> @GR (30 wt%) (FeB, Li <sub>3</sub> BO <sub>3</sub> , Fe <sub>2</sub> B) | 9.4                   | 400  | 100  | 150             | 100/375      |            | 7.0                   | 350  | vac  | 80                        | 9.4  | <sup>c</sup> | 10   | 59   | 99       | 190 |
| Ni/C (20 wt%) (Ni <sub>2</sub> B)  | n.a.                  | n.a. | n.a. | n.a.            | 200/340      |            | 12.2                  | 320  | 0.01 | 180                       | 8.9  | 320          | 15   | 72   | 99       | 191 |
| Ni@GR (10 + 20 wt%)  | 9.2                   | 300  | 100  | 200             | 130/285      |            | 7.5                   | 200  | vac  | 600                       | 9.2  | 300          | 100  | 92   | 106      | 192 |
|  |                       |      |      |                 |              |            | 9.2                   | 300  | vac  | 175                       |      |              |  |      |          |     |
| CoNi/C (40 wt%)  | 11.9                  | 370  | 100  | 50              | 130/355      |            | 11.9                  | 350  | vac  | 100                       | 9.4  | <sup>d</sup> | 10   | 82   | 95       | 193 |
| Nb(OEt) <sub>5</sub> (4 mol%) (Li <sub>3</sub> BO <sub>3</sub> , NbH)                                      | 6.3                   | 350  | 50   | 60              | 190/340      |            | 4.5                   | 350  | vac  | 20                        | 7.9  | <sup>e</sup> | 30   | 91   | 127      | 194 |
|  | 7.9                   | 500  | 50   | 20              |              |            | 7.0                   | 350  | vac  | 60                        |      |              |  |      |          |     |
| Ni/GR (20 wt%)   | n.a.                  | n.a. | n.a. | n.a.            | 180/275, 465 |            | 12.8                  | 450  | 1    | 45                        | 15.2 | <sup>f</sup> | 30   | 64   | n.a.     | 195 |
| NbBH <sub>4</sub>  |                       |      |      |                 |              |            |                       |      |      |                           |      |              |  |      |          |     |
| ZrCl <sub>4</sub> (10 wt%)   | n.a.                  | n.a. | n.a. | n.a.            | 350/500      |            | n.a.                  | n.a. | n.a. | n.a.                      | n.a. | n.a.         | n.a.   | n.a. | 162      | 199 |
|  |                       |      |      |                 |              |            |                       |      |      |                           |      |              |  |      |          |     |
| Mg(BH <sub>4</sub> ) <sub>2</sub>  |                       |      |      |                 |              |            |                       |      |      |                           |      |              |  |      |          |     |
| GR (40 wt%)  | n.a.                  | n.a. | n.a. | n.a.            | 154/199      |            | 5.7                   | 175  | n.a. | 80                        | 9.0  | 250          | 6  | 36   | 29       | 200 |
|  |                       |      |      |                 |              |            | 9.0                   | 250  |      | 50                        |      |              |  |      |          |     |
| Ti <sub>2</sub> C (30 wt%) (Ti)  | 10.2                  | 300  | 100  | 480             | 132/281      |            | 10.2                  | 260  | n.a. | 360                       | 10.2 | 260          | 3  | 32   | 42       | 181 |
| VH <sub>2</sub> @Ti <sub>3</sub> C <sub>2</sub> (20 wt%) (VH <sub>2.01</sub> , Ti)                         | 2.7                   | 275  | 90   | 360             | 90/n.a.      |            | 5                     | 275  | n.a. | 60                        | 2.7  | 275          | 4  | 65   | 172      | 201 |
|  |                       |      |      |                 |              |            | 8.2                   | 275  | n.a. | 300                       |      |              |  |      |          |     |
| NaCl + NbF <sub>5</sub> (48 + 10 wt%) (NbB <sub>2</sub> )  | n.a.                  | n.a. | n.a. | n.a.            | 135/n.a.     |            | 5.6                   | 500  | n.a. | 250                       | 5.6  | 500          | 3  | 71   | n.a.     | 202 |
| K <sub>2</sub> TiF <sub>6</sub> (3 mol%) (KBH <sub>4</sub> , TiH <sub>2</sub> )                            | n.a.                  | n.a. | n.a. | n.a.            | 105/n.a.     |            | 6.4                   | 280  | n.a. | 200                       | 6.4  | 280          | 2  | 36   | n.a.     | 203 |
| K <sub>2</sub> NbF <sub>7</sub> (3 mol%) (KBH <sub>4</sub> , TiH <sub>2</sub> )                            | n.a.                  | n.a. | n.a. | n.a.            | 118/n.a.     |            | 6.6                   | 280  | n.a. | 200                       | 6.6  | 280          | 2  | 41   | n.a.     | 203 |
| Ti (TiH <sub>1.024</sub> , TiB, TiB <sub>2</sub> )   | n.a.                  | n.a. | n.a. | n.a.            | n.a.         |            | 7.9                   | 290  | n.a. | 2000                      | 6.2  | 270          | 4  | 48   | 57       | 204 |
| Ni/CNT (5 wt%)   | n.a.                  | n.a. | n.a. | n.a.            | 93/n.a.      |            | 6.7                   | 300  | 4    | 60                        | n.a. | n.a.         | n.a.   | n.a. | 120      | 205 |
| NbVH/Ti <sub>3</sub> C <sub>2</sub> (30 wt%)   | n.a.                  | n.a. | n.a. | n.a.            | 106/n.a.     |            | 9.4                   | 230  | vac  | 1800                      | 6.0  | 250          | 10   | 70   | 104, 125 | 206 |
|  |                       |      |      |                 |              |            | 7.4                   | 270  | vac  | 60                        |      |              |  |      |          |     |
| Ca(BH <sub>4</sub> ) <sub>2</sub>  |                       |      |      |                 |              |            |                       |      |      |                           |      |              |  |      |          |     |
| Ti(OEt) <sub>4</sub> (10 mol%) (TiO <sub>2</sub> )   | 4.7                   | 320  | 90   | 1400            | n.a./318     |            | 4.7                   | 270  | n.a. | 400                       | n.a. | n.a.         | n.a.   | n.a. | 118      | 207 |
| TiCl <sub>3</sub> (24 mol%) (Ti)   | 1.7                   | 300  | 90   | 500             | 200/260      |            | n.a.                  | n.a. | n.a. | n.a.                      | n.a. | n.a.         | n.a.   | n.a. | n.a.     | 208 |

<sup>a</sup> RT = room temperature, GMF = wrinkled graphene microflowers, FL-GR = few-layer graphene, GR = graphene, NS = nanosheet, CNT = carbon nanotube, NC = nitrogen-doped carbon nanocages, vac = vacuum, n.a. = not available. <sup>b</sup> Desorption and absorption at 320 and 400 °C, respectively. <sup>c</sup> Desorption and absorption at 400 and 450 °C, respectively. <sup>d</sup> Desorption and absorption at 350 and 400 °C, respectively. <sup>e</sup> Desorption and absorption at 400 and 500 °C, respectively. <sup>f</sup> Dehydrogenation and rehydrogenation at 550 and 400 °C, respectively.



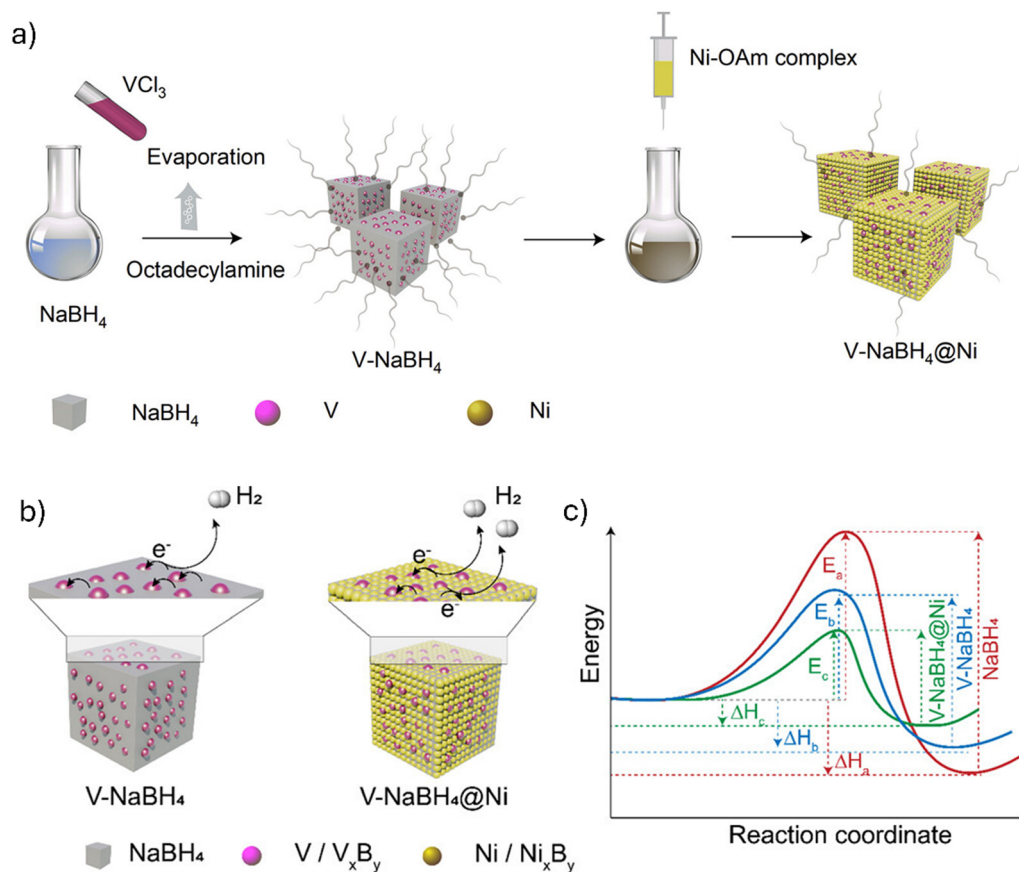


Fig. 5 (a) Illustration of the synthesis of vanadium-doped cube-like NaBH<sub>4</sub> with nickel shells, (b) the hydrogen release via the electron transfer process, and (c) the energy diagram showing altered thermodynamics and kinetics compared to pristine NaBH<sub>4</sub>. Reproduced from ref. 198 with permission from the American Chemical Society, copyright 2023.

graphene,<sup>189</sup> Ni nanocrystal decorated graphene (which has been reported to have the best performance in terms of cycle number),<sup>192</sup> and bimetallic (NiCo) nanoporous carbon nanosheets.<sup>197</sup> Nanocarbon provides a platform for heat and electron transport, structural support, and interface for catalysts and BH<sub>4</sub><sup>-</sup> ions. Transition metals and *in situ* formed transition metal borides catalyse the hydrogen uptake and release.

Currently, in general, tetrahydroborates underperform compared to the Mg/MgH<sub>2</sub> system in hydrogen storage due to factors like higher temperature and hydrogen pressure needed for recharging, slower kinetics (longer charging and discharging time) and poor hydrogen cycling stability (fewer cycles and lower capacity retention) (compare Table 5 with Table 6 and see Fig. 6 for selected data). Further improvements to establish reversible long-term cycling at lower than the current operating temperatures are necessary for practical applications. The advantages of the use of tetrahydroborates, compared to the Mg/MgH<sub>2</sub> system, are the higher hydrogen storage capacity per unit weight, larger additive tolerance concerning DOE targets, tunability through chemical design, and safety. Their stability in air increases as the ionic character of the salt increases, namely increasing stability from Li toward K and from Mg to Ca.<sup>149</sup> KBH<sub>4</sub> is stable in dry air and not hygroscopic. NaBH<sub>4</sub> is stable in dry air and can be stored in an airtight container for a

long time. It absorbs water from moist air and decomposes slowly with the liberation of hydrogen. LiBH<sub>4</sub> is extremely hygroscopic and decomposes rapidly in moist air.<sup>149</sup> Mg(BH<sub>4</sub>)<sub>2</sub> is hygroscopic and hydrolyses in moist air.<sup>211</sup> Ca(BH<sub>4</sub>)<sub>2</sub> is stable in dry air and slowly hydrolyses in water. An application advantage of NaBH<sub>4</sub> is that it is produced on a large scale in the industry (global production reached around 826 000 tons in 2023),<sup>212</sup> e.g., from NaH and B(OCH<sub>3</sub>)<sub>3</sub>.<sup>149</sup> All other tetrahydroborates can be synthesized by metathesis reaction from NaBH<sub>4</sub> (Scheme 2).<sup>149,211–215</sup>

#### 2.4. Alkali and alkali earth metal tetrahydroaluminates

Tetrahydroaluminates and tetrahydroborates are structural analogues, but tetrahydroaluminates have lower gravimetric hydrogen storage capacity due to the replacement of the light boron atom with the heavier aluminium. LiAlH<sub>4</sub> can tolerate a maximum 39 wt% of additive to fulfill DOE target requirements considering that all hydrogen is released from the storage material; these values are 13, 30, and 18 wt% for Na, Mg, and Ca-tetrahydroaluminates, respectively (see Tables 1 and 2). In general, tetrahydroaluminates decompose and release hydrogen at lower temperature than tetrahydroborates and the only volatile decomposition product is hydrogen, and the solid residue consists of metals and/or alloys. The last step of the multi-step hydrogen release is the decomposition of alkali or



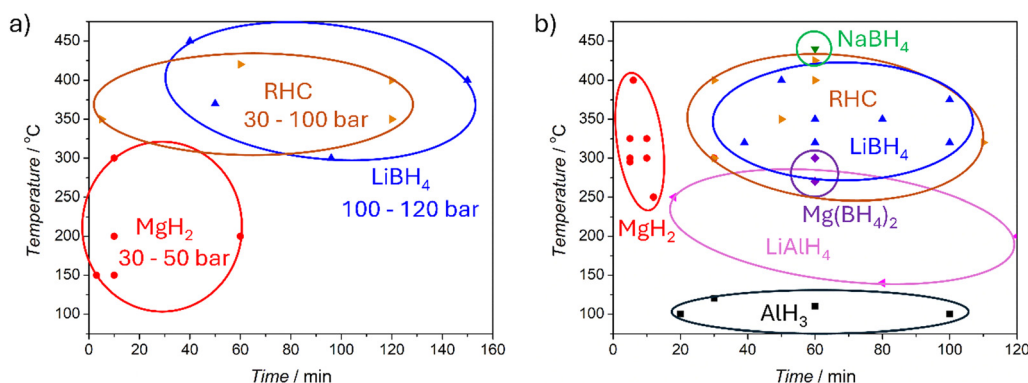
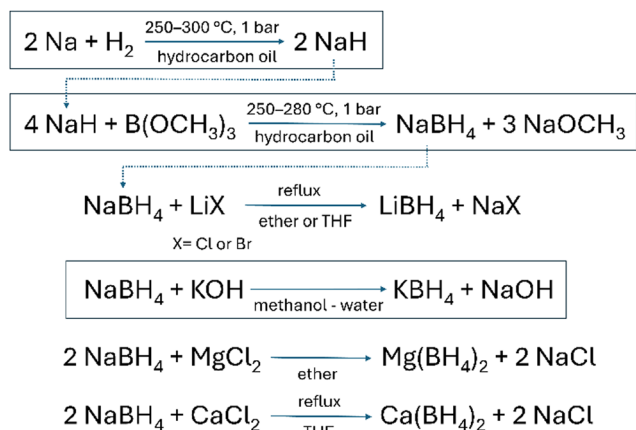


Fig. 6 Relationship between temperature and time for (a) hydrogen uptake of dehydrogenated systems, where uptake is higher than 6.0 wt% within 160 min, and (b) hydrogen release from investigated systems, where the amount of released hydrogen is above 6.5 wt% and release time is within 120 min.



Scheme 2 Synthesis of tetrahydroborates (industrial processes are indicated by boxes).<sup>149,211–215</sup>

alkali earth binary hydrides, which is practically not accessible due to the high temperatures required. If hydrogen discharge is conducted below their decomposition temperatures, the maximum hydrogen release from Li, Na, Mg, and Ca-tetrahydroaluminates would be 8.0, 5.6, 7.0, and 5.9 wt%, respectively. This places NaAlH<sub>4</sub> and Ca(AlH<sub>4</sub>)<sub>2</sub> on the list of unsatisfactory compounds for hydrogen storage, while LiAlH<sub>4</sub> and Mg(AlH<sub>4</sub>)<sub>2</sub> can tolerate only 9% and 7% additive, respectively. One of the major challenges of practical application of tetrahydroaluminates in hydrogen storage is that regenerating dehydrogenated tetrahydroaluminates requires high temperatures and hydrogen pressures.<sup>46,171,173,178</sup> LiAlH<sub>4</sub>, Mg(AlH<sub>4</sub>)<sub>2</sub> and Ca(AlH<sub>4</sub>)<sub>2</sub> are metastable and their rehydrogenation is thermodynamically not favoured.<sup>216,217</sup> The reason for the thermodynamic instability of LiAlH<sub>4</sub> and Ca(AlH<sub>4</sub>)<sub>2</sub> is the formation of stable intermediates, namely Li<sub>3</sub>AlH<sub>6</sub> and CaAlH<sub>5</sub>, respectively.<sup>218,219</sup> According to thermodynamic calculations, more than 1000 bar hydrogen partial pressure is required for the hydrogen absorption reaction of Li<sub>3</sub>AlH<sub>6</sub> → LiAlH<sub>4</sub> and CaAlH<sub>5</sub> → Ca(AlH<sub>4</sub>)<sub>2</sub> above room temperature.<sup>218,219</sup> Practical reversible hydrogen storage with LiAlH<sub>4</sub> and Ca(AlH<sub>4</sub>)<sub>2</sub> is therefore not possible without thermodynamically stabilizing these materials (and/or destabilizing intermediates). As an attempt to

achieve this, the thermodynamic stabilization of LiAlH<sub>4</sub> within the nanopores of N-doped ordered mesoporous carbon by lithium coordination to nitrogen binding sites was demonstrated recently.<sup>216</sup> The decomposition of LiAlH<sub>4</sub> bypassed the Li<sub>3</sub>AlH<sub>6</sub> intermediate and more than 80% of LiAlH<sub>4</sub> could be regenerated under 1000 bar hydrogen pressure. Mg(AlH<sub>4</sub>)<sub>2</sub> decomposes without the formation of a complex hydride intermediate; the first dehydrogenation step to MgH<sub>2</sub> and Al is exothermic, which makes the reverse process infeasible.<sup>220</sup> It appears likely that this first dehydrogenation step consists of two events, the endothermic decomposition of Mg(AlH<sub>4</sub>)<sub>2</sub> and a consecutive exothermic event which could be the re-crystallization of non-crystalline MgH<sub>2</sub>. The second dehydrogenation step has a relatively low temperature of 282 °C due to the formation of the intermetallic phase Mg<sub>2</sub>Al<sub>3</sub>.<sup>220</sup> Considering thermodynamic instability, LiAlH<sub>4</sub>, Mg(AlH<sub>4</sub>)<sub>2</sub> and Ca(AlH<sub>4</sub>)<sub>2</sub> may be best applied as one-way hydrogen storage materials, similarly to AlH<sub>3</sub> discussed above (Table 7). This consideration leaves NaAlH<sub>4</sub> as the only realistic target for reversible hydrogen storage but only if full dehydrogenation/rehydrogenation can be realized (Table 8). This material has the advantage of consisting only abundant elements, namely Na and Al. To address challenges, a wide range of transition and rare earth metal compounds and carbon-based materials, including oxides, chlorides, fluorides, nitrides, and borides, have been investigated to promote lower reaction temperatures and improved kinetics for tetrahydroaluminates.<sup>221–255</sup> General methods are like those used for main group binary hydrides and tetrahydroborates, discussed above, namely nanoconfinement and using additives and catalysts. Catalyst precursors (see examples in Tables 7 and 8) play a critical role as *in situ* formed transition metals, *e.g.* Ti, Zn, and Ni,<sup>224,244,248</sup> transition metal oxides, *e.g.* Ti<sub>2</sub>O<sub>3</sub>, NaFeO<sub>2</sub>, and NiO,<sup>233,244,251</sup> and Al-alloys, *e.g.* Al<sub>3</sub>Zr,<sup>223</sup> Al<sub>3</sub>Ti,<sup>225</sup> Al<sub>3</sub>Ni,<sup>233</sup> NiAl, Al<sub>3</sub>Ti and Ni<sub>2</sub>Al<sub>3</sub>,<sup>245</sup> AlCo,<sup>246</sup> Al<sub>13</sub>Co<sub>4</sub> and Al<sub>0.9</sub>Ni<sub>4.22</sub>,<sup>247</sup> as well as synergic multivalent Ti-species (Ti<sup>0</sup>, Ti<sup>3+</sup>)<sup>252,253</sup> or Ni and Ti species (Ni, NiO, Ti, Ti<sub>2</sub>O<sub>3</sub>)<sup>251</sup> are believed to catalyse the hydrogen uptake and release. The mechanism of catalytic action involved weakening the Al-H bonds, *e.g.* NiTiO<sub>3</sub> and Ni,<sup>251,255</sup> enhancing hydrogen transfer by shortening the diffusion path,<sup>244,247,254,255</sup> *e.g.* Ti shell,<sup>255</sup> and/or



Table 7 Effect of catalysts on the hydrogen release properties of LiAlH<sub>4</sub>, Mg(AlH<sub>4</sub>)<sub>2</sub>, and Ca(AlH<sub>4</sub>)<sub>2</sub>

| Catalyst precursor                             | Active form <sup>a</sup>   | Capacity <sup>b</sup><br>(wt%) | Decomp. temp. <sup>c</sup><br>onset/peak (°C) | Isothermal H <sub>2</sub> release<br>wt%/°C min <sup>-1</sup> | E <sub>a</sub> <sup>c</sup> (des.)<br>(kJ mol <sup>-1</sup> H <sub>2</sub> ) | Ref. |
|--|--|--------------------------------|---|---|--|------|
| LiAlH <sub>4</sub>                             |  |                                |   |   |  |      |
| ZrF <sub>4</sub> (10 wt%)                      | Al <sub>3</sub> Zr, LiF  | n.a.                           | 80, 130/219, 258                              | 5.6/100/120   | 60, 80   | 223  |
| Ti <sub>3</sub> C <sub>2</sub> (5 wt%)         | Ti, Ti <sup>3+</sup>   | 6.5                            | 59/n.a.                                       | 4.2/150/10<br>5.5/200/35                                      | 80, 100  | 224  |
| TiF <sub>3</sub> (2 mol%)                      | Al <sub>3</sub> Ti   | 7.3                            | 35/108  | 7.0/140/80<br>7.3/250/18                                      | 67, 88   | 225  |
| Ni <sub>0.6</sub> Zn <sub>0.4</sub> O (10 wt%) | NiO, Zn  | 5.6                            | 124, 170/n.a.                                 | 3.1/90/120  | 73, 85   | 244  |
| Ni-C@TiO <sub>2</sub> (7 wt%)                  | NiAl, Al <sub>3</sub> Ti, Ni <sub>2</sub> Al <sub>3</sub>                | 7.2                            | 56, 131/n.a.                                  | 6.3/200/20  | 59, 68   | 245  |
| Co-B (5 wt%)                                   | AlCo   | 7.7                            | n.a./135, 167                                 | 7.7/200/120   | 83   | 246  |
| Co <sub>3</sub> O <sub>4</sub> @CoNi (7 wt%)   | Al <sub>1.3</sub> Co <sub>4</sub> , Al <sub>0.9</sub> Ni <sub>4.22</sub> | 6.9                            | n.a./85, 177                                  | 6.3/200/120   | 80, 90   | 247  |
| Mg(AlH <sub>4</sub> ) <sub>2</sub>             |  |                                |   |   |  |      |
| TiCl <sub>3</sub> (1 mol%)                     | Ti   | 9                              | 60/n.a.                                       | 1.5/90/150<br>6/150/n.a.                                      | n.a.   | 248  |
| No catalyst                                    | —  | 9.0                            | 125/300, 415                                  | 5.5/135/125   | 123  | 249  |
| Ca(AlH <sub>4</sub> ) <sub>2</sub>             |  |                                |   |   |  |      |
| TiCl <sub>3</sub> (1 mol%)                     | n.a.   | n.a.                           | n.a./231, 295                                 | n.a.  | n.a.   | 242  |
| TiF <sub>3</sub> (10 wt%) <sup>d</sup>         | Ti   | n.a.                           | n.a./116, 218                                 | n.a.  | 57   | 243  |

<sup>a</sup> Catalytically active component formed during ball milling of precursors; ss = solid solution. <sup>b</sup> Experimentally determined maximum storage capacity. <sup>c</sup> Consecutive two dehydrogenation stages, n.a. = not available. <sup>d</sup> Ca(AlH<sub>4</sub>)<sub>2</sub>·2NaCl, synthesized by ball milling NaAlH<sub>4</sub> and CaCl<sub>2</sub>.

providing active sites to promote the nucleation and growth of dehydrogenation products, *e.g.* NiAl, Al<sub>3</sub>Ti, Ni<sub>2</sub>Al<sub>3</sub>,<sup>245</sup> and AlCo.<sup>246</sup> Ti<sub>3</sub>C<sub>2</sub> was found to effectively interact with tetrahydroaluminates and destabilize the Al-H bond through interfacial charge transfer.<sup>224</sup> Nanosizing and nanoconfinement are mainly used to control the hydride particle size, and their effect is kinetic rather than thermodynamic by creating nucleation sites and shortening diffusion paths. N-doped carbon, however, was shown to alter thermodynamics by Li adatom formation and charge redistribution between the metal hydride and the host.<sup>216</sup> As a new strategy of research, the concept of light-driven reversible hydrogen storage was validated recently on NaAlH<sub>4</sub>, using the catalytic effect of TiO<sub>2</sub> and the photothermal effect of nanolayered carbon.<sup>256</sup>

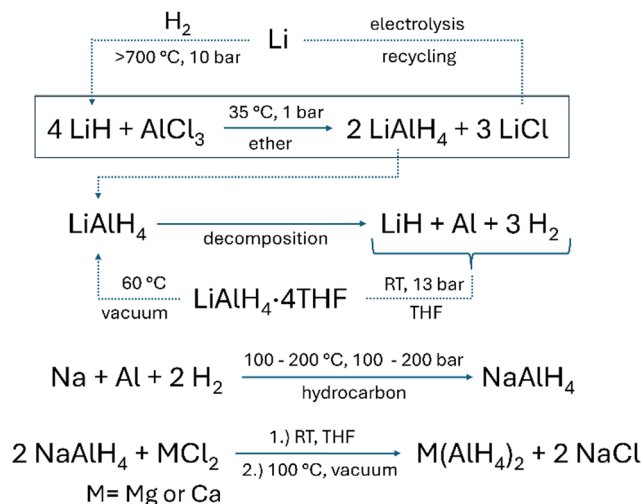
Handling tetrahydroaluminates requires more caution than handling tetrahydroborates due to the flammability of tetrahydroaluminates when exposed to oxygen and humidity. Tetrahydroaluminates hydrolyse in moist air and react violently with liquid water.<sup>149,257</sup> Although they are stable and not pyrophoric in the absence of moisture under ambient conditions, they are considered highly explosive in air when finely divided. Considering the one-way hydrogen delivery of LiAlH<sub>4</sub>, its performance is approaching that of AlH<sub>3</sub>, although the kinetics of LiAlH<sub>4</sub> dehydrogenation are a little slower (compare Table 4 and Table 7 and see Fig. 6); production cost and sustainability are expected to be decisive in their application. LiAlH<sub>4</sub> is produced in the industry, which is not the case for AlH<sub>3</sub>. In addition, producing AlH<sub>3</sub> from LiAlH<sub>4</sub> makes AlH<sub>3</sub> more expensive than

Table 8 Effect of catalysts on the hydrogen absorption and desorption kinetics of NaAlH<sub>4</sub><sup>a</sup>

| Catalyst (active form)   | Isothermal absorption |      |      |      | Non-isoth. des. <sup>b</sup><br>onset/peak |     | Isothermal desorption |      |      |      | Cycles/capacity retention |      |      |                                     | E <sub>a</sub> <sup>b</sup> (abs/des) |  | Ref. |
|--|-----------------------|------|------|------|--|-----|-----------------------|------|------|------|---------------------------|------|------|-------------------------------------|---------------------------------------|--|------|
|  | wt%                   | °C   | bar  | min  | °C/°C                                      | wt% | °C                    | bar  | min  | wt%  | °C                        | No.  | %    | kJ mol <sup>-1</sup> H <sub>2</sub> |                                       |  |      |
| NiFe <sub>2</sub> O <sub>4</sub> (3 mol%)<br>(NaFeO <sub>2</sub> , Al <sub>3</sub> Ni) | 3.7                   | 150  | 50   | 30   | 93, 147, 316/n.a.                          | 4.6 | 150                   | vac  | 60   | 3.5  | 150                       | 5    | 95   | —/54, 73, 113                       | 233                                   |  |      |
| CNT (8 mol%)   | 4.2                   | 150  | 140  | 600  | n.a.                                       | 3.3 | 160                   | vac  | 120  | 3.7  | 150                       | 8    | n.a. | n.a.                                | 237                                   |  |      |
| CeB <sub>6</sub> (2 mol%)  | 4.9                   | 120  | 120  | 20   | n.a.                                       | 4.9 | 160                   | 0.1  | 120  | 4.9  | 150                       | 15   | 92   | —/69, 99                            | 250                                   |  |      |
| NiTiO <sub>3</sub> (10 wt%)<br>(Ni, NiO, Ti, Ti <sub>2</sub> O <sub>3</sub> )          | 3.7                   | 60   | 100  | 90   | 89/139, 173                                | 3.3 | 110                   | 0.01 | 120  | 4.6  | 150                       | 5    | 95   | 12/104, 74                          | 251                                   |  |      |
| C@TiO <sub>2</sub> /Ti <sub>3</sub> C <sub>2</sub> (10 wt%)                            | n.a.                  | n.a. | n.a. | n.a. | 85/120, 160                                | 4.0 | 140                   | vac  | 13   | 5.0  | 200                       | 10   | 93   | —/72, 64                            | 252                                   |  |      |
| Ti <sub>3</sub> C <sub>2</sub> (7 wt%) (Ti, Ti <sup>3+</sup> )                         | 4.3                   | 80   | 100  | 180  | 100/140                                    | 3.2 | 100                   | vac  | 180  | 4.8  | 200                       | 10   | 97   | —/87. 88                            | 253                                   |  |      |
|  | 4.6                   | 120  | 100  | 60   |  | 4.7 | 140                   | vac  | 100  |      |                           |      |      |                                     |                                       |  |      |
| CoTiO <sub>3</sub> (10 wt%)<br>(AlTi <sub>3</sub> , Al <sub>3</sub> Co)                | n.a.                  | n.a. | n.a. | n.a. | n.a./135, 185                              | 3.5 | 150                   | vac  | 30   | n.a. | n.a.                      | n.a. | n.a. | —/86. 92                            | 254                                   |  |      |
| TiCl <sub>3</sub> (Ti)   | 4.0                   | 180  | 130  | 75   | 155/180, 250                               | 4.0 | 180                   | 0.1  | 150  | 4.0  | 180                       | 3    | 100  | n.a.                                | 255                                   |  |      |
| TiO <sub>2</sub> /C (10 wt%) <sup>f</sup>  | 4                     | 202  | 80   | 60   | n.a.                                       | 4   | 202                   | vac. | 7    | 4    | 202                       | 10   | 85   | n.a./56                             | 256                                   |  |      |
| CeCl <sub>3</sub> (2 mol%)   | 4                     | 120  | 100  | 10   | n.a.                                       | 3.9 | 180                   | 1.3  | n.a. | 3.9  | 180                       | 36   | 100  | n.a.                                | 261                                   |  |      |

<sup>a</sup> RT = room temperature, CNT = carbon nanotube, vac = vacuum, n.a. = not available. <sup>b</sup> Values for the first, second and third decomposition step are separated by comma. <sup>c</sup> Desorption at 160 °C and absorption at 120 °C. <sup>d</sup> Desorption at 170 °C and absorption at 120 °C. <sup>e</sup> Under the light intensity of 5 and 10 sun during absorption and desorption, respectively (1 sun = 100 mW cm<sup>-2</sup>).





Scheme 3 Synthesis of tetrahydroaluminates (industrial processes are indicated by a box, RT = room temperature).<sup>149,217,242,258</sup>

$\text{LiAlH}_4$  (Scheme 1). Considering the economics,  $\text{LiAlH}_4$  production can be improved by recycling the  $\text{LiCl}$  by-product as only 25% of  $\text{Li}$  is converted to  $\text{LiAlH}_4$  (Scheme 3).<sup>149</sup> Although dehydrogenated  $\text{LiAlH}_4$  cannot be re-hydrogenated in the solid phase, it can be hydrogenated in THF slurry to form an  $\text{LiAlH}_4 \cdot 4\text{THF}$  adduct ( $\Delta G = -1.65 \text{ kJ mol}^{-1} \text{LiAlH}_4$ );<sup>258</sup> the latter can be

desolvated in vacuum at a low temperature of  $60 \text{ }^\circ\text{C}$ .<sup>258–260</sup>

Dimethyl ether can be used at sub-ambient temperature for this conversion and vents naturally with the excess hydrogen.<sup>259,260</sup>

Detailed studies for the hydrogen delivery of magnesium and calcium tetrahydroaluminates are yet to be undertaken.  $\text{NaAlH}_4$  can reversibly deliver hydrogen in catalysed reactions (Fig. 7a, b and Table 8); however, the limited storage capacity, below the 6.5 wt% DOE target, and the cyclic instability are drawbacks for its application as a hydrogen storage material. It is worth noting that prototypes of hydrogen storage tanks using  $0.087 \text{ kg}$ ,<sup>261</sup>  $8 \text{ kg}$ ,<sup>262</sup> and  $20 \text{ kg}$ <sup>257</sup>  $\text{NaAlH}_4$  have been developed and material gravimetric capacity of 3.9 wt% (36 cycles) and 3.6 wt% (18 cycles), and system gravimetric capacity of 2 wt% (25 cycles) could be achieved, respectively. Industry, currently, is not producing  $\text{NaAlH}_4$ ,  $\text{Mg}(\text{AlH}_4)_2$  and  $\text{Ca}(\text{AlH}_4)_2$  on a large scale; these materials can be synthesized using various laboratory techniques from elements, hydrides and aluminium halides.<sup>217</sup> Selected frequently used methods are summarized in Scheme 3.

### 2.5. Reactive hydride composites

There is a vast possibility to combine metal hydrides, tetrahydroborates, and tetrahydroaluminates to create RHCs, especially as not only two but several components in various ratios could be mixed (Table 9). The concept of RHCs is that components of this system mutually destabilize each other and enhance the hydrogen desorption/adsorption kinetics, but without losing hydrogen

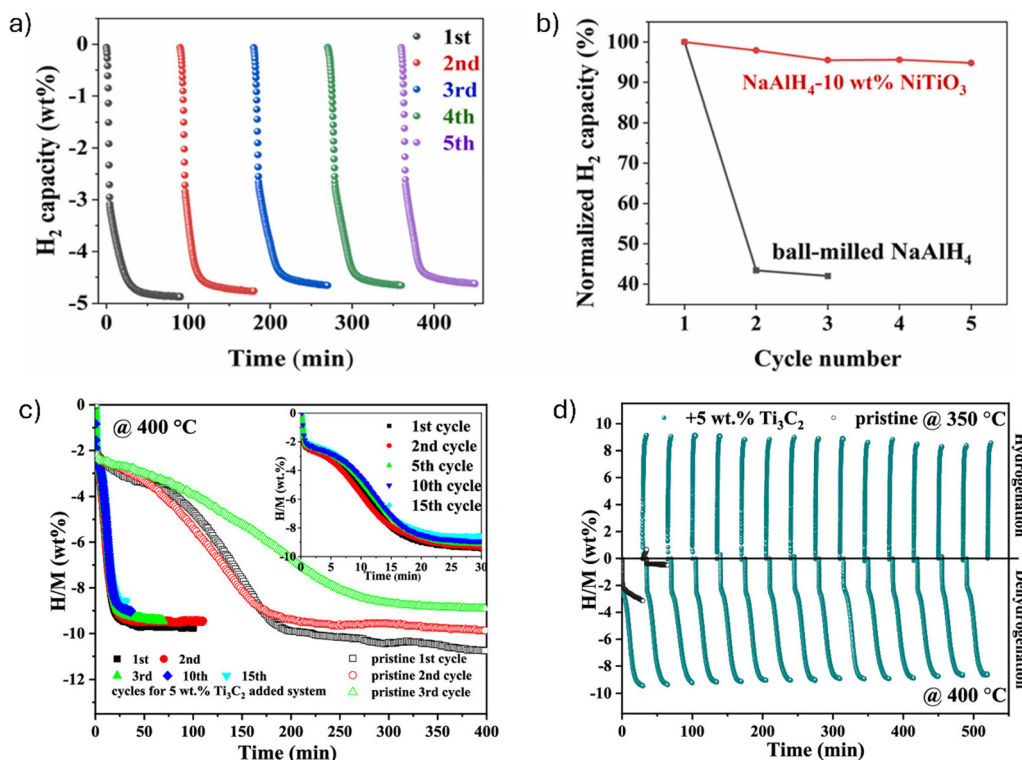


Fig. 7 (a) Isothermal dehydrogenation cyclic curves of  $\text{NiTiO}_3$  nanorod-doped  $\text{NaAlH}_4$  and (b) cyclic capacity retention of undoped and  $\text{NiTiO}_3$  nanorod-doped  $\text{NaAlH}_4$ . Reproduced from ref. 251 with permission from Elsevier B. V., copyright 2023. (c) and (d) Cyclic performance of the  $2\text{LiBH}_4 + \text{MgH}_2/2\text{LiH} + \text{MgB}_2$  system with and without  $\text{Ti}_3\text{C}_2$  catalysts: (c) dehydrogenation curves and (d) cyclic curves. Reproduced from ref. 280 with permission from the American Chemical Society, copyright 2019.



storage capacity as the additive/destabilizing agent is also a hydrogen storage material. The presence of a secondary phase introduces new phase boundaries where dehydrogenation can be preferential, compared to the pristine material, may initiate metathesis reaction between components or react to form intermediate phases altering thereby the reaction path, and modify the overall thermodynamics by alloy or metal boride formation. Experiments have confirmed lower onset decomposition temperature, faster dehydrogenation/rehydrogenation rate, and improved hydrogen yield for composites of tetrahydroborates, tetrahydroaluminates and metal hydrides compared to their pristine constituents.<sup>263–289</sup> In addition, nano-sizing, nanoconfinement, and catalysis have further improved hydrogen storage performances.<sup>273–287</sup> There are also challenges for RHC systems, such as the formation of stable intermediates, which block the reversibility of the dehydrogenation, phase separation of components during hydrogenation or rehydrogenation, or increased interdiffusion barriers, which must be prevented by using additives and catalysts. A simplified view of RHC hydrogen release considers RHC components confined in each other and consecutive decomposition steps; the first step is the decomposition of one of the components, forming fine and well dispersed reagent particles on the surface of the second component, and the second step is the dehydrogenation of the second component. The formation of alloys and borides can thermodynamically reduce the dehydrogenation enthalpy. An example is the  $6\text{LiBH}_4 + \text{Mg}(\text{AlH}_4)_2$  system, where  $\text{Mg}(\text{AlH}_4)_2$  decomposes to  $\text{MgH}_2$  and Al in the initiating step,  $\text{MgH}_2$  and Al react further to form  $\text{Mg}_2\text{Al}_3$ , and  $\text{Mg}_2\text{Al}_3$  and Al particles enhance the subsequent dehydrogenation of  $\text{LiBH}_4$  to form  $\text{MgAlB}_4$ ,  $\text{AlB}_2$  and LiH.<sup>279</sup> The products of this RHC decomposition, however, could be rehydrogenated only to  $\text{LiBH}_4 + \text{MgH}_2 + \text{Al}$  (due to the thermodynamic instability of  $\text{Mg}(\text{AlH}_4)_2$  discussed above). The  $2\text{LiBH}_4 + \text{MgH}_2$  system, the second example, is a typical RHC system exhibiting a high storage capacity of 11.5 wt%.<sup>284</sup> The RHC releases hydrogen in two steps, the first is the  $\text{MgH}_2$  decomposition to Mg and  $\text{H}_2$ , and the second is the reaction of Mg with  $\text{LiBH}_4$  to produce  $\text{MgB}_2$  and LiH. The formation of  $\text{MgB}_2$  provides thermodynamic stabilization for the system and is essential for the reversibility of hydrogen release. There is however a very long incubation period after the first step (more than 10 hours) which is attributed to the sluggish nucleation process of  $\text{MgB}_2$ .<sup>284,290</sup> Catalysing the nucleation by  $\text{VB}_2$  nanoparticles (having a lattice constant close to that of  $\text{MgB}_2$ ) resulted in an excellent cycling performance of 9.3 wt% over 10 cycles with 100% retention, and without the nucleation period.<sup>284</sup> It was observed in a similar system that the formation of  $\text{MgB}_2$  crystallites preferentially occurs on  $\text{TiB}_2$  nanoparticle surfaces, generated *in situ* from a  $3\text{TiCl}_3\text{-AlCl}_3$  additive, due to reduced elastic strain energy density compared to that of the  $\text{MgB}_2/\text{Mg}$  interface.<sup>290</sup> A similar action of  $\text{NbB}_2$ ,<sup>275</sup>  $\text{MgNi}_3\text{B}_2$  and  $\text{CoB}$ <sup>281</sup> nanoparticles has also been confirmed, highlighting an important catalytic role of transition metal borides. In general, catalysts and additives have been confirmed to act as active “hydrogen pumps”,<sup>274</sup> preventing aggregation of nanoparticles,<sup>273,277</sup> providing nucleation sites,<sup>274,275,280–284</sup> enhancing diffusion,<sup>283</sup> and destabilizing the

$\text{BH}_4^-$  anion by elongating the B–H bond.<sup>283</sup> Nanoconfinement was found to inhibit the formation of  $\text{B}_{12}\text{H}_{12}^{2-}$  clusters.<sup>273</sup> As an example, *in situ* generated  $\text{Ni}_2\text{B}$  nanoparticles were found to act as bidirectional electron transfer catalysts in tetrahydroborate systems, destabilize the tetrahydroborate anion and reduce the kinetic barrier for its formation.<sup>273</sup>  $\text{VH}_{2.01}$ , formed from  $\text{V}_2\text{C}$ , exhibited multiple roles; it enhanced  $\text{H}_2$  diffusion due to its open crystal structure, increased the hydrogen atom diffusion rate by providing pathways, and effectively weakened the B–H bonds and catalysed hydrogen release/absorption through a “hydrogen pump” effect.<sup>274</sup> The effect of  $\text{Ti}_2\text{C}$ ,  $\text{V}_2\text{C}$  and  $\text{Ti}_3\text{CN}$  MXenes was also found to be multiple as they prevented the aggregation of hydrides and generated active metal, e.g. Ti,<sup>277</sup> metal hydride, e.g.  $\text{VH}_{2.01}$ ,<sup>274</sup> or metal boride, e.g.  $\text{TiB}_2$ ,<sup>282</sup> species. The traditional focus of catalytic tuning of hydrogenation kinetics is on transition metal cations; however, the perspective of additional anion tuning was proposed recently by highlighting the role of  $\text{S}^{2-}$  anions in  $\text{Li}^+$  ion migration and destabilization of B–H bonds using  $\text{TiS}_2$ ,  $\text{MoS}_2$ , or  $\text{ZrS}_2$  for catalysing the dehydrogenation/hydrogenation of  $2\text{LiBH}_4 + \text{MgH}_2$ .<sup>283</sup>

The concept of forming RHCs by combining two or more hydrides has been proven to work in practice and combining hydrides has significantly improved the hydrogen storage performance of these composites, compared to their pristine constituents (Fig. 7c, d and Table 9). Challenges, however, remain the same for practical applications as for their constituents, namely further reduction of the operating temperature, enhancement of the kinetics, and especially improving reversibility of the hydrogen release and cyclic stability (Fig. 6). The  $\text{VB}_2$  catalysed  $2\text{LiBH}_4 + \text{MgH}_2$  system exhibits currently the best performance in terms of storage capacity and capacity retention during cycling (Table 9), which is the result of combining the relatively low decomposition temperature of  $\text{MgH}_2$ , the reactivity of Mg with  $\text{LiBH}_4$ , the thermodynamic stabilization by  $\text{MgB}_2$  formation, and the catalytic activity of  $\text{VB}_2$  nanoparticles on  $\text{MgB}_2$  nucleation.<sup>284</sup>

### 3. Conclusion

Developing solid-phase hydrogen storage materials for practical applications is of high importance for boosting the hydrogen industry. Light main group metal hydrides ( $\text{LiH}$ ,  $\text{MgH}_2$ ,  $\text{AlH}_3$ ), their tetrahydroborates ( $\text{LiBH}_4$ ,  $\text{NaBH}_4$ ,  $\text{KBH}_4$ ,  $\text{Ca}(\text{BH}_4)_2$  and  $\text{Mg}(\text{BH}_4)_2$ ), and tetrahydroaluminates ( $\text{LiAlH}_4$ ,  $\text{NaAlH}_4$ ,  $\text{Ca}(\text{AlH}_4)_2$  and  $\text{Mg}(\text{AlH}_4)_2$ ), as well as their hydride composites have high gravimetric hydrogen storage capacities, capable of fulfilling the minimum storage capacity requirements targeted by the DOE. The practical application of these materials, however, suffers from high operating temperatures, poor reversibility, slow kinetics, and low cyclic performance. To address these issues, large efforts have been devoted to tune hydrogen storage properties and recent research has justified that enhanced hydrogen storage can be achieved by nanostructuring and nanoconfining storage materials and incorporating catalysts. It has been found that small particle size and interaction between solid particles are vital elements for these catalysed reactions to enhance hydrogen



Table 9 Effect of catalysts on the hydrogen absorption and desorption kinetics of RHCs<sup>a</sup>

| Catalyst (active form)  | Isothermal absorption |      |      | Non-isoth. Des. <sup>b</sup> onset/peak |                   |      | Isothermal desorption |     |      | Cycles/capacity retention |      |      | $E_a^b$ (des) |                                 | Ref. |
|---|-----------------------|------|------|---|-------------------|------|-----------------------|-----|------|---------------------------|------|------|---------------|---------------------------------|------|
|   | wt%                   | °C   | bar  | min                                     | °C/°C             | wt%  | °C                    | bar | min  | wt%                       | °C   | No.  | %             | $\text{kJ mol}^{-1} \text{H}_2$ |      |
| LiBH <sub>4</sub> + KBH <sub>4</sub>  | 6.7                   | 400  | 100  | 120                                     | n.a./238          | 7.0  | 300                   | vac | 30   | 6.7                       | c    | 50   | 94            | 101                             | 273  |
| NiCp <sub>2</sub> C (40 wt%) (Ni <sub>2</sub> B)                              | n.a.                  | 300  | 100  | 360                                     | 80/280            | 4.5  | 275                   | vac | 50   | 7.3                       | 300  | 4    | 42            | 118, 125                        | 274  |
| LiBH <sub>4</sub> + Mg(BH <sub>4</sub> ) <sub>2</sub>                         | n.a.                  | 400  | 100  | 480                                     | 124/198           | 10.1 | 350                   | vac | 50   | 9.6                       | 260  | 4    | 37            | 106, 95, 122                    | 277  |
| V <sub>2</sub> C (20 wt%) (VH <sub>2,01</sub> )                               | n.a.                  | 400  | 100  | 480                                     | 124/198           | 6.5  | 200                   | 300 | 300  | 9.6                       | 260  | 4    | 37            | 106, 95, 122                    | 277  |
| Ti <sub>2</sub> C (30 wt%) (Ti)   | n.a.                  | 400  | 100  | 480                                     | 124/198           | 9.6  | 260                   | 300 | 300  | 9.6                       | 260  | 4    | 37            | 106, 95, 122                    | 277  |
| KBH <sub>4</sub> + 4LiAlH <sub>4</sub>  | 6.5                   | 420  | 33   | 60                                      | 82, 138, 484/n.a. | 1.7  | 420                   | 1   | 60   | n.a.                      | n.a. | n.a. | n.a.          | 153                             | 278  |
| no cat.   | 6.4                   | 400  | 30   | 300                                     | n.a.              | 11.8 | 400                   | 1   | 200  | n.a.                      | n.a. | n.a. | n.a.          | n.a.                            | 279  |
| 6LiBH <sub>4</sub> + Mg(AlH <sub>4</sub> ) <sub>2</sub>                       | 9.4                   | 350  | 100  | 5                                       | n.a.              | 9.5  | 400                   | 4   | 30   | 9.0                       | d    | 15   | 92            | 114                             | 280  |
| No cat. (Mg <sub>2</sub> Al <sub>3</sub> , Al)                                | n.a.                  | n.a. | n.a. | n.a.                                    | n.a.              | 5.5  | 380                   | 4   | 360  | 9.4                       | 400  | 10   | 96            | n.a.                            | 281  |
| 2LiBH <sub>4</sub> + MgH <sub>2</sub>   | n.a.                  | n.a. | n.a. | n.a.                                    | n.a.              | 9.4  | 400                   | 4   | 270  | 8.9                       | d    | 20   | 93            | 121, 119                        | 282  |
| Ti <sub>3</sub> C <sub>2</sub> (5 wt%) (TiB <sub>2</sub> )                    | 9.4                   | 350  | 75   | 5                                       | 236/342, 404, 435 | 9.0  | 400                   | 2   | 60   | 8.9                       | d    | 20   | 93            | 121, 119                        | 282  |
| NiCo@NC (10 wt%) (MgNi <sub>3</sub> B <sub>2</sub> , CoB)                     | 8.4                   | 350  | 40   | 120                                     | 221/n.a.          | 8.7  | 425                   | 4   | 60   | 9.3                       | 420  | 50   | 91            | 82, 101                         | 283  |
| Ti <sub>3</sub> CN (5 wt%) (TiB <sub>2</sub> )                                | 9.3                   | 350  | 60   | n.a.                                    | n.a.              | 9.23 | 400                   | 4   | 120  | 9.3                       | d    | 10   | 100           | n.a.                            | 284  |
| TiS <sub>2</sub> (10 wt%) (MgS, TiB <sub>2</sub> )                            | n.a.                  | n.a. | 70   | n.a.                                    | 339/n.a.          | n.a. | n.a.                  | 1   | n.a. | 9.1                       | 400  | 10   | 32            | n.a.                            | 285  |
| VB <sub>2</sub> (10 wt%) Ca(BH <sub>4</sub> ) <sub>2</sub> + MgH <sub>2</sub> | n.a.                  | n.a. | 70   | n.a.                                    | n.a.              | n.a. | n.a.                  | 1   | n.a. | 9.1                       | 400  | 10   | 45            | n.a.                            | 285  |
| No cat.   | 11.6                  | 450  | 80   | 960                                     | n.a.              | 11.6 | 450                   | 1   | 240  | 11.6                      | 450  | 10   | 61            | n.a.                            | 286  |
| NbF <sub>5</sub> (2 mol%)   | 3.8                   | 320  | 33   | 180                                     | 60/n.a.           | 1.7  | 320                   | 1   | 60   | n.a.                      | n.a. | n.a. | n.a.          | 80, 109, 137                    | 287  |
| 6LiBH <sub>4</sub> + CaH <sub>2</sub>   | 3.5                   | 420  | 30   | 60                                      | 125/n.a.          | 3.0  | 420                   | 1   | 60   | n.a.                      | n.a. | n.a. | n.a.          | 143, 147                        | 288  |
| TiCl <sub>3</sub> (1 mol%)  | 7.6                   | 350  | 90   | 1080                                    | 320/339           | 6.9  | 320                   | vac | 110  | 8.1                       | 350  | 10   | 77            | n.a.                            | 289  |
| 2Li[AlH <sub>4</sub> ] + Mg[BH <sub>4</sub> ] <sub>2</sub>                    |                       |      |      |   |                   |      |                       |     |      |                           |      |      |               |                                 |      |
| TiF <sub>3</sub> (5 wt%) (MgF <sub>2</sub> , LiF, TiH <sub>2</sub> )          |                       |      |      |   |                   |      |                       |     |      |                           |      |      |               |                                 |      |
| 2NaAlH <sub>4</sub> + Ca(BH <sub>4</sub> ) <sub>2</sub>                       |                       |      |      |   |                   |      |                       |     |      |                           |      |      |               |                                 |      |
| No cat.   |                       |      |      |   |                   |      |                       |     |      |                           |      |      |               |                                 |      |
| Ca(BH <sub>4</sub> ) <sub>2</sub> + 2LiBH <sub>4</sub> + 2MgH <sub>2</sub>    |                       |      |      |   |                   |      |                       |     |      |                           |      |      |               |                                 |      |
| No cat. (CaMgH <sub>3,72</sub> )  |                       |      |      |   |                   |      |                       |     |      |                           |      |      |               |                                 |      |

<sup>a</sup> RT = room temperature, CNT = carbon nanotube, NC = nanoporous carbon, vac = vacuum, n.a. = not available. <sup>b</sup> Values for the first, second and third decomposition step are separated by comma. <sup>c</sup> Desorption at 300 °C and absorption at 400 °C. <sup>d</sup> Desorption at 400 °C and absorption at 350 °C.



diffusion and mass transport, and preventing particle growth is a fundamental requirement for good cyclic performances. In addition, enhancement of storage properties is largely attributed to the *in situ* formation of active metal species or metal compounds during the synthesis and operation of storage material composites, as well as to high dispersion of catalytic species. It has become clear that multicomponent catalysts outperform conventional single catalyst systems due to their ability to address several steps of the multi-step processes of hydrogen release and absorption. Recent research has also highlighted that it is crucially important to prevent the crystallite growth and agglomeration, the separation of phases of storage components, and the redistribution of catalytic species or phases during hydrogen cycling. Incorporating additives for enhancing hydrogen and heat transport is also fundamentally important. All these requirements can only be fulfilled if the synergistic effect of multiple phases introduced into storage materials *in situ* and by mixing with additives is utilized.

Not all hydride and tetrahydroaluminate compounds are feasible targets for reversible hydrogen storage as  $\text{AlH}_3$ ,  $\text{LiAlH}_4$ ,  $\text{Ca}(\text{AlH}_4)_2$  and  $\text{Mg}(\text{AlH}_4)_2$  are metastable and their rehydrogenation is infeasible. They may serve as one-way hydrogen source media if their alternative economical synthesis is established. Their best performers can already operate with fast hydrogen release around and below 100 °C and could serve PEM fuel cells. Currently the Mg/MgH<sub>2</sub> system is the best performer concerning reversibility, kinetics and cyclic properties. MgH<sub>2</sub> can be discharged and recharged with relatively fast kinetics, but only at high temperatures of 300–400 °C and pressures of 20–80 bar, respectively. In addition, a stable cycling for at least 1500 cycles has not been achieved yet. The required pressure for recharging discharged tetrahydroborates and their composites is even higher (30–120 bar at 300–400 °C). The challenge for NaAlH<sub>4</sub> is the same and if only partially discharged the storage capacity is insufficient for DOE targets. Currently, none of the discussed hydrogen storage systems can fulfill the requirements of close to ambient working conditions, namely below 10 bar pressure and 100 °C. The improvement for practical application, however, has seen extensive progress and recently developed catalysed and confined systems operate at much lower temperatures and pressures, exhibit faster kinetics and much lower capacity decay during cycling than their corresponding pristine derivatives. There is still room for improvement as for example modifying template materials by doping to alter thermodynamics and anionic tuning to enhance kinetics has hardly been utilized. The novel concept of light-driven reversible hydrogen storage is validated recently on binary hydrides, tetrahydroborates and tetrahydroaluminates, and opens a new direction for the development of storage systems. There are reasons for optimism when it comes to solving storage issues and future research is expected to focus on exploiting the advantage of synergistic effects of catalysis using multiple catalysts, nanoconfinement, nanostructuring, and host material doping. Understanding the mechanism of hydrogen release/absorption is crucial for storage material design; therefore future work is expected to shift stronger toward full understanding of catalytic mechanisms by using high-resolution *operando* techniques. Research in this field will gradually move from storage materials

toward developing engineered storage systems for real world applications. As current research is conducted at a small scale, scaling up for practical applications is expected to present new challenges especially in material and thermal transport.

## Author contributions

Conceptualization and design: M. K.; acquisition of data: M. K. and T. P.; analysis and interpretation of data: M. K., T. P., S. S. and V. P. T.; writing – original draft: M. K. and T. P.; writing – review and editing: M. K., T. P., S. S. and V. P. T.; final version of the manuscript is approved by M. K., T. P., S. S. and V. P. T.

## Conflicts of interest

The authors declare no conflicts of interest.

## Data availability

No primary research results, software or code have been included, and no new data were generated or analysed as part of this review.

## Acknowledgements

This research was funded by the Australian Renewable Energy Agency, grant number 2023/TRAC733 (PRO-1050).

## References

- H. Ritchie and P. Rosado, *Energy Mix*, 2020, updated in 2024, <https://ourworldindata.org/energy-mix> (accessed on 9 March 2025).
- L. Pang, L. Liu, X. Zhou, M. Hafeez, S. Ullah and M. T. Sohail, How does natural resource depletion affect energy security risk? New insights from major energy-consuming countries, *Energy Strat. Rev.*, 2024, **54**, 101460, DOI: [10.1016/j.esr.2024.101460](https://doi.org/10.1016/j.esr.2024.101460).
- P. Friedlingstein, *et al.*, Global Carbon Budget 2021, *Earth Syst. Sci. Data*, 2022, **14**, 1917–2005, DOI: [10.5194/essd-14-1917-2022](https://doi.org/10.5194/essd-14-1917-2022).
- International Energy Agency (IEA), 2023, *Global Hydrogen Review 2023*, <https://www.iea.org/reports/global-hydrogen-review-2023> (accessed on 9 March 2025).
- Hydrogen Europe 2025*. Available on-line: <https://hydrogeneurope.eu/> (accessed on 9 March 2025).
- Road Map to a US Hydrogen Economy*. Available on-line: <https://static1.squarespace.com/static/53ab1fee4b0bef0179a1563/t/5e7ca9c03c2524311f3bef36/1585228227720/Road+map+to+a+US+hydrogen+economy+Exec+Sum+Web+Final.pdf> (accessed on 9 March 2025).
- T. Li, W. Liu, *et al.*, *China's Green Hydrogen New Era: A 2030 Renewable Hydrogen 100 GW Roadmap*, RMI, China Hydrogen Alliance Research Institute, 2022, [https://rmi.org/wp-content/uploads/dlm\\_uploads/2022/09/china\\_green\\_hydrogen\\_new\\_era\\_renewable\\_hydrogen\\_roadmap.pdf](https://rmi.org/wp-content/uploads/dlm_uploads/2022/09/china_green_hydrogen_new_era_renewable_hydrogen_roadmap.pdf) (accessed on 21 April 2025).



- 8 (a) N. Hyun-woo, *Gov't unveils roadmap for hydrogen-powered economy*, Korea Times, 2019. Available on-line: [https://www.koreatimes.co.kr/www/tech/2019/01/419\\_262238.html](https://www.koreatimes.co.kr/www/tech/2019/01/419_262238.html); (b) K. Yoon-seung, *Korea seeks to produce 6.2 million hydrogen cars by 2040*, Yonhap News Agency, 2019, Available on-line: <https://en.yna.co.kr/view/AEN20190117001400320?section=economy/economy> (accessed on 9 March 2025).
- 9 E. W. Lemmon, I. H. Bell, M. L. Huber and M. O. McLinden, Thermophysical Properties of Fluid Systems, in *NIST Chemistry WebBook, NIST Standard Reference Database Number 69*, ed. P. J. Linstrom and W. G. Mallard, National Institute of Standards and Technology, Gaithersburg MD, 2025, p. 20899, DOI: [10.18434/t4d303](https://doi.org/10.18434/t4d303) (accessed on 5 November, 2025).
- 10 DOE Technical Targets for Onboard Hydrogen Storage for Light-Duty Vehicles. <https://www.energy.gov/eere/fuelcells/doe-technical-targets-onboard-hydrogen-storage-light-duty-vehicles> (accessed on 9 March 2025).
- 11 J. C. Mankins, Technology readiness assessments: A retrospective, *Acta Astronaut.*, 2009, **65**, 1216–1223, DOI: [10.1016/j.actaastro.2009.03.058](https://doi.org/10.1016/j.actaastro.2009.03.058).
- 12 J. A. Gómez and D. M. F. Santos, The Status of On-Board Hydrogen Storage in Fuel Cell Electric Vehicles, *Designs*, 2023, **7**, 97, DOI: [10.3390/designs7040097](https://doi.org/10.3390/designs7040097).
- 13 J. Li, X. Chai, Y. Gu, P. Zhang, X. Yang, Y. Wen, Z. Xu, B. Jiang, J. Wang and G. Jin, *et al.*, Small-Scale High-Pressure Hydrogen Storage Vessels: A Review, *Materials*, 2024, **17**, 721, DOI: [10.3390/ma17030721](https://doi.org/10.3390/ma17030721).
- 14 J. Fesmire, A. Swanger, J. Jacobson and W. Notardonato, Energy efficient large-scale storage of liquid hydrogen, *IOP Conf. Series: Mater. Sci. Eng.*, 2022, **1240**, 012088, DOI: [10.1088/1757-899X/1240/1/012088](https://doi.org/10.1088/1757-899X/1240/1/012088).
- 15 T. Zhang, J. Uratani, Y. Huang, L. Xu, S. Griffiths and Y. Ding, Hydrogen liquefaction and storage: Recent progress and perspectives, *Renewable Sustainable Energy Rev.*, 2023, **176**, 113204, DOI: [10.1016/j.rser.2023.113204](https://doi.org/10.1016/j.rser.2023.113204).
- 16 M. H. Hirscher, L. Zhang and H. Oh, Nanoporous adsorbents for hydrogen storage, *Appl. Phys. A: Mater. Sci. Process.*, 2023, **129**, 112, DOI: [10.1007/s00339-023-06397-4](https://doi.org/10.1007/s00339-023-06397-4).
- 17 M. D. Allendorf, Z. Hulvey, T. Gennett, A. Ahmed, T. Autrey, J. Camp, E. S. Cho, H. Furukawa, M. Haranczyk, M. Head-Gordon, S. Jeong, A. Karkamkar, D.-J. Liu, J. R. Long, K. R. Meilhaus, I. H. Nayyar, R. Nazarov, D. J. Siegel, V. Stavila, J. J. Urban, S. Prasad Veccham and B. C. Wood, An assessment of strategies for the development of solid-state adsorbents for vehicular hydrogen storage, *Energy Environ. Sci.*, 2018, **11**, 2784, DOI: [10.1039/c8ee01085d](https://doi.org/10.1039/c8ee01085d).
- 18 A. R. Yuvaraj, A. Jayarama, D. Sharma, S. S. Nagarkar, S. P. Duttagupta and R. Pinto, Role of metal–organic framework in hydrogen gas storage: A critical review, *Int. J. Hydren Energy*, 2024, **59**, 1434–1458, DOI: [10.1016/j.ijhydene.2024.02.060](https://doi.org/10.1016/j.ijhydene.2024.02.060).
- 19 D. W. Kim, Y. Chen, H. Kim, N. Kim, Y. H. Lee, H. Oh, Y. G. Chung and C. S. Hong, High Hydrogen Storage in Trigonal Prismatic Monomer-Based Highly Porous Aromatic Frameworks, *Adv. Mater.*, 2024, **36**, 2401739, DOI: [10.1002/adma.202401739](https://doi.org/10.1002/adma.202401739).
- 20 J. B. von Colbe, J.-R. Ares, J. Barale, M. Baricco, C. Buckley, G. Capurso, N. Gallandat, D. M. Grant, M. N. Guzik, I. Jacob, E. H. Jensen, T. Jensen, J. Jepsen, T. Klassen, M. V. Lototsky, K. Manickam, A. Montone, J. Puzskiel, S. Sartori, D. A. Sheppard, A. Stuart, G. Walker, C. J. Webb, H. Yang, V. Yartys, A. Züttel and M. Dornheim, Application of hydrides in hydrogen storage and compression: Achievements, outlook and perspectives, *Int. J. Hydren Energy*, 2019, **44**, 7780–7808, DOI: [10.1016/j.ijhydene.2019.01.104](https://doi.org/10.1016/j.ijhydene.2019.01.104).
- 21 M. V. Lototsky, B. P. Tarasov and V. A. Yartys, Gas-phase applications of metal hydrides, *J. Energy Storage*, 2023, **72**, 108165, DOI: [10.1016/j.est.2023.108165](https://doi.org/10.1016/j.est.2023.108165).
- 22 A. Bishnoi, S. Pati and P. Sharma, Architectural design of metal hydrides to improve the hydrogen storage characteristics, *J. Power Sourc.*, 2024, **608**, 234609, DOI: [10.1016/j.jpowsour.2024.234609](https://doi.org/10.1016/j.jpowsour.2024.234609).
- 23 A. S. Mehr, A. D. Phillips, M. P. Brandon, M. T. Pryce and J. G. Carton, Recent challenges and development of technical and techno-economic aspects for hydrogen storage, insights at different scales; A state of art review, *Int. J. Hydren Energy*, 2024, **70**, 786–815, DOI: [10.1016/j.ijhydene.2024.05.182](https://doi.org/10.1016/j.ijhydene.2024.05.182).
- 24 M. Niermann, A. Beckendorff, M. Kaltschmitt and K. Bonhoff, Liquid Organic Hydrogen Carrier (LOHC) – Assessment based on chemical and economic properties, *Int. J. Hydren Energy*, 2019, **44**, 6631–6654, DOI: [10.1016/j.ijhydene.2019.01.199](https://doi.org/10.1016/j.ijhydene.2019.01.199).
- 25 A. Lin and G. Bagnato, Revolutionising energy storage: The Latest Breakthrough in liquid organic hydrogen carriers, *Int. J. Hydren Energy*, 2024, **63**, 315–329, DOI: [10.1016/j.ijhydene.2024.03.146](https://doi.org/10.1016/j.ijhydene.2024.03.146).
- 26 H. Li, X. Zhang, C. Zhang, Z. Ding and X. Jin, Application and Analysis of Liquid Organic Hydrogen Carrier (LOHC) Technology in Practical Projects, *Energies*, 2024, **17**, 1940, DOI: [10.3390/en17081940](https://doi.org/10.3390/en17081940).
- 27 M.-J. Zhou, Y. Miao, Y. Gu and Y. Xie, Recent Advances in Reversible Liquid Organic Hydrogen Carrier Systems: From Hydrogen Carriers to Catalysts, *Adv. Mater.*, 2024, **36**, 2311355, DOI: [10.1002/adma.202311355](https://doi.org/10.1002/adma.202311355).
- 28 AHEAD. *World's first international transport of hydrogen - Foreign-produced hydrogen has arrived in Japan for the first time from Brunei Darussalam*. 2019. Available online: [https://www.ahead.or.jp/en/pdf/20191218\\_ahead\\_press.pdf](https://www.ahead.or.jp/en/pdf/20191218_ahead_press.pdf) (accessed on 10 March 2025).
- 29 W. Liu, C. J. Webb and E. MacA, Gray, Review of hydrogen storage in AB<sub>3</sub> alloys targeting stationary fuel cell applications, *Int. J. Hydren Energy*, 2016, **41**, 3485–3507, DOI: [10.1016/j.ijhydene.2015.12.054](https://doi.org/10.1016/j.ijhydene.2015.12.054).
- 30 G. Sandrock, A panoramic overview of hydrogen storage alloys from a gas reaction point of view, *J. Alloys Compd.*, 1999, **293–295**, 877–888, DOI: [10.1016/S0925-8388\(99\)00384-9](https://doi.org/10.1016/S0925-8388(99)00384-9).
- 31 M. V. Lototsky, I. Tolj, M. W. Davids, Y. V. Klochko, A. Parsons, D. Swanepoel, R. Ehlers, G. Louw, B. van der Westhuizen, F. Smith, B. G. Pollet, C. Sita and V. Linkov, Metal hydride hydrogen storage and supply systems for electric forklift with low-temperature proton exchange



- membrane fuel cell power module, *Int. J. Hydren Energy*, 2016, **41**, 13831–13842, DOI: [10.1016/j.ijhydene.2016.01.148](https://doi.org/10.1016/j.ijhydene.2016.01.148).
- 32 T. Sawa, T. Aoki, I. Yamamoto, S. Tsukioka, H. Yoshida, T. Hyakudome, S. Ishibashi, T. Inada, T. Kabeno, R. Sasamoto and Y. Nasuno, Performance of the fuel cell underwater vehicle URASHIMA, *Acoust. Sci. Tech.*, 2005, **26**, 249–257, DOI: [10.1250/ast.26.249](https://doi.org/10.1250/ast.26.249).
- 33 A. I. Bevan, A. Züttel, D. Booka and I. R. Harris, Performance of a metal hydride store on the “Ross Barlow” hydrogen powered canal boat, *Faraday Discuss.*, 2011, **151**, 353–367, DOI: [10.1039/C0FD00025F](https://doi.org/10.1039/C0FD00025F).
- 34 M. Jakubowski and C. Pałczyński, Chapter 30 - Beryllium, ed. G. F. Nordberg, B. A. Fowler and M. Nordberg, *Handbook on the Toxicology of Metals*, 4th edn, Academic Press, 2015, pp. 635–653, DOI: [10.1016/B978-0-444-59453-2.00030-5](https://doi.org/10.1016/B978-0-444-59453-2.00030-5).
- 35 U. Wietelmann, M. Felderhoff and P. Rittmeyer, *Hydrides. Ullman's Encyclopedia in Industrial Chemistry*, Wiley-VCH Verlag GmbH & Co. KGaA, Weinheim, 2016, DOI: [10.1002/14356007.a13\\_199.pub2](https://doi.org/10.1002/14356007.a13_199.pub2).
- 36 I. Dovgaliuk, D. A. Safin, N. A. Tumanov, F. Morelle, A. Moulai, R. Cerný, Z. Lodziana, M. Devillers and Y. Filinchuk, Solid Aluminum Borohydrides for Prospective Hydrogen Storage, *ChemSusChem*, 2017, **10**, 4725–4734, DOI: [10.1002/cssc.201701629](https://doi.org/10.1002/cssc.201701629).
- 37 D. Harrison and T. Thonhauser, Suppressing diborane production during the hydrogen release of metal borohydrides: The example of alloyed Al(BH<sub>4</sub>)<sub>3</sub>, *Int. J. Hydren Energy*, 2016, **41**, 3571–3578, DOI: [10.1016/j.ijhydene.2015.12.159](https://doi.org/10.1016/j.ijhydene.2015.12.159).
- 38 K. Miwa, N. Ohba, S. Towata, Y. Nakamori, A. Zuttel and S. Orimo, First-principles study on thermodynamical stability of metal borohydrides: Aluminum borohydride Al(BH<sub>4</sub>)<sub>3</sub>, *J. Alloys Compd.*, 2007, **446–447**, 310–314, DOI: [10.1016/j.jallcom.2006.11.140](https://doi.org/10.1016/j.jallcom.2006.11.140).
- 39 T. Eggeman, *Hydrides, Kirk-Othmer Encyclopedia of Chemical Technology*, John Wiley & Sons, Inc., 2001, vol. 13, 607–631, DOI: [10.1002/0471238961.0825041819211212.a01.pub2](https://doi.org/10.1002/0471238961.0825041819211212.a01.pub2).
- 40 N. Eisenreich, A. Keßler, A. Koleczko and V. Weiser, On the kinetics of AlH<sub>3</sub> decomposition and the subsequent Al oxidation, *Int. J. Hydren Energy*, 2014, **39**, 6286–6294, DOI: [10.1016/j.ijhydene.2014.01.167](https://doi.org/10.1016/j.ijhydene.2014.01.167).
- 41 V. N. Konoplev and V. M. Bakulina, Some properties of magnesium borohydride, *Russ. Chem. Bull.*, 1971, **20**, 136–138, DOI: [10.1007/BF00849335](https://doi.org/10.1007/BF00849335).
- 42 C. Comanescu, G. Capurso and A. Maddalena, Nanoconfinement in activated mesoporous carbon of calcium borohydride for improved reversible hydrogen storage, *Nanotechnology*, 2012, **23**, 385401, DOI: [10.1088/0957-4484/23/38/385401](https://doi.org/10.1088/0957-4484/23/38/385401).
- 43 S.-C. Chung and H. Morioka, Thermochemistry and crystal structures of lithium, sodium and potassium alanates as determined by *ab initio* simulations, *J. Alloys Compd.*, 2004, **372**, 92–96, DOI: [10.1016/j.jallcom.2003.09.130](https://doi.org/10.1016/j.jallcom.2003.09.130).
- 44 M. Fichtner, J. Engel, O. Fuhr, A. Glöss, O. Rubner and R. Ahlrichs, The Structure of Magnesium Alanate, *Inorg. Chem.*, 2003, **42**, 7060–7066, DOI: [10.1021/ic034160y](https://doi.org/10.1021/ic034160y).
- 45 A. Züttel, Materials for hydrogen storage, *Materialstoday*, 2003, **6**, 24–33, DOI: [10.1016/S1369-7021\(03\)00922-2](https://doi.org/10.1016/S1369-7021(03)00922-2).
- 46 Q. Lai, M. Paskevicius, D. A. Sheppard, C. E. Buckley, A. W. Thornton, M. R. Hill, Q. Gu, J. Mao, Z. Huang, H. K. Liu, Z. Guo, A. Banerjee, S. Chakraborty, R. Ahuja and K.-F. Aguey-Zinsou, Hydrogen Storage Materials for Mobile and Stationary Applications: Current State of the Art, *ChemSusChem*, 2015, **8**, 2789–2825, DOI: [10.1002/cssc.201500231](https://doi.org/10.1002/cssc.201500231).
- 47 Y. T. Ge, Characterisation of pressure-concentration-temperature profiles for metal hydride hydrogen storage alloys with model development, *Energy Storage*, 2024, **6**, e504, DOI: [10.1002/est2.504](https://doi.org/10.1002/est2.504).
- 48 J. Huot, Metal hydrides, in *Handbook of Hydrogen Storage*, ed. M. Hirscher, Wiley-VCH Verlag GmbH & Co. KGaA, Weinheim, 2010, DOI: [10.1002/9783527629800.ch4](https://doi.org/10.1002/9783527629800.ch4).
- 49 S. Qian and D. O. Northwood, Hysteresis in metal-hydrogen systems: a critical review of the experimental observations and theoretical models, *Int. J. Hydren Energy*, 1988, **13**, 25–35, DOI: [10.1016/0360-3199\(88\)90006-7](https://doi.org/10.1016/0360-3199(88)90006-7).
- 50 B. Bogdanovic, K. Bohmhammel, B. Christ, A. Reiser, K. Schlichte, R. Vehlen and U. Wolf, Thermodynamic investigation of the magnesium–hydrogen system, *J. Alloys Compd.*, 1999, **282**, 84–92, DOI: [10.1016/S0925-8388\(98\)00829-9](https://doi.org/10.1016/S0925-8388(98)00829-9).
- 51 E. M. Dematteis, D. M. Dreistadt, G. Capurso, J. Jepsen, F. Cuevas and M. Latroche, Fundamental hydrogen storage properties of TiFe-alloy with partial substitution of Fe by Ti and Mn, *J. Alloys Compd.*, 2021, **874**, 159925, DOI: [10.1016/j.jallcom.2021.159925](https://doi.org/10.1016/j.jallcom.2021.159925).
- 52 R. M. R. Wellen and E. L. Canedo, On the Kissinger equation and the estimate of activation energies for non-isothermal cold crystallization of PET, *Polym. Test.*, 2014, **40**, 33–38, DOI: [10.1016/j.polymertesting.2014.08.008](https://doi.org/10.1016/j.polymertesting.2014.08.008).
- 53 S. Vyazovkin, Kissinger Method in Kinetics of Materials: Things to Beware and Be Aware of, *Molecules*, 2020, **25**, 2813, DOI: [10.3390/molecules25122813](https://doi.org/10.3390/molecules25122813).
- 54 J. M. Criado and A. Ortega, Non-Isothermal Transformation Kinetics: Remarks on the Kissinger Method, *J. Non-Cryst. Solids*, 1986, **87**, 302–311, DOI: [10.1016/S0022-3093\(86\)80004-7](https://doi.org/10.1016/S0022-3093(86)80004-7).
- 55 S. Shrinivasan, H.-Y. Tien, M. Tanniru and S. S. V. Tatiparti, On the parameters of Johnson–Mehl–Avrami–Kolmogorov equation for the hydride growth mechanisms: A case of MgH<sub>2</sub>, *J. Alloys Compd.*, 2018, **742**, 1002–1005, DOI: [10.1016/j.jallcom.2017.12.283](https://doi.org/10.1016/j.jallcom.2017.12.283).
- 56 Y. Pang and Q. Li, A review on kinetic models and corresponding analysis methods for hydrogen storage materials, *Int. J. Hydren Energy*, 2016, **41**, 18072–18087, DOI: [10.1016/j.ijhydene.2016.08.018](https://doi.org/10.1016/j.ijhydene.2016.08.018).
- 57 M. T. Todinov, On Some Limitations of the Johnson–Mehl–Avrami–Kolmogorov Equation, *Acta Mater.*, 2000, **48**, 4217–4224, DOI: [10.1016/S1359-6454\(00\)00280-9](https://doi.org/10.1016/S1359-6454(00)00280-9).
- 58 M. Fanfoni and M. Tomellini, The Johnson–Mehl–Avrami–Kolmogorov model: A brief review, *Nouv Cim D*, 1998, **20**, 1171–1182, DOI: [10.1007/BF03185527](https://doi.org/10.1007/BF03185527).
- 59 T. Huang and C. Zhou, Surface Diffusion-Controlled Johnson–Mehl–Avrami–Kolmogorov Model for Hydrogenation of Mg-based Alloys, *J. Phys. Chem. C*, 2023, **127**, 13900–13910, DOI: [10.1021/acs.jpcc.3c02650](https://doi.org/10.1021/acs.jpcc.3c02650).



- 60 M. J. Starink, Analysis of hydrogen desorption from linear heating experiments: Accuracy of activation energy determinations, *Int. J. Hydrogen Energy*, 2018, **43**, 6632–6641, DOI: [10.1016/j.ijhydene.2018.02.064](https://doi.org/10.1016/j.ijhydene.2018.02.064).
- 61 H. Cheng, C. Lu, J. Liu, Y. Yan, X. Han, H. Jin, Y. Wang, Y. Liu and C. Wu, Synchrotron radiation X-ray powder diffraction techniques applied in hydrogen storage materials - A review, *Progr. Nat. Sci.: Mater. Int.*, 2017, **27**, 66–73, DOI: [10.1016/j.pnsc.2016.12.007](https://doi.org/10.1016/j.pnsc.2016.12.007).
- 62 A. Fitch, Synchrotron radiation and powder diffraction, Synchrotron radiation and powder diffraction, in *International Tables for Crystallography*, vol. H, ch. 2.2, 2019, pp. 51–65, DOI: [10.1107/97809553602060000937](https://doi.org/10.1107/97809553602060000937).
- 63 X. Zhang, Y. Sun, G. Xia and X. Yu, Light-weight solid-state hydrogen storage materials characterized by neutron scattering, *J. Alloys Compd.*, 2022, **899**, 163254, DOI: [10.1016/j.jallcom.2021.163254](https://doi.org/10.1016/j.jallcom.2021.163254).
- 64 A. Ramirez-Cuesta, R. B. Xicohtencatl and Y. Cheng, Inelastic neutron scattering: A unique tool to study hydrogen in materials, *J. Mater. Res.*, 2024, **39**, 727–736, DOI: [10.1557/s43578-024-01284-x](https://doi.org/10.1557/s43578-024-01284-x).
- 65 D. K. Ross, 6 - Neutron scattering studies for analysing solid-state hydrogen storage, in *Woodhead Publishing Series in Electronic and Optical Materials, Solid-State Hydrogen Storage*, ed. G. Walker, Woodhead Publishing, 2008, pp. 135–173, DOI: [10.1533/9781845694944.2.135](https://doi.org/10.1533/9781845694944.2.135).
- 66 M. Schmidtman, P. Coster, P. F. Henry, V. P. Ting, M. T. Wellere and C. C. Wilson, Determining hydrogen positions in crystal engineered organic molecular complexes by joint neutron powder and single crystal X-ray diffraction, *CrystEngComm*, 2014, **16**, 1232–1236, DOI: [10.1039/C3CE42070A](https://doi.org/10.1039/C3CE42070A).
- 67 V. P. Ting, A. J. Ramirez-Cuesta, N. Bimbo, J. E. Sharpe, A. Noguera-Diaz, V. Presser, S. Rudic and T. J. Mays, Direct Evidence for Solid-like Hydrogen in a Nanoporous Carbon Hydrogen Storage Material at Supercritical Temperatures, *ACS Nano*, 2015, **9**, 8249–8254, DOI: [10.1021/acs.nano.5b02623](https://doi.org/10.1021/acs.nano.5b02623).
- 68 D. Yang, S. Rochat, M. Krzystyniak, A. Kulak, J. Olivier, V. P. Ting and M. Tian, Investigation of the Dynamic Behaviour of H<sub>2</sub> and D<sub>2</sub> in a Kinetic Quantum Sieving System, *ACS Appl. Mater. Interfaces*, 2024, **16**, 12467–12478, DOI: [10.1021/acsami.3c17965](https://doi.org/10.1021/acsami.3c17965).
- 69 J. Matsuda, *In situ* TEM studies on hydrogen-related issues: hydrogen storage, hydrogen embrittlement, fuel cells and electrolysis, *Microscopy*, 2024, **73**, 196–207, DOI: [10.1093/jmicro/dfad060](https://doi.org/10.1093/jmicro/dfad060).
- 70 J. Kim, J. O. Fadonougbo, J.-H. Bae, M. K. Cho, J. Hong, Y. W. Cho, J. W. Roh, G. H. Kim, J. H. Han, Y.-S. Lee, J. Y. Cho, K. H. Lee, J.-Y. Suh and D. W. Chun, Real-Time Monitoring of the Dehydrogenation Behavior of a Mg<sub>2</sub>FeH<sub>6</sub>-MgH<sub>2</sub> Composite by *In Situ* Transmission Electron Microscopy, *Adv. Funct. Mater.*, 2022, **32**, 2204147, DOI: [10.1002/adfm.202204147](https://doi.org/10.1002/adfm.202204147).
- 71 F. Wu and N. Yao, *In Situ* Transmission Electron Microscopy Studies in Gas/Liquid Environment. In *Microscopy and Analysis*, ed. S. G. Stanciu, InTech, 2016, DOI: [10.5772/62551](https://doi.org/10.5772/62551).
- 72 G. L. Soloveichik, Y. Gao, J. Rijssenbeek, M. Andrus, S. Kniajanski, R. C. Bowman, Jr., S.-J. Hwang and J.-C. Zhao, Magnesium borohydride as a hydrogen storage material: Properties and dehydrogenation pathway of unsolvated Mg(BH<sub>4</sub>)<sub>2</sub>, *Int. J. Hydrogen Energy*, 2009, **34**, 916–928, DOI: [10.1016/j.ijhydene.2008.11.016](https://doi.org/10.1016/j.ijhydene.2008.11.016).
- 73 L. Wang, M. Z. Qadir and K.-F. Aguey-Zinsou, Ni coated LiH nanoparticles for reversible hydrogen Storage, *Int. J. Hydrogen Energy*, 2016, **41**, 6376–6386, DOI: [10.1016/j.ijhydene.2016.01.173](https://doi.org/10.1016/j.ijhydene.2016.01.173).
- 74 Y. Yang, X. Zhang, L. Zhang, W. Zhang, H. Liu, Z. Huang, L. Yang, C. Gu, W. Sun, M. Gao, Y. Liu and H. Pan, Recent advances in catalyst-modified Mg-based hydrogen storage materials, *J. Mat. Sci. Technol.*, 2023, **163**, 182–211, DOI: [10.1016/j.jmst.2023.03.063](https://doi.org/10.1016/j.jmst.2023.03.063).
- 75 K.-F. Aguey-Zinsou and J.-R. Ares-Fernández, Hydrogen in magnesium: new perspectives toward functional stores, *Energy Environ. Sci.*, 2010, **3**, 526–543, DOI: [10.1039/b921645f](https://doi.org/10.1039/b921645f).
- 76 Z. Han, M. L. Yeboah, R. Jiang, X. Li and S. Zhou, Hybrid activation mechanism of thermal annealing for hydrogen storage of magnesium based on experimental evidence and theoretical validation, *Appl. Surf. Sci.*, 2020, **504**, 144491, DOI: [10.1016/j.apsusc.2019.144491](https://doi.org/10.1016/j.apsusc.2019.144491).
- 77 H. Yun, H. Wang, J. Bai, X. Wang, X. Dai, X. Hou and Y. Xu, Activation and hydrogen storage properties of Mg-based composites synthesized by catalytic mechanochemical hydrogenation strategy, *Int. J. Hydrogen Energy*, 2024, **50**, 1025–1039, DOI: [10.1016/j.ijhydene.2023.08.311](https://doi.org/10.1016/j.ijhydene.2023.08.311).
- 78 Y. Kang, K. Zhang and X. Lin, Surface Modifications of Magnesium-Based Materials for Hydrogen Storage and Nickel-Metal Hydride Batteries: A Review, *Coatings*, 2023, **13**, 1100, DOI: [10.3390/coatings13061100](https://doi.org/10.3390/coatings13061100).
- 79 Y. Xu, Y. Li, Q. Hou, Y. Hao and Z. Ding, Ball Milling Innovations Advance Mg-Based Hydrogen Storage Materials Towards Practical Applications, *Materials*, 2024, **17**, 2510, DOI: [10.3390/ma17112510](https://doi.org/10.3390/ma17112510).
- 80 G. Parry and R. J. Pulham, Rate of Reaction of Hydrogen with Liquid Lithium: Comparison with Sodium and Potassium, *J. Chem. Soc., Dalton Trans.*, 1975, 1915–1917, DOI: [10.1039/DT9750001915](https://doi.org/10.1039/DT9750001915).
- 81 L. Wang, M. Z. Qadir and K.-F. Aguey-Zinsou, Direct and reversible hydrogen storage of lithium hydride (LiH) nanoconfined in high surface area graphite, *Int. J. Hydrogen Energy*, 2016, **41**, 18088–18094, DOI: [10.1016/j.ijhydene.2016.07.073](https://doi.org/10.1016/j.ijhydene.2016.07.073).
- 82 R. T. Howie, O. Narygina, C. L. Guillaume, S. Evans and E. Gregoryanz, High-pressure synthesis of lithium hydride, *Phys. Rev. B: Condens. Matter Mater. Phys.*, 2012, **86**, 064108, DOI: [10.1103/PhysRevB.86.064108](https://doi.org/10.1103/PhysRevB.86.064108).
- 83 R. C. Muduli, Z. Chen, F. Guo, A. Jain, H. Miyaoka, T. Ichikawa and P. Kale, Enhancing the solid-state hydrogen storage properties of lithium hydride through thermodynamic tuning with porous silicon nanowires, *Energy Adv.*, 2024, **3**, 2212–2219, DOI: [10.1039/d4ya00389f](https://doi.org/10.1039/d4ya00389f).
- 84 J. J. Vajo, F. Mertens, C. C. Ahn, R. C. Bowman, Jr. and B. Fultz, Altering Hydrogen Storage Properties by Hydride Destabilization through Alloy Formation: LiH and



- MgH<sub>2</sub> Destabilized with Si, *J. Phys. Chem. B*, 2004, **108**, 13977–13983, DOI: [10.1021/jp040060h](https://doi.org/10.1021/jp040060h).
- 85 R. C. Muduli, Z. Chen, K. Shinzato, F. Guo, T. Ichikawa, A. Jain, H. Miyaoka and P. Kale, Thermodynamic improvement of lithium hydrides for hydrogen absorption and desorption by incorporation of porous silicon, *Int. J. Hydren Energy*, 2024, **50**, 1094–1102, DOI: [10.1016/j.ijhydene.2023.09.015](https://doi.org/10.1016/j.ijhydene.2023.09.015).
- 86 J. Graetz and J. J. Reilly, Thermodynamics of the  $\alpha$ ,  $\beta$  and  $\gamma$  polymorphs of AlH<sub>3</sub>, *J. Alloys Compd.*, 2006, **424**, 262–265, DOI: [10.1016/j.jallcom.2005.11.086](https://doi.org/10.1016/j.jallcom.2005.11.086).
- 87 J. Graetz and J. J. Reilly, Decomposition Kinetics of the AlH<sub>3</sub> Polymorphs, *J. Phys. Chem. B*, 2005, **109**, 22181–22185, DOI: [10.1021/jp0546960](https://doi.org/10.1021/jp0546960).
- 88 J. F. Fernandez and C. R. Sanchez, Rate determining step in the absorption and desorption of hydrogen by magnesium, *J. Alloys Compd.*, 2002, **340**, 189–198, DOI: [10.1016/S0925-8388\(02\)00120-2](https://doi.org/10.1016/S0925-8388(02)00120-2).
- 89 A. S. Pedersen, J. Kj ller, B. Larsen, B. VigeHolm and J. A. Jensen, Long-Term Cycling of the Magnesium Hydrogen System, *Int. J. Hydren Energy*, 1984, **9**, 799–802, DOI: [10.1016/0360-3199\(84\)90283-0](https://doi.org/10.1016/0360-3199(84)90283-0).
- 90 J. Graetz, J. J. Reilly, V. A. Yartys, J. P. Maehlen, B. M. Bulychev, V. E. Antonov, B. P. Tarasov and I. E. Gabis, Aluminum hydride as a hydrogen and energy storage material: Past, present and future, *J. Alloys Compd.*, 2011, **509S**, S517–S528, DOI: [10.1016/j.jallcom.2010.11.115](https://doi.org/10.1016/j.jallcom.2010.11.115).
- 91 G. Sandrock, J. Reilly, J. Graetz, W.-M. Zhou, J. Johnson and J. Wegrzyn, Accelerated thermal decomposition of AlH<sub>3</sub> for hydrogen-fueled vehicles, *Appl. Phys. A: Mater. Sci. Process.*, 2005, **80**, 687–690, DOI: [10.1007/s00339-004-3105-0](https://doi.org/10.1007/s00339-004-3105-0).
- 92 S. He, G. Li, Y. Wang, L. Liu, Z. Lu, L. Xu, P. Sheng, X. Wang, H. Chen, C. Huang, Z. Lan, W. Zhou, J. Guo and H. Liu, Achieving both high hydrogen capacity and low decomposition temperature of the metastable AlH<sub>3</sub> by proper ball milling with TiB<sub>2</sub>, *Int. J. Hydren Energy*, 2023, **48**, 3541–3551, DOI: [10.1016/j.ijhydene.2022.10.198](https://doi.org/10.1016/j.ijhydene.2022.10.198).
- 93 H. Liu, L. Zhang, H. Ma, C. Lu, H. Luo, X. Wang, X. Huang, Z. Lan and J. Guo, Aluminum hydride for solid-state hydrogen storage: Structure, synthesis, thermodynamics, kinetics, and regeneration, *J. Energy Chem.*, 2021, **52**, 428–440, DOI: [10.1016/j.jechem.2020.02.008](https://doi.org/10.1016/j.jechem.2020.02.008).
- 94 Y. Nakagawa, C.-H. Lee, K. Matsui, K. Kousaka, S. Isobe, N. Hashimoto, S. Yamaguchi, H. Miyaoka, T. Ichikawa and Y. Kojima, Doping effect of Nb species on hydrogen desorption properties of AlH<sub>3</sub>, *J. Alloys Compd.*, 2018, **734**, 55–59, DOI: [10.1016/j.jallcom.2017.10.273](https://doi.org/10.1016/j.jallcom.2017.10.273).
- 95 L. Liang, Q. Yang, S. Zhao, L. Wang and F. Liang, Excellent catalytic effect of LaNi<sub>5</sub> on hydrogen storage properties for aluminium hydride at mild temperature, *Int. J. Hydrogen Energy*, 2021, **46**, 38733–38740, DOI: [10.1016/j.ijhydene.2021.09.130](https://doi.org/10.1016/j.ijhydene.2021.09.130).
- 96 H. Liu, S. He, G. Li, Y. Wang, L. Xu, P. Sheng, X. Wang, T. Jiang, C. Huang, Z. Lan, W. Zhou and J. Guo, Directed Stabilization by Air-Milling and Catalyzed Decomposition by Layered Titanium Carbide Toward Low-Temperature and High-Capacity Hydrogen Storage of Aluminum Hydride, *ACS Appl. Mater. Interfaces*, 2022, **14**, 42102–42112, DOI: [10.1021/acsami.2c11805](https://doi.org/10.1021/acsami.2c11805).
- 97 Y. Yang, F. Liang, Y. Cheng, D. Yin and L. Wang, Improvement of dehydrogenation performance by adding CeO<sub>2</sub> to  $\alpha$ -AlH<sub>3</sub>, *Int. J. Hydren Energy*, 2020, **45**, 2119–2126, DOI: [10.1016/j.ijhydene.2019.11.086](https://doi.org/10.1016/j.ijhydene.2019.11.086).
- 98 L. Liang, C. Wang, M. Ren, S. Li, Z. Wu, L. Wang and F. Liang, Unraveling the Synergistic Catalytic Effects of TiO<sub>2</sub> and Pr<sub>6</sub>O<sub>11</sub> on Superior Dehydrogenation Performances of  $\alpha$ -AlH<sub>3</sub>, *ACS Appl. Mater. Interfaces*, 2021, **13**, 26998–27005, DOI: [10.1021/acsami.1c04534](https://doi.org/10.1021/acsami.1c04534).
- 99 Y. Zhao, Q. Wang, D. Yin, S. Li, C. Wang, L. Liang, S. Zhao, C. Zhang, L. Wang and Y. Cheng, Superior catalytic effect of Bi@C on dehydrogenation performance of  $\alpha$ -AlH<sub>3</sub>, *Int. J. Hydren Energy*, 2024, **50**, 1164–1173, DOI: [10.1016/j.ijhydene.2023.09.049](https://doi.org/10.1016/j.ijhydene.2023.09.049).
- 100 Y. Zhao, Q. Wang, D. Yin, X. Wang, S. Li, C. Wang, L. Liang, S. Zhao, L. Wang and Y. Cheng, Hollow structured Fe@C nanorods for boosting dehydrogenation properties of  $\alpha$ -AlH<sub>3</sub>, *Nano Res.*, 2024, **17**, 8184–8191, DOI: [10.1007/s12274-024-6867-z](https://doi.org/10.1007/s12274-024-6867-z).
- 101 Y. Shanga, C. Pistiddaa, G. Gizer, T. Klassena and M. Dornheim, Mg-based materials for hydrogen storage, *J. Magn. Alloys*, 2021, **9**, 1837–1860, DOI: [10.1016/j.jma.2021.06.007](https://doi.org/10.1016/j.jma.2021.06.007).
- 102 Y. Li, Y. Zhang, H. Shang, Y. Qi, P. Li and D. Zhao, Investigation on structure and hydrogen storage performance of as-milled and cast Mg<sub>90</sub>Al<sub>10</sub> alloys, *Int. J. Hydren Energy*, 2018, **43**, 6642–6653, DOI: [10.1016/j.ijhydene.2018.02.086](https://doi.org/10.1016/j.ijhydene.2018.02.086).
- 103 A. Andreasen, Hydrogenation properties of Mg–Al alloys, *Int. J. Hydren Energy*, 2008, **33**, 7489–7497, DOI: [10.1016/j.ijhydene.2008.09.095](https://doi.org/10.1016/j.ijhydene.2008.09.095).
- 104 T. Liu, T. Zhang, X. Zhang and X. Li, Synthesis and hydrogen storage properties of ultrafine Mg–Zn particles, *Int. J. Hydren Energy*, 2011, **36**, 3515–3520, DOI: [10.1016/j.ijhydene.2010.12.049](https://doi.org/10.1016/j.ijhydene.2010.12.049).
- 105 M. Peška, A. Dębski, W. Gąsior, S. Dyjak, W. Gierlotka, A. Baran, D. J. Zasada and M. Polanski, Hydrogenation Behavior of Mg–Li Alloys, *ACS Appl. Energy Mater.*, 2025, **8**, 1994–2002, DOI: [10.1021/acsaem.4c02396](https://doi.org/10.1021/acsaem.4c02396).
- 106 A. S. Pedersen, B. VigeHolm, J. Kj ller and B. Larsen, The effect of cycling in impure hydrogen on the hydrogen capacity of magnesium powder, *Int. J. Hydren Energy*, 1987, **12**, 765–771, DOI: [10.1016/0360-3199\(87\)90092-9](https://doi.org/10.1016/0360-3199(87)90092-9).
- 107 M. Krebsz, R. Y. Hodgetts, S. Johnston, C. K. Nguyen, Y. Hora, D. R. MacFarlane and A. N. Simonov, Reduction of dinitrogen to ammonium through a magnesium-based electrochemical process at close-to-ambient temperature, *Energy Environ. Sci.*, 2024, **17**, 4481, DOI: [10.1039/d4ee01090f](https://doi.org/10.1039/d4ee01090f).
- 108 M. Krebsz, S. Johnston, C. K. Nguyen, Y. Hora, B. Roy, A. N. Simonov and D. R. MacFarlane, High-Performance Magnesium Electrochemical Cycling with Hybrid Mg–Li Electrolytes, *ACS Appl. Mater. Interfaces*, 2022, **14**, 34552–34561, DOI: [10.1021/acsami.2c04073](https://doi.org/10.1021/acsami.2c04073).
- 109 L. Ouyang, F. Liu, H. Wang, J. Liu, X.-S. Yang, L. Sun and M. Zhu, Magnesium-based hydrogen storage compounds:



- A review, *J. Alloys Compd.*, 2020, **832**, 154865, DOI: [10.1016/j.jallcom.2020.154865](https://doi.org/10.1016/j.jallcom.2020.154865).
- 110 Y. Liu, Y. Guo, Y. Jiang, L. Feng, Y. Sun and Y. Wang, Recent progress in thermodynamic and kinetics modification of magnesium hydride hydrogen storage materials, *Mater. Rep.: Energy*, 2024, **4**, 100252, DOI: [10.1016/j.matre.2024.100252](https://doi.org/10.1016/j.matre.2024.100252).
- 111 X. Yang, W. Li, J. Zhang and Q. Hou, Hydrogen Storage Performance of Mg/MgH<sub>2</sub> and Its Improvement Measures: Research Progress and Trends, *Materials*, 2023, **16**, 1587, DOI: [10.3390/ma16041587](https://doi.org/10.3390/ma16041587).
- 112 J. Zhang, M. Liu, J. Qi, N. Lei, S. Guo, J. Li, X. Xiao and L. Ouyang, Advanced Mg-based materials for energy storage: fundamental, progresses, challenges and perspectives, *Progr. Mater. Sci.*, 2025, **148**, 101381, DOI: [10.1016/j.pmatsci.2024.101381](https://doi.org/10.1016/j.pmatsci.2024.101381).
- 113 Z. Ding, Y. Li, H. Yang, Y. Lu, J. Tan, J. Li, Q. Li, Y. Chen, L. L. Shaw and F. Pan, Tailoring MgH<sub>2</sub> for hydrogen storage through nanoengineering and Catalysis, *J. Magn. Alloys*, 2022, **10**, 2946–2967, DOI: [10.1016/j.jma.2022.09.028](https://doi.org/10.1016/j.jma.2022.09.028).
- 114 Y. Zhang, F. Wu, S. Guemou, H. Yu, L. Zhang and Y. Wang, Constructing Mg<sub>2</sub>Co–Mg<sub>2</sub>CoH<sub>5</sub> nano hydrogen pumps from LiCoO<sub>2</sub> nanosheets for boosting the hydrogen storage property of MgH<sub>2</sub>, *Dalton Trans.*, 2022, **51**, 16195, DOI: [10.1039/d2dt02090d](https://doi.org/10.1039/d2dt02090d).
- 115 M. Dai, J. A. Bolarin, G. Lei, Z. Li, T. He, H. Cao and P. Chen, Potassium hydride reduced black TiO<sub>2-x</sub> for boosting the hydrogenation of magnesium at room temperature, *J. Alloys Compd.*, 2022, **897**, 162750, DOI: [10.1016/j.jallcom.2021.162750](https://doi.org/10.1016/j.jallcom.2021.162750).
- 116 L. Ren, Y. Li, Z. Li, X. Lin, C. Lu, W. Ding and J. Zou, Boosting Hydrogen Storage Performance of MgH<sub>2</sub> by Oxygen Vacancy-Rich H-V<sub>2</sub>O<sub>5</sub> Nanosheet as an Excited H-Pump, *Nano-Micro Lett.*, 2024, **16**, 160, DOI: [10.1007/s40820-024-01375-8](https://doi.org/10.1007/s40820-024-01375-8).
- 117 H. Liang, Z. Xie, R. Zhao, X. Wen, F. Hong, W. Shi, H. Chen, H. Liu, W. Zhou, J. Guo and Z. Lan, Facile synthesis of nickel-vanadium bimetallic oxide and its catalytic effects on the hydrogen storage properties of magnesium hydride, *Int. J. Hydrogen Energy*, 2022, **47**, 32969–32980, DOI: [10.1016/j.ijhydene.2022.07.012](https://doi.org/10.1016/j.ijhydene.2022.07.012).
- 118 L. Zhang, Z. Cai, Z. Yao, L. Ji, Z. Sun, N. Yan, B. Zhang, B. Xiao, J. Du, X. Zhu and L. Chen, A striking catalytic effect of facile synthesized ZrMn<sub>2</sub> nanoparticles on the de/rehydrogenation properties of MgH<sub>2</sub>, *J. Mater. Chem. A*, 2019, **7**, 5626–5634, DOI: [10.1039/C9TA00120D](https://doi.org/10.1039/C9TA00120D).
- 119 J. Lu, Y. J. Choi, Z. Z. Fang, H. Y. Sohn and E. Rönnebro, Hydrogen Storage Properties of Nanosized MgH<sub>2</sub>–0.1TiH<sub>2</sub> Prepared by Ultrahigh-Energy–High-Pressure Milling, *J. Am. Chem. Soc.*, 2009, **131**, 15843–15852, DOI: [10.1021/ja906340u](https://doi.org/10.1021/ja906340u).
- 120 L. Zhang, L. Ji, Z. Yao, N. Yan, Z. Sun, X. Yang, X. Zhu, S. Hu and L. Chen, Facile synthesized Fe nanosheets as superior active catalyst for hydrogen storage in MgH<sub>2</sub>, *Int. J. Hydrogen Energy*, 2019, **44**, 21955–21964, DOI: [10.1016/j.ijhydene.2019.06.065](https://doi.org/10.1016/j.ijhydene.2019.06.065).
- 121 S. Gao, X. Wang, H. Liu, T. He, Y. Wang, S. Li and M. Yan, CNTs decorated with CoFeB as a dopant to remarkably improve the dehydrogenation/rehydrogenation performance and cyclic stability of MgH<sub>2</sub>, *Int. J. Hydrogen Energy*, 2020, **45**, 28964–28973, DOI: [10.1016/j.ijhydene.2020.07.148](https://doi.org/10.1016/j.ijhydene.2020.07.148).
- 122 X. Lu, L. Zhang, H. Yu, Z. Lu, J. He, J. Zheng, F. Wu and L. Chen, Achieving superior hydrogen storage properties of MgH<sub>2</sub> by the effect of TiFe and carbon nanotubes, *Chem. Eng. J.*, 2021, **422**, 130101, DOI: [10.1016/j.cej.2021.130101](https://doi.org/10.1016/j.cej.2021.130101).
- 123 Z.-Y. Dai, P. Wu, L.-R. Xiao, H. Kimura, C.-X. Hou, X.-Q. Sun, S.-J. Guo, W. Du and X.-B. Xie, Non-stoichiometric Ni<sub>3</sub>ZnCo<sub>0.7</sub> carbide loading on melamine sponge-derived carbon for hydrogen storage performance improvement of MgH<sub>2</sub>, *Rare Met.*, 2025, **44**, 515–530, DOI: [10.1007/s12598-024-02943-y](https://doi.org/10.1007/s12598-024-02943-y).
- 124 K. Nie, J. Li, H. Lu, R. Zhang, Y. Chen and F. Pan, Enhanced hydrogen storage properties of MgH<sub>2</sub> with alkali-ized Nb<sub>2</sub>CT<sub>x</sub> MXene: The role of enlarged interlayer spacing and optimized surface, *Sep. Purif. Technol.*, 2025, **354**, 129069, DOI: [10.1016/j.seppur.2024.129069](https://doi.org/10.1016/j.seppur.2024.129069).
- 125 H. Wan, S. Zhou, D. Wei, J. Qiu, Z. Ding, Y. Chen, J. Wang and F. Pan, Enhancing hydrogen storage properties of MgH<sub>2</sub> via reaction-induced construction of Ti/Co/Mn-based multiphase catalytic system, *Sep. Purif. Technol.*, 2025, **355**, 129776, DOI: [10.1016/j.seppur.2024.129776](https://doi.org/10.1016/j.seppur.2024.129776).
- 126 M. S. El-Eskandarany, F. Al-Ajmi, M. Banyan and A. Al-Duweesh, Synergetic effect of reactive ball milling and cold pressing on enhancing the hydrogen storage behavior of nanocomposite MgH<sub>2</sub>/10 wt% TiMn<sub>2</sub> binary system, *Int. J. Hydrogen Energy*, 2019, **44**, 26428–26443, DOI: [10.1016/j.ijhydene.2019.08.093](https://doi.org/10.1016/j.ijhydene.2019.08.093).
- 127 C. Peng, Y. Li and Q. Zhang, Amorphous mixed transition metal oxides: A novel catalyst for boosting dehydrogenation of MgH<sub>2</sub>, *Scr. Mater.*, 2024, **248**, 116149, DOI: [10.1016/j.scriptamat.2024.116149](https://doi.org/10.1016/j.scriptamat.2024.116149).
- 128 H. Liu, X. Duan, Z. Wu, H. Luo, X. Wang, C. Huang, Z. Lan, W. Zhou, J. Guo and M. Ismail, Exfoliation of compact layered Ti<sub>2</sub>AlC<sub>2</sub> MAX to open layered Ti<sub>2</sub>VC<sub>2</sub> MXene towards enhancing the hydrogen storage properties of MgH<sub>2</sub>, *Chem. Eng. J.*, 2023, **468**, 143688, DOI: [10.1016/j.cej.2023.143688](https://doi.org/10.1016/j.cej.2023.143688).
- 129 W. Sun, H. Zhang, Q. He, R. Zhang, J. Wu, Y. Wang, Y. Bu, B. Li, L. Sun, F. Xu, Y. Lu, T. Yu, Z. Yang and L. Geng, Monolithic nickel-doped molybdenum nitride improves hydrogen storage properties of MgH<sub>2</sub>, *J. Alloys Compd.*, 2025, **1010**, 177000, DOI: [10.1016/j.jallcom.2024.177000](https://doi.org/10.1016/j.jallcom.2024.177000).
- 130 Y. Chen, B. Sun, G. Zhang, S. Ni, C. Li, J. Tian, Y. Zhang and X. Li, MOF-derived Ni<sub>3</sub>Fe/Ni/NiFe<sub>2</sub>O<sub>4</sub>@C for enhanced hydrogen storage performance of MgH<sub>2</sub>, *J. Energy Chem.*, 2025, **101**, 333–344, DOI: [10.1016/j.jechem.2024.09.048](https://doi.org/10.1016/j.jechem.2024.09.048).
- 131 C. Peng, X. Chen and Q. Zhang, Enhancing dehydrogenation kinetics of MgH<sub>2</sub> through doping with the Nb<sub>2</sub>O<sub>5</sub>-C/Ti<sub>3</sub>C<sub>2</sub>T<sub>x</sub> catalyst synthesized by fast Joule heating, *J. Alloys Compd.*, 2025, **1014**, 178709, DOI: [10.1016/j.jallcom.2025.178709](https://doi.org/10.1016/j.jallcom.2025.178709).
- 132 H. Gao, M. Song, B. Zhao, J. Liu, R. Shi, Y. Liu, X. Hu and Y. Zhu, Assisting molybdenum trioxide catalysis by engineering oxygen vacancy for enhancing hydrogen storage performance of magnesium hydride, *J. Colloid Interface Sci.*, 2025, **678**, 343–352, DOI: [10.1016/j.jcis.2024.09.056](https://doi.org/10.1016/j.jcis.2024.09.056).



- 133 X. Lu, X. Yang, X. Liang, J. Su, J. Kong, Y. Pan and Q. Hou, MXene  $\text{Ti}_3\text{C}_2@\text{NiO}$  catalysts for improving the kinetic performance of  $\text{MgH}_2$  hydrogen storage, *J. Alloys Compd.*, 2025, **1010**, 177963, DOI: [10.1016/j.jallcom.2024.177963](https://doi.org/10.1016/j.jallcom.2024.177963).
- 134 L. Wang, T. Zhong, F. Wu, D. Chen, Z. Yao, L. Chen and L. Zhang, Anions intercalated two-dimension high entropy layered metal oxides for enhanced hydrogen storage in magnesium hydride, *Chem. Eng. J.*, 2025, **505**, 159591, DOI: [10.1016/j.cej.2025.159591](https://doi.org/10.1016/j.cej.2025.159591).
- 135 X. Ou, J. Li, H. Lv, L. Wang and T. Yang, Effect of nanosized nickel diselenide on hydrogen storage properties of ball-milled magnesium hydride, *Int. J. Hydrogen Energy*, 2025, **101**, 594–604, DOI: [10.1016/j.ijhydene.2024.12.465](https://doi.org/10.1016/j.ijhydene.2024.12.465).
- 136 H. Chu, C. Yin, Y. Xia, Y. S. Chua, S. Qiu, F. Xu and L. Sun, Highly dispersed Ni nanoparticles decorated  $\text{TiO}_2$  microspheres for enhancing hydrogen storage properties of magnesium hydride, *J. Alloys Compd.*, 2024, **997**, 174927, DOI: [10.1016/j.jallcom.2024.174927](https://doi.org/10.1016/j.jallcom.2024.174927).
- 137 H. Xiao, F. Qian, X. Zhang, H. Hu, R. Tang, C. Hu, W. Zhou, X. He, Z. Pu, C. Ma, R. Wang, L. Yi and Q. Chen, Effect of  $\text{Ce}_{0.6}\text{Zr}_{0.4}\text{O}_2$  nanocrystals on boosting hydrogen storage performance of  $\text{MgH}_2$ , *Chem. Eng. J.*, 2024, **494**, 153203, DOI: [10.1016/j.cej.2024.153203](https://doi.org/10.1016/j.cej.2024.153203).
- 138 S. Long, Y. Qin, H. Fu, J. Hu, H. Xue, Y. Chen and F. Pan, Hydrogen storage properties of  $\text{MgH}_2$  modified by efficient  $\text{Co}_3\text{V}_2\text{O}_8$  catalyst, *Sep. Purif. Technol.*, 2024, **341**, 126901, DOI: [10.1016/j.seppur.2024.126901](https://doi.org/10.1016/j.seppur.2024.126901).
- 139 K. Nie, J. Li, H. Lu, R. Zhang, Y. Chen and F. Pan, Cubic  $\text{NaNbO}_3$  synthesized by alkali treatment of  $\text{Nb}_2\text{C}$  MXene for enhancing the hydrogen storage of  $\text{MgH}_2$ , *Sep. Purif. Technol.*, 2025, **359**, 130839, DOI: [10.1016/j.seppur.2024.130839](https://doi.org/10.1016/j.seppur.2024.130839).
- 140 C. Ge, P. Wu, C. Ni, B. Wang, C. Hou, X. Sun, X. Yang, W. Du and X. Xie, Effect of  $\text{Al}_3\text{V}$  alloy on the hydrogen storage properties of  $\text{MgH}_2$ , *Int. J. Hydrogen Energy*, 2025, **97**, 738–747, DOI: [10.1016/j.ijhydene.2024.11.417](https://doi.org/10.1016/j.ijhydene.2024.11.417).
- 141 Z. Lu, H. Liu, H. Luo, Z. Wu, H. Ning, Y. Fan, X. Wang, X. Huang, C. Huang, Z. Lan, W. Zhou and J. Guo, Effect of  $\text{Ti}_{0.9}\text{Zr}_{0.1}\text{Mn}_{1.5}\text{V}_{0.3}$  alloy catalyst on hydrogen storage kinetics and cycling stability of magnesium hydride, *Chem. Eng. J.*, 2024, **479**, 147893, DOI: [10.1016/j.cej.2023.147893](https://doi.org/10.1016/j.cej.2023.147893).
- 142 X. Xie, L. Xiao, H. Kimura, P. Wu, W. Du and Y. Wu, Effects of layered walnut  $\text{NiS@NTA}$  on hydrogen storage performance of  $\text{MgH}_2$ , *Sep. Purif. Technol.*, 2025, **359**, 130837, DOI: [10.1016/j.seppur.2024.130837](https://doi.org/10.1016/j.seppur.2024.130837).
- 143 Q. Yuan, C. Peng, C. Yang, Y. Li, Q. Zhang, Y. Lv, G. Liu and D. Liu, Facilitated hydrogen storage properties of  $\text{MgH}_2$  by Ni nanoparticles anchored on  $\text{Mo}_2\text{C@C}$  nanosheets, *Int. J. Hydrogen Energy*, 2024, **85**, 12–19, DOI: [10.1016/j.ijhydene.2024.08.292](https://doi.org/10.1016/j.ijhydene.2024.08.292).
- 144 T. Zhong, T. Xu, L. Zhang, F. Wu, Y. Jiang and X. Yu, Designing multivalent NiMn-based layered nanosheets with high specific surface area and abundant active sites for solid-state hydrogen storage in magnesium hydride, *J. Magn. Alloys*, 2025, **13**, 148–160, DOI: [10.1016/j.jma.2024.04.027](https://doi.org/10.1016/j.jma.2024.04.027).
- 145 S. N. Nyamsi, M. V. Lototskyy, V. A. Yartys, G. Capurso, M. W. Davids and S. Pasupathi, 200 NL  $\text{H}_2$  hydrogen storage tank using  $\text{MgH}_2\text{-TiH}_2\text{-C}$  nanocomposite as H storage material, *Int. J. Hydrogen Energy*, 2021, **46**, 19046–19059, DOI: [10.1016/j.ijhydene.2021.03.055](https://doi.org/10.1016/j.ijhydene.2021.03.055).
- 146 X. Zhang, S. Ju, C. Li, J. Hao, Y. Sun, X. Hu, W. Chen, J. Chen, L. He, G. Xia, F. Fang, D. Sun and X. Yu, Atomic reconstruction for realizing stable solar-driven reversible hydrogen storage of magnesium hydride, *Nat. Commun.*, 2024, **15**, 2815, DOI: [10.1038/s41467-024-47077-y](https://doi.org/10.1038/s41467-024-47077-y).
- 147 Z. Cheng, Y. Guan, H. Wen, Z. Li, K. Cui, Q. Pei, S. Wang, C. Pistidda, J. Guo, H. Cao and P. Chen, Light-Driven De/Rehydrogenation of a LiH Surface under Ambient Conditions, *J. Phys. Chem. Lett.*, 2024, **15**, 6662–6667, DOI: [10.1021/acs.jpcclett.4c00874](https://doi.org/10.1021/acs.jpcclett.4c00874).
- 148 J. P. Weiler, Meridian Lightweight Technologies, Inc., *Global Magnesium Market: Supply, Demand, and Future Outlook*. Available online (assessed on 5 July 2025): <https://www.lightmetalage.com/news/industry-news/magnesium/global-magnesium-market-supply-demand-and-future-outlook/>.
- 149 U. Wietelmann, M. Felderhoff and P. Rittmeyer, *Hydrides. In Ullmann's Encyclopedia of Industrial Chemistry*, Wiley-VCH, 2016, DOI: [10.1002/14356007.a13\\_199.pub2](https://doi.org/10.1002/14356007.a13_199.pub2).
- 150 H. Uesugi, T. Sugiyama, H. Nii, T. Ito and I. Nakatsugawa, Industrial production of  $\text{MgH}_2$  and its application, *J. Alloys Compd.*, 2011, **509S**, S650–S653, DOI: [10.1016/j.jallcom.2010.11.047](https://doi.org/10.1016/j.jallcom.2010.11.047).
- 151 P. Yao, H. Zhao, M. Zhang, C. Xia, T. Yang and Q. Li, Synthesis of  $\alpha\text{-AlH}_3$  by organic liquid reduction method and its hydrogen desorption performance, *Int. J. Hydrogen Energy*, 2023, **48**, 34132–34140, DOI: [10.1016/j.ijhydene.2023.05.170](https://doi.org/10.1016/j.ijhydene.2023.05.170).
- 152 M. J. Krause, F. Orlandi, A. T. Saurage and J. R. Zietz Jr., Aluminum Compounds, Organic. In *Ullmann's Encyclopedia of Industrial Chemistry*, Wiley-VCH, 2020, DOI: [10.1002/14356007.a01\\_543](https://doi.org/10.1002/14356007.a01_543).
- 153 L. Wang, A. Rawal, M. Z. Quadir and K.-F. Aguey-Zinsou, Formation of aluminium hydride ( $\text{AlH}_3$ ) via the decomposition of organoaluminium and hydrogen storage properties, *Int. J. Hydrogen Energy*, 2018, **43**, 16749–16757, DOI: [10.1016/j.ijhydene.2017.12.052](https://doi.org/10.1016/j.ijhydene.2017.12.052).
- 154 P. Mauron, F. Buchter, O. Friedrichs, A. Remhof, M. Biemann, C. N. Zwicky and A. Züttel, Stability and Reversibility of  $\text{LiBH}_4$ , *J. Phys. Chem. B*, 2008, **112**, 906–910, DOI: [10.1021/jp077572r](https://doi.org/10.1021/jp077572r).
- 155 A. Züttel, P. Wenger, S. Rentsch, P. Sudan, P. Mauron and C. Emmenegger,  $\text{LiBH}_4$  a new hydrogen storage material, *J. Power Sources*, 2003, **118**, 1–7, DOI: [10.1016/S0378-7753\(03\)00054-5](https://doi.org/10.1016/S0378-7753(03)00054-5).
- 156 A. Züttel, A. Borgschulte and S. Orimo, Tetrahydroborates as new hydrogen storage materials, *Scripta Mater.*, 2007, **56**, 823–828, DOI: [10.1016/j.scriptamat.2007.01.010](https://doi.org/10.1016/j.scriptamat.2007.01.010).
- 157 P. Martelli, R. Caputo, A. Remhof, P. Mauron, A. Borgschulte and A. Züttel, Stability and Decomposition of  $\text{NaBH}_4$ , *J. Phys. Chem. C*, 2010, **114**, 7173–7177, DOI: [10.1021/jp909341z](https://doi.org/10.1021/jp909341z).
- 158 S. Kumar, A. Jain, H. Miyaoka, T. Ichikawa and Y. Kojima, Study on the thermal decomposition of  $\text{NaBH}_4$  catalyzed by  $\text{ZrCl}_4$ , *Int. J. Hydrogen Energy*, 2017, **42**, 22432–22437, DOI: [10.1016/j.ijhydene.2017.02.060](https://doi.org/10.1016/j.ijhydene.2017.02.060).
- 159 S. Kumar, Y. Kojima and G. Kumar Dey, Synergic effect of  $\text{ZrCl}_4$  on thermal dehydrogenation kinetics of  $\text{KBH}_4$ ,



- J. Alloys Compd.*, 2017, **718**, 134–138, DOI: [10.1016/j.jallcom.2017.05.118](https://doi.org/10.1016/j.jallcom.2017.05.118).
- 160 I. Saldan, Decomposition and formation of magnesium borohydride, *Int. J. Hydren Energy*, 2016, **41**, 11201–11224, DOI: [10.1016/j.ijhydene.2016.05.062](https://doi.org/10.1016/j.ijhydene.2016.05.062).
- 161 R. J. Newhouse, V. Stavila, S.-J. Hwang, L. E. Klebanoff and J. Z. Zhang, Reversibility and Improved Hydrogen Release of Magnesium Borohydride, *J. Phys. Chem. C*, 2010, **114**, 5224–5232, DOI: [10.1021/jp9116744](https://doi.org/10.1021/jp9116744).
- 162 H.-W. Li, K. Kikuchi, Y. Nakamori, N. Ohba, K. Miwa, S. Towata and S. Orimo, Dehydrogenating and rehydrogenating processes of well-crystallized Mg(BH<sub>4</sub>)<sub>2</sub> accompanying with formation of intermediate compounds, *Acta Mater.*, 2008, **56**, 1342–1347, DOI: [10.1016/j.actamat.2007.11.023](https://doi.org/10.1016/j.actamat.2007.11.023).
- 163 Y. Yan, D. Rentsch and A. Remhof, Controllable decomposition of Ca(BH<sub>4</sub>)<sub>2</sub> for reversible hydrogen storage, *Phys. Chem. Chem. Phys.*, 2017, **19**, 7788–7792, DOI: [10.1039/c7cp00448f](https://doi.org/10.1039/c7cp00448f).
- 164 C. J. Sahle, C. Sternemann, C. Giacobbe, Y. Yan, C. Weis, M. Harder, Y. Forov, G. Spiekermann, M. Tolan, M. Krischa and A. Remhof, Formation of CaB<sub>6</sub> in the thermal decomposition of the hydrogen storage material Ca(BH<sub>4</sub>)<sub>2</sub>, *Phys. Chem. Chem. Phys.*, 2016, **18**, 19866–19872, DOI: [10.1039/c6cp02495e](https://doi.org/10.1039/c6cp02495e).
- 165 E. Rönnebro and E. H. Majzoub, Calcium Borohydride for Hydrogen Storage: Catalysis and Reversibility, *J. Phys. Chem. B*, 2007, **111**, 12045–12047, DOI: [10.1021/jp0764541](https://doi.org/10.1021/jp0764541).
- 166 Y. Kim, D. Reed, Y.-S. Lee, J. Y. Lee, J.-H. Shim, D. Book and Y. W. Cho, Identification of the Dehydrogenated Product of Ca(BH<sub>4</sub>)<sub>2</sub>, *J. Phys. Chem. C*, 2009, **113**, 5865–5871, DOI: [10.1021/jp8094038](https://doi.org/10.1021/jp8094038).
- 167 X. Yang, J. Su, X. Lu, J. Kong, D. Huo, Y. Pan and W. Li, Application and development of LiBH<sub>4</sub> hydrogen storage materials, *J. Alloys Compd.*, 2024, **1001**, 175174, DOI: [10.1016/j.jallcom.2024.175174](https://doi.org/10.1016/j.jallcom.2024.175174).
- 168 Y. Xu, Y. Zhou, Y. Li, M. Ashuri and Z. Ding, Engineering LiBH<sub>4</sub>-Based Materials for Advanced Hydrogen Storage: A Critical Review of Catalysis, Nanoconfinement, and Composite Design, *Molecules*, 2024, **29**, 5774, DOI: [10.3390/molecules29235774](https://doi.org/10.3390/molecules29235774).
- 169 S. Wang, Z. Li, M. Gao, Y. Liu and H. Pan, Low-temperature and reversible hydrogen storage advances of light metal borohydrides, *Renewable Sustainable Energy Rev.*, 2025, **208**, 115000, DOI: [10.1016/j.rser.2024.115000](https://doi.org/10.1016/j.rser.2024.115000).
- 170 X. Yang, J. Kong, X. Lu, J. Su, Q. Hou and W. Li, Hydrogen storage properties of metal borohydrides and their improvements: Research progress and trends, *Int. J. Hydren Energy*, 2024, **60**, 308–323, DOI: [10.1016/j.ijhydene.2024.02.097](https://doi.org/10.1016/j.ijhydene.2024.02.097).
- 171 E. M. Dematteis, M. B. Amdisen, T. Autrey, J. Barale, M. E. Bowden, C. E. Buckley, Y. W. Cho, S. Deledda, M. Dornheim, P. de Jongh, J. B. Grinderslev, G. Gizer, V. Gulino, B. C. Hauback, M. Heere, T. W. Heo, T. D. Humphries, T. R. Jensen, S. Y. Kang, Y.-S. Lee, H.-W. Li, S. Li, K. T. Møller, P. Ngene, S. Orimo, M. Paskevicius, M. Polanski, S. Takagi, L. Wan, B. C. Wood, M. Hirscher and M. Baricco, Hydrogen storage in complex hydrides: past activities and new trends, *Prog. Energy*, 2022, **4**, 032009, DOI: [10.1088/2516-1083/ac7499](https://doi.org/10.1088/2516-1083/ac7499).
- 172 S. Wang, Z. Li, M. Gao, Y. Liu and H. Pan, Low-temperature and reversible hydrogen storage advances of light metal borohydrides, *Renewable Sustainable Energy Rev.*, 2025, **208**, 115000, DOI: [10.1016/j.rser.2024.115000](https://doi.org/10.1016/j.rser.2024.115000).
- 173 A. Jain, S. Agarwal and T. Ichikawa, Catalytic Tuning of Sorption Kinetics of Lightweight Hydrides: A Review of the Materials and Mechanism, *Catalysts*, 2018, **8**, 651, DOI: [10.3390/catal8120651](https://doi.org/10.3390/catal8120651).
- 174 C. J. Tomasso, A. L. Pham, T. M. Mattox and J. J. Urban, Using Additives to Control the Decomposition Temperature of Sodium Borohydride, *J. Energy Power Technol.*, 2020, **2**, 009, DOI: [10.21926/jept.2002009](https://doi.org/10.21926/jept.2002009).
- 175 T. D. Humphries, G. N. Kalantzopoulos, I. Llamas-Jansa, J. E. Olsen and B. C. Hauback, Reversible Hydrogenation Studies of NaBH<sub>4</sub> Milled with Ni-Containing Additives, *J. Phys. Chem. C*, 2013, **117**, 6060–6065, DOI: [10.1021/jp312105w](https://doi.org/10.1021/jp312105w).
- 176 J. Mao and D. H. Gregory, Recent Advances in the Use of Sodium Borohydride as a Solid State Hydrogen Store, *Energies*, 2015, **8**, 430–453, DOI: [10.3390/en8010430](https://doi.org/10.3390/en8010430).
- 177 C. Comanescu, Calcium Borohydride Ca(BH<sub>4</sub>)<sub>2</sub>: Fundamentals, Prediction and Probing for High-Capacity Energy Storage Applications, Organic Synthesis and Catalysis, *Energies*, 2023, **16**, 4536, DOI: [10.3390/en16114536](https://doi.org/10.3390/en16114536).
- 178 A. Schneemann, J. L. White, S. Y. Kang, S. Jeong, L. F. Wan, E. S. Cho, T. W. Heo, D. Prendergast, J. J. Urban, B. C. Wood, M. D. Allendorf and V. Stavila, Nanostructured Metal Hydrides for Hydrogen Storage, *Chem. Rev.*, 2018, **118**, 10775–10839, DOI: [10.1021/acs.chemrev.8b00313](https://doi.org/10.1021/acs.chemrev.8b00313).
- 179 X. Yang, J. Su, X. Lu, J. Kong, D. Huo, Y. Pan and W. Li, Application and development of LiBH<sub>4</sub> hydrogen storage materials, *J. Alloys Compd.*, 2024, **1001**, 175174, DOI: [10.1016/j.jallcom.2024.175174](https://doi.org/10.1016/j.jallcom.2024.175174).
- 180 M. A. Wahab, I. Urooj, M. Sohail, M. R. Karim, I. A. Alnaser, A. Abdala and R. Haque, Advancing Catalysts by Nanoconfinement and Catalysis for Enhanced Hydrogen Production from Magnesium Borohydride: A Review, *Chem. – Asian J.*, 2024, **19**, e202400174, DOI: [10.1002/asia.202400174](https://doi.org/10.1002/asia.202400174).
- 181 Y. Lv, Y. Jing, B. Zhang, Y. Li, G. Xia, X. Yu, P. Huang, H. Huang, B. Liu, J. Yuan and Y. Wu, 2D transition metal carbides trigger enhanced dehydrogenation and reversibility properties in Mg(BH<sub>4</sub>)<sub>2</sub>, *Chem. Eng. J.*, 2023, **478**, 147387, DOI: [10.1016/j.cej.2023.147387](https://doi.org/10.1016/j.cej.2023.147387).
- 182 I. L. Jansa, G. N. Kalantzopoulos, K. Nordholm and B. C. Hauback, Destabilization of NaBH<sub>4</sub> by Transition Metal Fluorides, *Molecules*, 2020, **25**, 780, DOI: [10.3390/molecules25040780](https://doi.org/10.3390/molecules25040780).
- 183 A. Nale, F. Pendolino, A. Maddalena and P. Colombo, Enhanced hydrogen release of metal borohydrides M(BH<sub>4</sub>)<sub>n</sub> (M = Li, Na, Mg, Ca) mixed with reduced graphene oxide, *Int. J. Hydrogen Energy*, 2016, **41**, 11225–11231, DOI: [10.1016/j.ijhydene.2016.04.191](https://doi.org/10.1016/j.ijhydene.2016.04.191).
- 184 M. Au and A. Jurgensen, Modified Lithium Borohydrides for Reversible Hydrogen Storage, *J. Phys. Chem. B*, 2006, **110**, 7062–7067, DOI: [10.1021/jp056240o](https://doi.org/10.1021/jp056240o).
- 185 Z. Li, K. Xian, H. Chen, M. Gao, S. Qu, M. Wu, Y. Yang, W. Sun, C. Gao, Y. Liu, X. Zhang and H. Pan, Enhanced



- reversible hydrogen storage properties of wrinkled graphene microflowers confined LiBH<sub>4</sub> system with high volumetric hydrogen storage capacity, *Mater. Rep.: Energy*, 2024, **4**, 100249, DOI: [10.1016/j.matre.2024.100249](https://doi.org/10.1016/j.matre.2024.100249).
- 186 Y. Jia, P. Zhou, X. Xiao, X. Wang, B. Han, J. Wang, F. Xu, L. Sun and L. Chen, Synergetic action of 0D/2D/3D N-doped carbon nanocages and NbB<sub>2</sub> nanocatalyst on reversible hydrogen storage performance of lithium borohydride, *Chem. Eng. J.*, 2024, **485**, 150090, DOI: [10.1016/j.cej.2024.150090](https://doi.org/10.1016/j.cej.2024.150090).
- 187 K. Xian, B. Nie, Z. Li, M. Gao, Z. Li, C. Shang, Y. Liu, Z. Guo and H. Pan, TiO<sub>2</sub> decorated porous carbonaceous network structures offer confinement, catalysis and thermal conductivity for effective hydrogen storage of LiBH<sub>4</sub>, *Chem. Eng. J.*, 2021, **407**, 127156, DOI: [10.1016/j.cej.2020.127156](https://doi.org/10.1016/j.cej.2020.127156).
- 188 S. Wang, M. H. Wu, Y. Y. Zhu, Z. L. Li, Y. X. Yang, Y. Z. Li, H. F. Liu and M. X. Gao, Reactive destabilization and bidirectional catalyzation for reversible hydrogen storage of LiBH<sub>4</sub> by novel waxberry-like nano-additive assembled from ultrafine Fe<sub>3</sub>O<sub>4</sub> particles, *J. Mater. Sci. Technol.*, 2024, **173**, 63–71, DOI: [10.1016/j.jmst.2023.07.020](https://doi.org/10.1016/j.jmst.2023.07.020).
- 189 W. Zhang, L. Zhou, X. Zhang, L. Zhang, Z. Lou, B. Guo, Z. Hong, M. Gao, W. Sun, Y. Liu and H. Pan, From nanorods to nanoparticles: Morphological engineering enables remarkable hydrogen storage by lithium borohydride, *Nano Energy*, 2024, **130**, 110128, DOI: [10.1016/j.nanoen.2024.110128](https://doi.org/10.1016/j.nanoen.2024.110128).
- 190 G. Na, W.-G. Cui, H. Shi, Z. Li, F. Gao, X. Wang, K. Wang, Y. Gao, Y. Yang, Z. Shen, Y. Liu, J. Miao and H. Pan, *In Situ* Generation and Stabilization of Multiple Catalysts by Introducing a Graphene-Supported FeF<sub>2</sub>/FeO<sub>x</sub> Additive for Enhancing the Hydrogen Storage of LiBH<sub>4</sub>, *ACS Appl. Energy Mater.*, 2025, **8**, 3802–3811, DOI: [10.1021/acsaem.4c02891](https://doi.org/10.1021/acsaem.4c02891).
- 191 Y. Liu, W. Chen, S. Ju, X. Yu and G. Xia, Stable hydrogen storage of lithium borohydrides *via* the catalytic effect of Ni<sub>2</sub>B induced by thermodynamic destabilization reaction, *J. Mat. Sci. Technol.*, 2024, **202**, 192–200, DOI: [10.1016/j.jmst.2024.03.035](https://doi.org/10.1016/j.jmst.2024.03.035).
- 192 X. Zhang, L. Zhang, W. Zhang, Z. Ren, Z. Huang, J. Hu, M. Gao, H. Pan and Y. Liu, Nano-synergy enables highly reversible storage of 9.2 wt% hydrogen at mild conditions with lithium borohydride, *Nano Energy*, 2021, **83**, 105839, DOI: [10.1016/j.nanoen.2021.105839](https://doi.org/10.1016/j.nanoen.2021.105839).
- 193 Y. Ding, C. Li, X. Zhang, W. Chen, X. Yu and G. Xia, Spatial Confinement of Lithium Borohydride in Bimetallic CoNi-Doped Hollow Carbon Frameworks for Stable Hydrogen Storage, *ACS Appl. Mater. Interfaces*, 2024, **16**, 50717–50725, DOI: [10.1021/acsaami.4c09512](https://doi.org/10.1021/acsaami.4c09512).
- 194 Z. Li, M. Gao, J. Gu, K. Xian, Z. Yao, C. Shang, Y. Liu, Z. Guo and H. Pan, *In Situ* Introduction of Li<sub>3</sub>BO<sub>3</sub> and NbH Leads to Superior Cyclic Stability and Kinetics of a LiBH<sub>4</sub>-Based Hydrogen Storage System, *ACS Appl. Mater. Interfaces*, 2020, **12**, 893–903, DOI: [10.1021/acsaami.9b19287](https://doi.org/10.1021/acsaami.9b19287).
- 195 J. Xu, Y. Li, J. Cao, R. Meng, W. Wang and Z. Chen, Preparation of graphene-supported highly dispersed nickel nanoparticles for the improved generation of hydrogen from ball-milled LiBH<sub>4</sub>, *Catal. Sci. Technol.*, 2015, **5**, 1821–1828, DOI: [10.1039/C4CY01276C](https://doi.org/10.1039/C4CY01276C).
- 196 L. Chong, J. Zou, X. Zengab and W. Ding, Effects of LnF<sub>3</sub> on reversible and cyclic hydrogen sorption behaviors in NaBH<sub>4</sub>: electronic nature of Ln versus crystallographic factors, *J. Mater. Chem. A*, 2015, **3**, 4493–4500, DOI: [10.1039/c4ta06556e](https://doi.org/10.1039/c4ta06556e).
- 197 W. Chen, S. Ju, Y. Sun, T. Zhang, J. Wang, J. Ye, G. Xia and X. Yu, Thermodynamically favored stable hydrogen storage reversibility of NaBH<sub>4</sub> inside of bimetallic nanoporous carbon nanosheets, *J. Mater. Chem. A*, 2022, **10**, 7122–7129, DOI: [10.1039/d1ta10361j](https://doi.org/10.1039/d1ta10361j).
- 198 M. S. Salman, M. Zubair, Y. Yang, N. M. Bedford and K.-F. Aguey-Zinsou, Doping and Structure-Promoted Destabilization of NaBH<sub>4</sub> Nanocubes for Hydrogen Storage, *ACS Appl. Nano Mater.*, 2023, **6**, 4178–4189, DOI: [10.1021/acsaem.2c05209](https://doi.org/10.1021/acsaem.2c05209).
- 199 S. Kumar, Y. Kojima and G. K. Dey, Synergic effect of ZrCl<sub>4</sub> on thermal dehydrogenation kinetics of KBH<sub>4</sub>, *J. Alloys Compd.*, 2017, **718**, 134–138, DOI: [10.1016/j.jallcom.2017.05.118](https://doi.org/10.1016/j.jallcom.2017.05.118).
- 200 H. Zhang, G. Xia, J. Zhang, D. Sun, Z. Guo and X. Yu, Graphene-Tailored Thermodynamics and Kinetics to Fabricate Metal Borohydride Nanoparticles with High Purity and Enhanced Reversibility, *Adv. Energy Mater.*, 2018, **8**, 1702975, DOI: [10.1002/aenm.201702975](https://doi.org/10.1002/aenm.201702975).
- 201 Z. Zhang, D. Gao, J. Zheng, A. Xia, Q. Zhang, L. Wang and L. Zhang, Heterostructured VF<sub>4</sub>@Ti<sub>3</sub>C<sub>2</sub> catalyst improving reversible hydrogen storage properties of Mg(BH<sub>4</sub>)<sub>2</sub>, *Chem. Eng. J.*, 2023, **460**, 141690, DOI: [10.1016/j.cej.2023.141690](https://doi.org/10.1016/j.cej.2023.141690).
- 202 X. Wang, X. Xiao, J. Zheng, X. Huang, M. Chen and L. Chen, *In-situ* synthesis of amorphous Mg(BH<sub>4</sub>)<sub>2</sub> and chloride composite modified by NbF<sub>5</sub> for superior reversible hydrogen storage properties, *Int. J. Hydrogen Energy*, 2020, **45**, 2044–2053, DOI: [10.1016/j.ijhydene.2019.11.023](https://doi.org/10.1016/j.ijhydene.2019.11.023).
- 203 J. Zheng, X. Wang, X. Xiao, H. Cheng, L. Zhang and L. Chen, Improved reversible dehydrogenation properties of Mg(BH<sub>4</sub>)<sub>2</sub> catalyzed by dual-cation transition metal fluorides K<sub>2</sub>TiF<sub>6</sub> and K<sub>2</sub>NbF<sub>7</sub>, *Chem. Eng. J.*, 2021, **412**, 128738, DOI: [10.1016/j.cej.2021.128738](https://doi.org/10.1016/j.cej.2021.128738).
- 204 X. Wang, X. Xiao, J. Zheng, Z. Hang, W. Lin, Z. Yao, M. Zhang and L. Chen, The dehydrogenation kinetics and reversibility improvements of Mg(BH<sub>4</sub>)<sub>2</sub> doped with Ti nanoparticles under mild conditions, *Int. J. Hydrogen Energy*, 2021, **46**, 23737–23747, DOI: [10.1016/j.ijhydene.2021.04.149](https://doi.org/10.1016/j.ijhydene.2021.04.149).
- 205 J. Yuan, H. Huang, Z. Jiang, Y. Lv, B. Liu, B. Zhang, Y. Yan and Y. Wu, Ni-Doped Carbon Nanotube-Mg(BH<sub>4</sub>)<sub>2</sub> Composites for Hydrogen Storage, *ACS Appl. Nano Mater.*, 2021, **4**, 1604–1612, DOI: [10.1021/acsaem.0c02738](https://doi.org/10.1021/acsaem.0c02738).
- 206 A. Xia, J. Zheng, Q. Zhang, M. Lv, Z. Ma and C. Su, Mxene-supported NbVH nanoparticles as efficient catalysts for reversible hydrogen storage in magnesium borohydride, *Chem. Eng. J.*, 2024, **496**, 154381, DOI: [10.1016/j.cej.2024.154381](https://doi.org/10.1016/j.cej.2024.154381).
- 207 J. Gu, M. Gao, H. Pan, Y. Liu, B. Li, Y. Yang, C. Liang, H. Fua and Z. Guo, Improved hydrogen storage performance of Ca(BH<sub>4</sub>)<sub>2</sub>: a synergetic effect of porous morphology and *in situ* formed TiO<sub>2</sub>, *Energy Environ. Sci.*, 2013, **6**, 847–858, DOI: [10.1039/C2EE24121H](https://doi.org/10.1039/C2EE24121H).



- 208 Q. Lai, C. Milanese and K.-F. Aguey-Zinsou, Stabilization of Nanosized Borohydrides for Hydrogen Storage: Suppressing the Melting with  $\text{TiCl}_3$  Doping, *ACS Appl. Energy Mater.*, 2018, **1**, 421–430, DOI: [10.1021/acsaem.7b00082](https://doi.org/10.1021/acsaem.7b00082).
- 209 L. Feng, Y. Liu, Y. Jiang, Y. Guo, Y. Sun and Y. Wang, Light-driven rapid dehydrogenation of  $\text{LiBH}_4\text{-TiF}_3\text{-TiO}_2$  hydrogen storage composite, *J. Alloys Compd.*, 2025, **1010**, 176848, DOI: [10.1016/j.jallcom.2024.176848](https://doi.org/10.1016/j.jallcom.2024.176848).
- 210 X. Zhang, C. Li, J. Ye, X. Hu, W. Chen, F. Fang, D. Sun, Y. Liu, X. Yu and G. Xia, Light-Enabled Reversible Hydrogen Storage of Borohydrides Activated by Photogenerated Vacancies, *J. Am. Chem. Soc.*, 2025, **147**, 2786–2796, DOI: [10.1021/jacs.4c15744](https://doi.org/10.1021/jacs.4c15744).
- 211 V. N. Konoplev and V. M. Bakulina, Some properties of magnesium borohydride, *Russ. Chem. Bull.*, 1971, **20**, 136–138, DOI: [10.1007/BF00849335](https://doi.org/10.1007/BF00849335).
- 212 *Global Sodium Borohydride Market to Hit Sales of USD 2606 Million by 2032, at 5.89% CAGR Growth: Astute Analytica*. <https://www.globenewswire.com/news-release/2024/03/25/2851764/0/en/Global-Sodium-Borohydride-Market-to-Hit-Sales-of-USD-2-606-Million-by-2032-at-5-89-CAGR-Growth-Astute-Analytica.html> (accessed on 5 July 2025).
- 213 H. Hagemann and R. Cerny, Synthetic approaches to inorganic borohydrides, *Dalton Trans.*, 2010, **39**, 6006–6012, DOI: [10.1039/b927002g](https://doi.org/10.1039/b927002g).
- 214 H. C. Brown, Y. M. Choi and S. Narasimhan, Convenient procedure for the conversion of sodium borohydride into lithium borohydride in simple ether solvents, *Inorg. Chem.*, 1981, **20**(12), 4454–4456, DOI: [10.1021/ic50226a091](https://doi.org/10.1021/ic50226a091).
- 215 K. Chłopek, C. Frommen, A. Leon, O. Zabara and M. Fichtner, Synthesis and properties of magnesium tetrahydroborate,  $\text{Mg}(\text{BH}_4)_2$ , *J. Mater. Chem.*, 2007, **17**, 3496–3503, DOI: [10.1039/b702723k](https://doi.org/10.1039/b702723k).
- 216 Y. J. Cho, S. Li, J. L. Snider, M. A. T. Marple, N. A. Strange, J. D. Sugar, F. El Gabaly, A. Schneemann, S. Kang, M. Kang, H. Park, J. Park, L. F. Wan, H. E. Mason, M. D. Allendorf, B. C. Wood, E. S. Cho and V. Stavila, Reversing the Irreversible: Thermodynamic Stabilization of  $\text{LiAlH}_4$  Nanoconfined Within a Nitrogen-Doped Carbon Host, *ACS Nano*, 2021, **15**, 10163–10174, DOI: [10.1021/acsnano.1c02079](https://doi.org/10.1021/acsnano.1c02079).
- 217 I. P. Jain, P. Jain and A. Jain, Novel hydrogen storage materials: A review of lightweight complex hydrides, *J. Alloys Compd.*, 2010, **503**, 303–339, DOI: [10.1016/j.jallcom.2010.04.250](https://doi.org/10.1016/j.jallcom.2010.04.250).
- 218 J.-W. Jang, J.-H. Shim, Y. W. Cho and B.-J. Lee, Thermodynamic calculation of  $\text{LiH} \leftrightarrow \text{Li}_3\text{AlH}_6 \leftrightarrow \text{LiAlH}_4$  reactions, *J. Alloys Compd.*, 2006, **420**, 286–290, DOI: [10.1016/j.jallcom.2005.10.040](https://doi.org/10.1016/j.jallcom.2005.10.040).
- 219 F. Habermann, A. Wirth, K. Burkmann, J. Kraus, B. Störr, H. Stöcker, J. Seidel, J. Kortus, R. Gumeniuk, K. Bohmhammel and F. Mertens, Thermodynamic and kinetic study of the effect of  $\text{LiCl}$  and  $\text{NaCl}$  on the thermal dehydrogenation of  $\text{Ca}(\text{AlH}_4)_2$ , *RSC Mechanochem.*, 2025, **2**, 603–615, DOI: [10.1039/D4mr00140k](https://doi.org/10.1039/D4mr00140k).
- 220 F. Habermann, A. Wirth, K. Burkmann, B. Störr, J. Seidel, R. Gumeniuk, K. Bohmhammel and F. Mertens, Heat Capacity Function, Enthalpy of Formation and Absolute Entropy of  $\text{Mg}(\text{AlH}_4)_2$ , *ChemPhysChem*, 2024, **25**, e202300748, DOI: [10.1002/cphc.202300748](https://doi.org/10.1002/cphc.202300748).
- 221 Rafi-ud-din, L. Zhang, L. Ping and Q. Xuanhui, Catalytic effects of nano-sized  $\text{TiC}$  additions on the hydrogen storage properties of  $\text{LiAlH}_4$ , *J. Alloys Compd.*, 2010, **508**, 119–128, DOI: [10.1016/j.jallcom.2010.08.008](https://doi.org/10.1016/j.jallcom.2010.08.008).
- 222 J. Wang, A. D. Ebner and J. A. Ritter, Physicochemical Pathway for Cyclic Dehydrogenation and Rehydrogenation of  $\text{LiAlH}_4$ , *J. Am. Chem. Soc.*, 2006, **128**, 5949–5954, DOI: [10.1021/ja060045l](https://doi.org/10.1021/ja060045l).
- 223 N. A. M. Y. Omar, Z. Omar, M. Ismail and N. S. M. Mustafa, Enhancing the dehydrogenation properties of  $\text{LiAlH}_4$  through the addition of  $\text{ZrF}_4$  for solid-state hydrogen storage, *J. Alloys Compd.*, 2025, **1010**, 177250, DOI: [10.1016/j.jallcom.2024.177250](https://doi.org/10.1016/j.jallcom.2024.177250).
- 224 Y. Xia, H. Zhang, Y. Sun, L. Sun, F. Xu, S. Sun, G. Zhang, P. Huang, Y. Du, J. Wang, S. P. Verevkin and A. A. Pimerzin, Dehydrogenation effect in improved dehydrogenation of  $\text{LiAlH}_4$  by doping with two-dimensional  $\text{Ti}_3\text{C}_2$ , *Mater. Today Nano*, 2019, **8**, 100054, DOI: [10.1016/j.mtnano.2019.100054](https://doi.org/10.1016/j.mtnano.2019.100054).
- 225 L. Zang, J. Cai, L. Zhao, W. Gao, J. Liu and Y. Wang, Improved hydrogen storage properties of  $\text{LiAlH}_4$  by mechanical milling with  $\text{TiF}_3$ , *J. Alloys Compd.*, 2015, **647**, 756–762, DOI: [10.1016/j.jallcom.2015.06.036](https://doi.org/10.1016/j.jallcom.2015.06.036).
- 226 S.-S. Liu, Z.-B. Li, C.-L. Jiao, X.-L. Si, L.-N. Yang, J. Zhang, H.-Y. Zhou, F.-L. Huang, Z. Gabelica, C. Schick, L.-X. Sun and F. Xu, Improved reversible hydrogen storage of  $\text{LiAlH}_4$  by nano-sized  $\text{TiH}_2$ , *Int. J. Hydrogen Energy*, 2013, **38**, 2770–2777, DOI: [10.1016/j.ijhydene.2012.11.042](https://doi.org/10.1016/j.ijhydene.2012.11.042).
- 227 S.-S. Liu, L.-X. Sun, Y. Zhang, F. Xu, J. Zhang, H.-L. Chu, M.-Q. Fan, T. Zhang, X.-Y. Song and J. P. Grolier, Effect of ball milling time on the hydrogen storage properties of  $\text{TiF}_3$ -doped  $\text{LiAlH}_4$ , *Int. J. Hydrogen Energy*, 2009, **34**, 8079–8085, DOI: [10.1016/j.ijhydene.2009.07.090](https://doi.org/10.1016/j.ijhydene.2009.07.090).
- 228 B. Bogdanovic and M. Schwickardi, Ti-doped alkali metal aluminium hydrides as potential novel reversible hydrogen storage materials, *J. Alloys Compd.*, 1997, **253–254**, 1–9, DOI: [10.1016/S0925-8388\(96\)03049-6](https://doi.org/10.1016/S0925-8388(96)03049-6).
- 229 N. A. Ali and M. Ismail, Modification of  $\text{NaAlH}_4$  properties using catalysts for solid-state hydrogen storage: A review, *Int. J. Hydrogen Energy*, 2021, **46**, 766–782, DOI: [10.1016/j.ijhydene.2020.10.011](https://doi.org/10.1016/j.ijhydene.2020.10.011).
- 230 J. Khan and I. P. Jain, Chloride catalytic effect on hydrogen desorption in  $\text{NaAlH}_4$ , *Int. J. Hydrogen Energy*, 2016, **41**, 8271–8276, DOI: [10.1016/j.ijhydene.2015.11.116](https://doi.org/10.1016/j.ijhydene.2015.11.116).
- 231 J. Khan and I. P. Jain, Catalytic effect of  $\text{Nb}_2\text{O}_5$  on dehydrogenation kinetics of  $\text{NaAlH}_4$ , *Int. J. Hydrogen Energy*, 2016, **41**, 8264–8270, DOI: [10.1016/j.ijhydene.2015.11.072](https://doi.org/10.1016/j.ijhydene.2015.11.072).
- 232 Q. Wan, P. Li, Z. Li, K. Zhao, Z. Liu, L. Wang, F. Zhai, X. Qu and A. A. Volinsky,  $\text{NaAlH}_4$  dehydrogenation properties enhanced by  $\text{MnFe}_2\text{O}_4$  nanoparticles, *J. Power Sourc.*, 2014, **248**, 388–395, DOI: [10.1016/j.jpowsour.2013.09.093](https://doi.org/10.1016/j.jpowsour.2013.09.093).
- 233 Y. Huang, P. Li, Q. Wan, J. Zhang, Y. Li, R. Li, X. Dong and X. Qu, Improved dehydrogenation performance of  $\text{NaAlH}_4$  using  $\text{NiFe}_2\text{O}_4$  nanoparticles, *J. Alloys Compd.*, 2017, **709**, 850–856, DOI: [10.1016/j.jallcom.2017.03.182](https://doi.org/10.1016/j.jallcom.2017.03.182).



- 234 N. S. Mustafa, N. A. Sazelee, N. A. Ali, N. N. Sulaiman and M. Ismail, Enhancement of hydrogen storage properties of NaAlH<sub>4</sub> catalyzed by CuFe<sub>2</sub>O<sub>4</sub>, *Int. J. Hydren Energy*, 2023, **48**, 35197–35205, DOI: [10.1016/j.ijhydene.2023.05.277](https://doi.org/10.1016/j.ijhydene.2023.05.277).
- 235 T. K. Nielsen, M. Polanski, D. Zasada, P. Javadian, F. Besenbacher, J. Bystrzycki, J. Skibsted and T. R. Jensen, Improved Hydrogen Storage Kinetics of Nanoconfined NaAlH<sub>4</sub> Catalyzed with TiCl<sub>3</sub> Nanoparticles, *ACS Nano*, 2011, **5**, 4056–4064, DOI: [10.1021/nm200643b](https://doi.org/10.1021/nm200643b).
- 236 M. Paskevicius, U. Fils, F. Karimi, J. Puzskiel, P. K. Pranzas, C. Pistidda, A. Hoell, E. Welter, A. Schreyer, T. Klassen, M. Dornheim and T. R. Jensen, Cyclic stability and structure of nanoconfined Ti-doped NaAlH<sub>4</sub>, *Int. J. Hydren Energy*, 2016, **41**, 4159–4167, DOI: [10.1016/j.ijhydene.2015.12.185](https://doi.org/10.1016/j.ijhydene.2015.12.185).
- 237 D. Pukazhselvan, B. K. Gupta, A. Srivastava and O. N. Srivastava, Investigations on hydrogen storage behavior of CNT doped NaAlH<sub>4</sub>, *J. Alloys Compd.*, 2005, **403**, 312–317, DOI: [10.1016/j.jallcom.2005.05.008](https://doi.org/10.1016/j.jallcom.2005.05.008).
- 238 B. Bogdanovic, M. Felderhoff, A. Pommerin, F. Schüth and N. Spielkamp, Advanced Hydrogen-Storage Materials Based on Sc-, Ce-, and Pr-Doped NaAlH<sub>4</sub>, *Adv. Mater.*, 2006, **18**, 1198–1201, DOI: [10.1002/adma.200501367](https://doi.org/10.1002/adma.200501367).
- 239 Y. Kima, E.-K. Lee, J.-H. Shima, Y. W. Cho and K. B. Yoon, Mechanochemical synthesis and thermal decomposition of Mg(AlH<sub>4</sub>)<sub>2</sub>, *J. Alloys Compd.*, 2006, **422**, 283–287, DOI: [10.1016/j.jallcom.2005.11.063](https://doi.org/10.1016/j.jallcom.2005.11.063).
- 240 V. Iosub, T. Matsunaga, K. Tange and M. Ishikiriya, Direct synthesis of Mg(AlH<sub>4</sub>)<sub>2</sub> and CaAlH<sub>5</sub> crystalline compounds by ball milling and their potential as hydrogen storage materials, *Int. J. Hydren Energy*, 2009, **34**, 906–912, DOI: [10.1016/j.ijhydene.2008.11.013](https://doi.org/10.1016/j.ijhydene.2008.11.013).
- 241 J. Wang, A. D. Ebner and J. A. Ritter, On the Reversibility of Hydrogen Storage in Novel Complex Hydrides, *Adsorption*, 2005, **11**, 811–816, DOI: [10.1007/s10450-005-6028-y](https://doi.org/10.1007/s10450-005-6028-y).
- 242 N. Morisaku, K. Komiya, L. Yuzhan, H. Yukawa, M. Morinaga, K. Ikeda and S. Orimo, Synthesis and Decomposition of Pure Ca(AlH<sub>4</sub>)<sub>2</sub>, *Adv. Mat. Res.*, 2007, **26–28**, 869–872, DOI: [10.4028/www.scientific.net/AMR.26-28.869](https://doi.org/10.4028/www.scientific.net/AMR.26-28.869).
- 243 C. Li, X. Xiao, P. Ge, J. Xue, S. Li, H. Ge and L. Chen, Investigation on synthesis, structure and catalytic modification of Ca(AlH<sub>4</sub>)<sub>2</sub> complex hydride, *Int. J. Hydren Energy*, 2012, **37**, 936–941, DOI: [10.1016/j.ijhydene.2011.03.151](https://doi.org/10.1016/j.ijhydene.2011.03.151).
- 244 N. A. Sazelee, N. A. Ali, H. Liu and M. Ismail, Improving the desorption properties of LiAlH<sub>4</sub> by the addition of Ni<sub>0.6</sub>Zn<sub>0.4</sub>O, *Int. J. Hydren Energy*, 2024, **56**, 543–551, DOI: [10.1016/j.ijhydene.2023.12.181](https://doi.org/10.1016/j.ijhydene.2023.12.181).
- 245 Y. Bu, L. Sun, F. Xu, Y. Luo, C. Zhang, S. Wei, G. Zhang, H. Pan, J. Zeng and Z. Cao, Improved dehydrogenation of LiAlH<sub>4</sub> by hollow 3D flower-like bimetallic composites M-NC@TiO<sub>2</sub> (M=Ni, Co, Fe, Cu), *Ceram. Int.*, 2024, **50**, 34251–34263, DOI: [10.1016/j.ceramint.2024.06.244](https://doi.org/10.1016/j.ceramint.2024.06.244).
- 246 X. Li, X. Zheng, Q. Ma, B. Xu, Y. Wang and Y. Li, Effect of Co-B on the hydrogen storage properties of LiAlH<sub>4</sub>, *Chem. Phys. Lett.*, 2025, **859**, 141764, DOI: [10.1016/j.cplett.2024.141764](https://doi.org/10.1016/j.cplett.2024.141764).
- 247 R. Cheng, Z. Liu, P. Manasa, Z. Zhao, H. Pan, F. Xu, L. Sun and F. Rosei, Nanoflower-engineered Co<sub>3</sub>O<sub>4</sub>@CoNi-LDO bimetallic oxide: A catalyst for revolutionizing hydrogen storage in LiAlH<sub>4</sub>, *Int. J. Hydrogen Energy*, 2025, **102**, 375–385, DOI: [10.1016/j.ijhydene.2025.01.085](https://doi.org/10.1016/j.ijhydene.2025.01.085).
- 248 J. Wang, A. D. Ebner and J. A. Ritter, On the Reversibility of Hydrogen Storage in Novel Complex Hydrides, *Adsorption*, 2005, **11**, 811–816, DOI: [10.1007/s10450-005-6028-y](https://doi.org/10.1007/s10450-005-6028-y).
- 249 Y. Liu, Y. Pang, X. Zhang, Y. Zhou, M. Gao and H. Pan, Synthesis and hydrogen storage thermodynamics and kinetics of Mg(AlH<sub>4</sub>)<sub>2</sub> submicron rods, *Int. J. Hydren Energy*, 2012, **37**, 18148–18154, DOI: [10.1016/j.ijhydene.2012.09.081](https://doi.org/10.1016/j.ijhydene.2012.09.081).
- 250 X. Fan, X. Xiao, L. Chen, L. Zhang, J. Shao, S. Li, H. Ge and Q. Wang, Significantly improved hydrogen storage properties of NaAlH<sub>4</sub> catalyzed by Ce-based nanoparticles, *J. Mater. Chem. A*, 2013, **1**, 9752–9759, DOI: [10.1039/c3ta11860f](https://doi.org/10.1039/c3ta11860f).
- 251 J. Chen, C. Li, W. Chen, X. Zhang, X. Yu and G. Xia, Tailoring reversible hydrogen storage performance of NaAlH<sub>4</sub> through NiTiO<sub>3</sub> nanorods, *J. Alloys Compd.*, 2024, **971**, 172689, DOI: [10.1016/j.jallcom.2023.172689](https://doi.org/10.1016/j.jallcom.2023.172689).
- 252 Z. Yuan, Y. Fan, Y. Chen, X. Liu, B. Liu and S. Han, Two-dimensional C@TiO<sub>2</sub>/Ti<sub>3</sub>C<sub>2</sub> composite with superior catalytic performance for NaAlH<sub>4</sub>, *Int. J. Hydren Energy*, 2020, **45**, 21666–21675, DOI: [10.1016/j.ijhydene.2020.05.243](https://doi.org/10.1016/j.ijhydene.2020.05.243).
- 253 R. Wu, H. Du, Z. Wang, M. Gao, H. Pan and Y. Liu, Remarkably improved hydrogen storage properties of NaAlH<sub>4</sub> doped with 2D titanium carbide, *J. Power Sourc.*, 2016, **327**, 519–525, DOI: [10.1016/j.jpowsour.2016.07.095](https://doi.org/10.1016/j.jpowsour.2016.07.095).
- 254 N. A. Ali, M. Ismail, M. M. Nasef and A. A. Jalil, Enhanced hydrogen storage properties of NaAlH<sub>4</sub> with the addition of CoTiO<sub>3</sub> synthesised via a solid-state method, *J. Alloys Compd.*, 2023, **934**, 167932, DOI: [10.1016/j.jallcom.2022.167932](https://doi.org/10.1016/j.jallcom.2022.167932).
- 255 C. Prathana and K.-F. Aguey-Zinsou, Tuning the hydrogen thermodynamics of NaAlH<sub>4</sub> by encapsulation within a titanium shell, *Int. J. Hydren Energy*, 2023, **48**, 29240–29255, DOI: [10.1016/j.ijhydene.2023.04.028](https://doi.org/10.1016/j.ijhydene.2023.04.028).
- 256 Y. Sun, X. Zhang, W. Chen, J. Ye, S. Ju, K.-F. Aguey-Zinsou, G. Xia, D. Sun and X. Yu, Light-Driven Reversible Hydrogen Storage in Light-Weight Metal Hydrides Enabled by Photo-thermal Effect, *Small*, 2022, **18**, 2202978, DOI: [10.1002/sml.202202978](https://doi.org/10.1002/sml.202202978).
- 257 D. A. Mosher, S. Arsenault, X. Tang and D. L. Anton, Design, fabrication and testing of NaAlH<sub>4</sub> based hydrogen storage systems, *J. Alloys Compd.*, 2007, **446–447**, 707–712, DOI: [10.1016/j.jallcom.2007.01.042](https://doi.org/10.1016/j.jallcom.2007.01.042).
- 258 J. Graetz, J. Wegrzyn and J. J. Reilly, Regeneration of Lithium Aluminum Hydride, *J. Am. Chem. Soc.*, 2008, **130**, 17790–17794, DOI: [10.1021/ja805353w](https://doi.org/10.1021/ja805353w).
- 259 T. D. Humphries, D. Birkmire, G. S. McGrady, B. C. Hauback and C. M. Jensen, Regeneration of LiAlH<sub>4</sub> at sub-ambient temperatures studied by multinuclear NMR Spectroscopy, *J. Alloys Compd.*, 2017, **723**, 1150–1154, DOI: [10.1016/j.jallcom.2017.06.300](https://doi.org/10.1016/j.jallcom.2017.06.300).
- 260 X. Liu, G. S. McGrady, H. W. Langmi and C. M. Jensen, Facile Cycling of Ti-Doped LiAlH<sub>4</sub> for High Performance Hydrogen Storage, *J. Am. Chem. Soc.*, 2009, **131**(14), 5032–5033, DOI: [10.1021/ja809917g](https://doi.org/10.1021/ja809917g).



- 261 I. Utz, M. Linder, N. Schmidt, J. J. Hu, M. Fichtner and A. Wörner, Experimental study of powder bed behavior of sodium alanate in a lab-scale H<sub>2</sub> storage tank with flow-through mode, *Int. J. Hydrogen Energy*, 2012, **37**, 7645–7653, DOI: [10.1016/j.ijhydene.2012.02.016](https://doi.org/10.1016/j.ijhydene.2012.02.016).
- 262 J. M. Bellosta von Colbe, O. Metz, G. A. Lozano, P. K. Pranzas, H. W. Schmitz, F. Beckmann, A. Schreyer, T. Klassen and M. Dornheim, Behavior of scaled-up sodium alanate hydrogen storage tanks during sorption, *Int. J. Hydrogen Energy*, 2012, **37**, 2807–2811, DOI: [10.1016/j.ijhydene.2011.03.153](https://doi.org/10.1016/j.ijhydene.2011.03.153).
- 263 N. A. Ali, N. A. Sazelee and M. Ismail, An overview of reactive hydride composite (RHC) for solid-state hydrogen storage materials, *Int. J. Hydrogen Energy*, 2021, **46**, 31674–31698, DOI: [10.1016/j.ijhydene.2021.07.058](https://doi.org/10.1016/j.ijhydene.2021.07.058).
- 264 C. Abetz, P. Georgopoulos, C. Pistidda, T. Klassen and V. Abetz, Reactive Hydride Composite Confined in a Polymer Matrix: New Insights into the Desorption and Absorption of Hydrogen in a Storage Material with High Cycling Stability, *Adv. Mater. Technol.*, 2022, **7**, 2101584, DOI: [10.1002/admt.202101584](https://doi.org/10.1002/admt.202101584).
- 265 Z.-Z. Fang, X.-D. Kang, P. Wang, H.-W. Li and S.-I. Orimo, Unexpected dehydrogenation behavior of LiBH<sub>4</sub>/Mg(BH<sub>4</sub>)<sub>2</sub> mixture associated with the *in situ* formation of dual-cation borohydride, *J. Alloys Compd.*, 2010, **491**, L1–L4, DOI: [10.1016/j.jallcom.2009.10.149](https://doi.org/10.1016/j.jallcom.2009.10.149).
- 266 J. Huang, M. Gao, Z. Li, X. Cheng, J. Gu, Y. Liu and H. Pan, Destabilization of combined Ca(BH<sub>4</sub>)<sub>2</sub> and Mg(AlH<sub>4</sub>)<sub>2</sub> for improved hydrogen storage properties, *J. Alloys Compd.*, 2016, **670**, 135–143, DOI: [10.1016/j.jallcom.2016.02.035](https://doi.org/10.1016/j.jallcom.2016.02.035).
- 267 N. N. Sulaiman, M. Ismail, S. N. Timmiati and K. L. Lim, Improved hydrogen storage performances of LiAlH<sub>4</sub> + Mg(BH<sub>4</sub>)<sub>2</sub> composite with TiF<sub>3</sub> addition, *Int. J. Energy Res.*, 2020, 1–17, DOI: [10.1002/er.5984](https://doi.org/10.1002/er.5984).
- 268 H. Xiao, H. Leng, Z. Yu, Q. Li and K.-C. Chou, Improved Hydrogen Storage Properties of Mg(BH<sub>4</sub>)<sub>2</sub>-Mg(AlH<sub>4</sub>)<sub>2</sub> Combined Systems, ed. J. S. Carpenter, *et al.*, *Characterization of Minerals, Metals, and Materials*, Springer, Cham, 2015, DOI: [10.1007/978-3-319-48191-3\\_49](https://doi.org/10.1007/978-3-319-48191-3_49).
- 269 J. J. Vajo, S. L. Skeith and F. Mertens, Reversible Storage of Hydrogen in Destabilized LiBH<sub>4</sub>, *J. Phys. Chem. B*, 2005, **109**, 3719–3722, DOI: [10.1021/jp040769o](https://doi.org/10.1021/jp040769o).
- 270 N. A. Ali and M. Ismail, Advanced hydrogen storage of the Mg–Na–Al system: A review, *J. Magnesium Alloys*, 2021, **9**, 1111–1122, DOI: [10.1016/j.jma.2021.03.031](https://doi.org/10.1016/j.jma.2021.03.031).
- 271 Y.-J. Kwak, M.-Y. Song and K.-T. Lee, Improvement in the Hydrogen Storage Properties of MgH<sub>2</sub> by Adding NaAlH<sub>4</sub>, *Metals*, 2024, **14**, 227, DOI: [10.3390/met14020227](https://doi.org/10.3390/met14020227).
- 272 M. Ismail, Study on the hydrogen storage properties and reaction mechanism of NaAlH<sub>4</sub>-MgH<sub>2</sub>-LiBH<sub>4</sub> ternary-hydride system, *Int. J. Hydrogen Energy*, 2014, **39**, 8340–8346, DOI: [10.1016/j.ijhydene.2014.03.166](https://doi.org/10.1016/j.ijhydene.2014.03.166).
- 273 S. Qu, Y. Yang, C. Yan, M. Gao, M. Wu, Z. Li, S. Wang, Y. Liu, W. Sun, C. Liang, X. Zhang and H. Pan, Catalyzed eutectic LiBH<sub>4</sub>-KBH<sub>4</sub> system nanoconfined at low temperature for superior hydrogen storage reversibility, *J. Mater. Chem. A*, 2025, **13**, 2757–2768, DOI: [10.1039/d4ta06500j](https://doi.org/10.1039/d4ta06500j).
- 274 Q. Zhang, J. Zheng, A. Xia, M. Lv, Z. Ma and M. Liu, Enhanced reversible hydrogen storage in LiBH<sub>4</sub>-Mg(BH<sub>4</sub>)<sub>2</sub> composite with V<sub>2</sub>C-Mxene, *Chem. Eng. J.*, 2024, **487**, 150629, DOI: [10.1016/j.ccej.2024.150629](https://doi.org/10.1016/j.ccej.2024.150629).
- 275 F. Karimi, P. K. Pranzas, J. A. Puzkiel, M. V. C. Riglos, C. Milanese, U. Vainio, C. Pistidda, G. Gizer, T. Klassen, A. Schreyer and M. Dornheim, A comprehensive study on lithium-based reactive hydride composite (Li-RHC) as a reversible solid-state hydrogen storage system toward potential mobile applications, *RSC Adv.*, 2021, **11**, 23122, DOI: [10.1039/d1ra03246a](https://doi.org/10.1039/d1ra03246a).
- 276 M. Ismail and N. S. Mustafa, Improved hydrogen storage properties of NaAlH<sub>4</sub>-MgH<sub>2</sub>-LiBH<sub>4</sub> ternary-hydride system catalyzed by TiF<sub>3</sub>, *Int. J. Hydrogen Energy*, 2016, **41**, 18107–18113, DOI: [10.1016/j.ijhydene.2016.07.090](https://doi.org/10.1016/j.ijhydene.2016.07.090).
- 277 Y. Lv, B. Zhang, H. Huang, X. Yu, T. Xu, J. Chen, B. Liu, J. Yuan, G. Xia and Y. Wu, Excellent low-temperature dehydrogenation performance and reversibility of 0.55LiBH<sub>4</sub>-0.45Mg(BH<sub>4</sub>)<sub>2</sub> composite catalyzed by few-layer Ti<sub>2</sub>C, *J. Alloys Compd.*, 2024, **972**, 172896, DOI: [10.1016/j.jallcom.2023.172896](https://doi.org/10.1016/j.jallcom.2023.172896).
- 278 N. A. Sazelee, N. A. Ali, S. Suwarno, S.-U. Rather and M. Ismail, Reaction mechanism and absorption/desorption kinetics performance of the destabilised KBH<sub>4</sub>-LiAlH<sub>4</sub> system, *Int. J. Hydrogen Energy*, 2025, **109**, 520–527, DOI: [10.1016/j.ijhydene.2025.02.104](https://doi.org/10.1016/j.ijhydene.2025.02.104).
- 279 D. Liu, Q. Liu, T. Si, Q. Zhang, F. Fang, D. Sun, L. Ouyang and M. Zhu, Superior hydrogen storage properties of LiBH<sub>4</sub> catalyzed by Mg(AlH<sub>4</sub>)<sub>2</sub>, *Chem. Commun.*, 2011, **47**, 5741–5743, DOI: [10.1039/C1CC11238D](https://doi.org/10.1039/C1CC11238D).
- 280 K. Xian, M. Gao, Z. Li, J. Gu, Y. Shen, S. Wang, Z. Yao, Y. Liu and H. Pan, Superior Kinetic and Cyclic Performance of a 2D Titanium Carbide Incorporated 2LiH + MgB<sub>2</sub> Composite toward Highly Reversible Hydrogen Storage, *ACS Appl. Energy Mater.*, 2019, **2**, 4853–4864, DOI: [10.1021/acsam.9b00557](https://doi.org/10.1021/acsam.9b00557).
- 281 W. Chen, Y. Sun, T. Xu, J. Ye, G. Xia, D. Sun and X. Yu, Reversible Hydrogen Storage Performance of 2LiBH<sub>4</sub>-MgH<sub>2</sub> Enabled by Dual Metal Borides, *ACS Appl. Energy Mater.*, 2022, **5**, 10501–10508, DOI: [10.1021/acsam.2c01142](https://doi.org/10.1021/acsam.2c01142).
- 282 H. Luo, Y. Yang, L. Lu, G. Li, X. Wang, X. Huang, X. Tao, C. Huang, Z. Lan, W. Zhou, J. Guo and H. Liu, Highly-dispersed nano-TiB<sub>2</sub> derived from the two-dimensional Ti<sub>3</sub>CN MXene for tailoring the kinetics and reversibility of the Li-Mg-B-H hydrogen storage material, *Appl. Surf. Sci.*, 2023, **610**, 155581, DOI: [10.1016/j.apsusc.2022.155581](https://doi.org/10.1016/j.apsusc.2022.155581).
- 283 Z. Ma, J. Zang, W. Hu, Q. Wang, Z. Sun, F. Fang, Y. Song and D. Sun, From Back to Stage: Superior Cycling Stability of 2LiBH<sub>4</sub>-MgH<sub>2</sub> Enabled by Anion Tuning, *Adv. Energy Mater.*, 2024, **14**, 2401156, DOI: [10.1002/aenm.202401156](https://doi.org/10.1002/aenm.202401156).
- 284 Y.-K. Liu, Y.-C. Pang, C.-Q. Li, X.-Y. Zhang, X.-C. Hu, W. Chen, X.-B. Yu and G.-L. Xia, Amorphous VB<sub>2</sub> nanoparticles for stable hydrogen storage of 2LiBH<sub>4</sub>-MgH<sub>2</sub>, *Rare Met.*, 2025, **44**, 5544–5553, DOI: [10.1007/s12598-025-03327-6](https://doi.org/10.1007/s12598-025-03327-6).
- 285 Y. Li, P. Li, Q. Tan, Z. Zhang, Q. Wan, Z. Liu, A. Subramanian and X. Qu, Thermal properties and cycling performance of Ca(BH<sub>4</sub>)<sub>2</sub>/MgH<sub>2</sub> composite for energy



- storage, *Chem. Phys. Lett.*, 2018, **700**, 44–49, DOI: [10.1016/j.cplett.2018.04.011](https://doi.org/10.1016/j.cplett.2018.04.011).
- 286 Y. Li, P. Li and X. Qu, Investigation on  $\text{LiBH}_4\text{-CaH}_2$  composite and its potential for thermal energy storage, *Sci. Rep.*, 2017, **7**, 41754, DOI: [10.1038/srep41754](https://doi.org/10.1038/srep41754).
- 287 N. N. Sulaiman, M. Ismail, S. N. Timmiati and K. L. Lim, Improved hydrogen storage performances of  $\text{LiAlH}_4^+$   $\text{Mg}(\text{BH}_4)_2$  composite with  $\text{TiF}_3$  addition, *Int. J. Energy Res.*, 2021, **45**, 2882–2898, DOI: [10.1002/er.5984](https://doi.org/10.1002/er.5984).
- 288 N. S. Mustafa, F. A. Halim Yap, M. S. Yahya and M. Ismail, The hydrogen storage properties and reaction mechanism of the  $\text{NaAlH}_4 + \text{Ca}(\text{BH}_4)_2$  composite system, *Int. J. Hydrogen Energy*, 2018, **43**, 11132.e11140, DOI: [10.1016/j.ijhydene.2018.04.234](https://doi.org/10.1016/j.ijhydene.2018.04.234).
- 289 M. Gao, J. Gu, H. Pan, Y. Wang, Y. Liu, C. Liang and Z. Guo,  $\text{Ca}(\text{BH}_4)_2\text{-LiBH}_4\text{-MgH}_2$ : a novel ternary hydrogen storage system with superior long-term cycling performance, *J. Mater. Chem. A*, 2013, **1**, 12285, DOI: [10.1039/c3ta12472j](https://doi.org/10.1039/c3ta12472j).
- 290 O. Jin, Y. Shang, X. Huang, D. V. Szabó, T. T. Le, S. Wagner, T. Klassen, C. Kübel, C. Pistidda and A. Pundt, Transformation Kinetics of  $\text{LiBH}_4\text{-MgH}_2$  for Hydrogen Storage, *Molecules*, 2022, **27**, 7005, DOI: [10.3390/molecules27207005](https://doi.org/10.3390/molecules27207005).

